Quantitative Magnetic Resonance Imaging in Multiple Sclerosis: Neuropathology and Genetics Correlates

Inaugural dissertation
to
be awarded the degree of Dr. sc. med.
presented at
the Faculty of Medicine
of the University of Basel

by
Reza Rahmanzadeh
from Amol, Iran

Basel, 2021

Approved by the Faculty of Medicine

On application of

Prof. Dr. med. Dr. Phil. Cristina Granziera, First supervisor

Prof. Dr. rer. nat. Sven Cichon, Second supervisor

Prof. Dr. med. Matilde Inglese, External reviewer

Basel, 31.01.2022

Prof. Dr. Primo Leo Schär

Dean

Contents

Summary

Multiple sclerosis (MS) is a chronic inflammatory demyelinating disease of the central nervous system characterized by multifocal inflammatory infiltrates, microglial activation and degradation of oligodendrocytes, myelin and axons. The imbalance between the damage to the myelin/axonal structure and axonal repair is considered to be one of the drivers of disability in MS patients. MS patients exhibit a high heterogeneity in disease progression and in the extent of myelin/axonal damage and the underlying mechanisms are currently poorly understood. Hence, the overall goals & findings of this doctoral thesis were:

i) to study the interplay between myelin and axonal damage/repair in various MS lesion types and different brain regions using myelin water imaging for myelin water fraction (MWF) and multi-shell diffusion imaging. Our findings showed that particular lesion types (e.g. paramagnetic rim lesions & periventricular lesions) exhibit more damage to myelin and axons, and myelin and axon pathology in lesions is related to MS disability and global measures of neuroaxonal damage.

ii) to propose a new approach to distinguish MS lesion types using clinically-compatible qMRI techniques. In a cross-sectional/longitudinal in vivo study with post-mortem verification, we have shown that quantitative susceptibility mapping (QSM) could identify remyelinated, chronic active and chronic inactive MS lesions with high accuracy.

iii) to evaluate the reproducibility of MWF, QSM, quantitative T1 mapping (qT1), magnetization transfer saturation imaging (MTsat). and their relative sensitivity to MS pathology. Our findings showed that quantitative magnetic resonance imaging (qMRIs) exhibit differential sensitivity to focal and diffuse WM and GM pathology in MS patients and are highly reproducible.

iv) to study the relationship between genetic risk factors and myelin/axonal damage/repair in MS. Our study identified novel genetic loci that might be associated with myelin and axonal pathology in MS Patients.

1. Introduction

1.1. MS pathogenesis & pathology

Multiple sclerosis (MS) is the most common non-traumatic neurological disorder of the central nervous system. Damage to the myelin sheath and the neuroaxonal unit is a characteristic feature of MS; however, underlying mechanisms responsible for that is still unclear. Three main pathological processes in MS have been shown to be involved in axonal and myelin damage:

a. CNS-invading autoimmunity: it is believed that a CNS-invading auto-reactive T-lymphocytes attack mediated by auto-reactive T lymphocytes is involved in the pathogenesis of MS. Inflammation may directly injure myelin/axons via secretion of proteolytic enzymes, cytokines and free-radical species, inducing the expression of neurotransmitters and their receptors, and CD8 T cell- or antibody- mediated inflammatory processes(Rahmanzadeh *et al.*, 2018a; Rahmanzadeh *et al.*, 2018c).

b. Activated Microglia: Neuropathological investigations in normal appearing white matter (NAWM) showed that there are clusters of activated microglia areas without BBB damage and apparent myelin/axonal changes. In such areas, iron deposition exists, microglia are in activated status and production of noxious reactive oxygen species (ROS) are up-regulated and mitochondrial genes involved in respiratory chain are down-regulated (Mahad *et al.*, 2008). Nevertheless, although the total amount of myelin seems to be unchanged, oligodendrocyte pathology has been shown in these areas(Marik *et al.*, 2007; Mahad *et al.*, 2008; Mahad *et al.*, 2015).

c. Oligodendrocyte-intrinsic abnormalities: In some MS lesions, myelin sheaths appear to be distorted, a process that appears to be intrinsic to the oligodendrocytes and that starts in the innermost myelin layers showing swelling and numerous organelles (Rodriguez *et al.*, 1993; Cui *et al.*, 2017). In addition, it has been shown that nascent primitive MS lesions in acute MS patients show a preferential myelin associated glycoprotein (MAG) loss in areas without infiltration of inflammatory cells (Itoyama *et al.*, 1980; Aboul-Enein *et al.*, 2003; Rahmanzadeh *et al.*, 2018b).

1.2. MS lesion heterogeneity

MS lesions are heterogeneous in terms of cellular composition of the inflammatory infiltrate, target of injury and degree of demyelination and axonal loss (Lucchinetti *et al.*, 2000). In neuropathological studies, lesion-wise variation has been observed intra- and inter-individually and among lesions in different locations and at different stages of development (Barnett and Prineas, 2004; Metz *et al.*, 2014). Recently, Kuhlmann et al. (Kuhlmann *et al.*, 2017) have proposed a new neuropathological classification of MS lesions: i) active MS lesions harbor macrophages/microglia ii) mixed-active/inactive are the ones with an activated macrophages/microglia at lesion border surrounding the demyelinated lesion center iii) inactive MS lesions are sharply demarcated hypocellular lesions almost devoid of oligodentrocytes, macrophages/microglia and lymphocytes. In addition, remyelination might be present to some extent in all above-mentioned MS lesion types and is characterized by the presence of thinner myelin sheath and oligodendrocyte progenitor cells.

MS lesions might show partial to almost complete remyelination (Lassmann, 2018a). Also, periventricular lesions exhibit much more pronounced myelin and axon loss than juxtacortical lesions (Patrikios *et al.*, 2006; Patani *et al.*, 2007). On the other hand, chronic active lesions show a more pronounced axon loss in their inactive center compared to other lesions (eg. acute and inactive), and a surrounding rim with iron-laden macrophages, demyelination and axon end-bulbs (Kuhlmann *et al.*, 2017). Besides, previous pathological and imaging studies revealed that axon/myelin damage is not limited to the plaque area, but rather extend to the tissue surrounding it (Lieury *et al.*, 2014; Mustafi *et al.*, 2019). Further, the pathological characteristics of WM lesions seem to be similar between plaques found in relapsing remitting MS (RRMS) and progressive MS (PMS) patients (Lucchinetti *et al.*, 2000). During my doctoral studies, I have attempted at identifying different neuropathological MS lesion types in vivo in MS patients.

1.3. Advanced qMRIs of myelin and axonal structures

There are a number of advanced MRI techniques that are sensitive to myelin and axonal damage, as well as toiron content within the CNS (Granziera *et al.*, 2021).

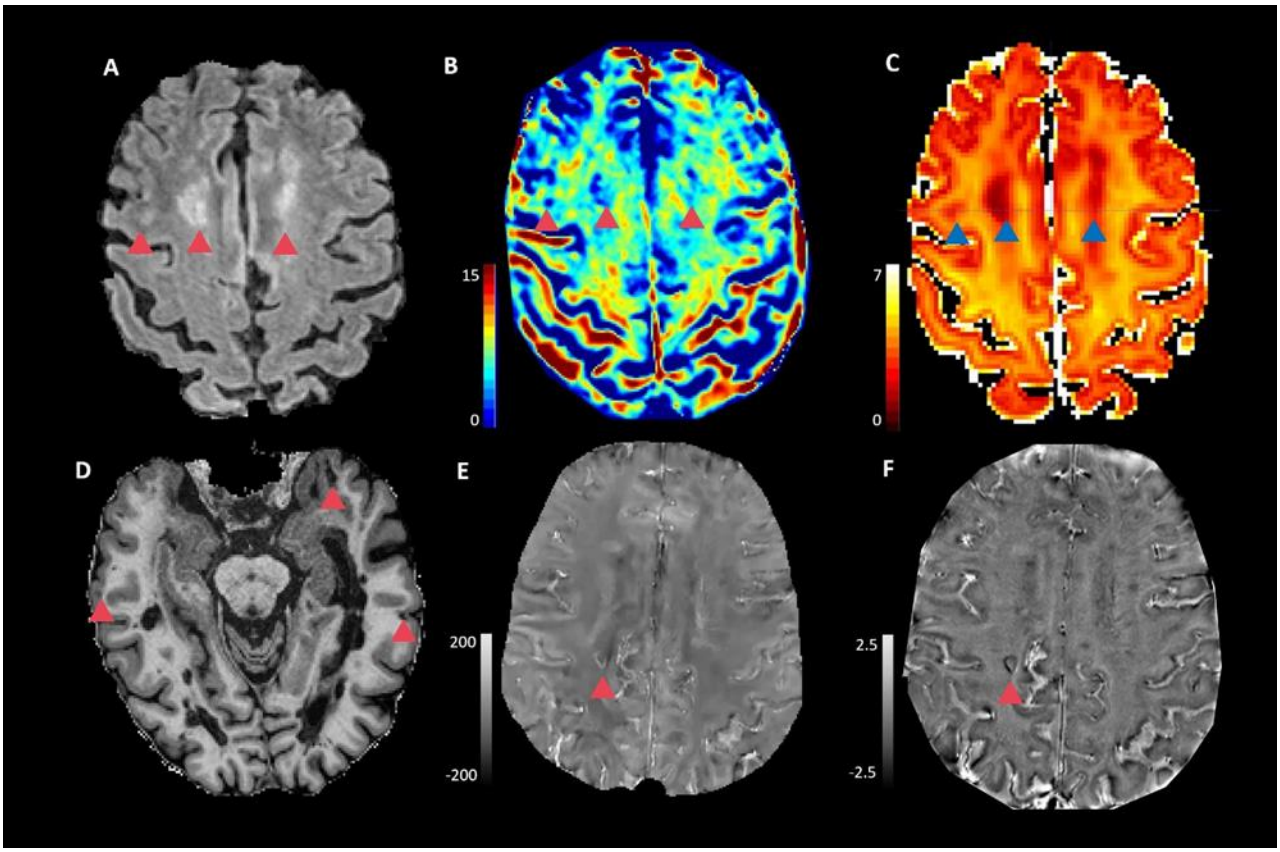

Figure 1. Axial images in one exemplary MS patient: A) FLAIR B) MWF map C) NODDI-NDI map D) MP2RAGE E) 3D-EPI QSM F) 3D-EPI unwrapped phase. Red/Blue triangles show WM lesions (A, B, C), Cortical lesions (D) and lesions with paramagnetic rim (E, F).

Magnetization Transfer Imaging (MTI) has been traditionally exploited to provide semi-quantitative or quantitative measures of myelin integrity in MS patients, whereas Diffusion Tensor Imaging (DTI) has supported with coarse measures of axon content, especially in WM(Enzinger *et al.*, 2015). On the other hand, Myelin

water imaging (MWI) (Nguyen *et al.*, 2016) and biophysical models applied to multishell diffusion MRI (Cercignani and Gandini Wheeler-Kingshott, 2019) have shown to provide more specific surrogate measures of myelin and axon integrity than MTI and DTI.

MWI quantifies the water between myelin layers by distinguishing multiple water components in T2 relaxometry data and supports with measures (e.g. myelin water fraction; MWF), which have been validated postmortem (Moore *et al.*, 2000; Kozlowski *et al.*, 2014). Neurite orientation dispersion and density imaging (NODDI) mathematically models multi-shell diffusion data to estimate axon and dendrite density (neurite density index; NDI) and the orientation of tissue components in the central nervous system (Zhang *et al.*, 2012). The advantage of NODDI over DTI is that NODDI does not assume a Gaussian distribution of diffusion processes and, hence, models non-Gaussian diffusion in biological tissue providing more specific measures of tissue microstructure (Colgan *et al.*, 2016; Grussu *et al.*, 2017). Multi-compartment microscopic diffusion imaging (MCMDI) is an alternative technique to the NODDI model that provides estimates of intra- and extra-neurite compartments in the brain, which has also been applied to MS patients (Kaden *et al.*, 2016; Bagnato *et al.*, 2018).

Quantitative susceptibility mapping (QSM) quantifies the spatial distribution of magnetic susceptibility in biological tissue(Liu *et al.*, 2012) and has been shown to be sensitive to iron content and to myelin integrity(Wisnieff *et al.*, 2015; Hametner *et al.*, 2018). QSM is a field-to-source inversion method to map the local susceptibility sources in the tissue from the shift in the magnetic field created by these sources which can be measured from gradient echo data.

Quantitative T1 mapping (qT1)(Taylor *et al.*, 2016) quantifies T1 relaxation times that are sensitive to water content and macro/micro molecules changes within a tissue, such as the one provoked by demyelination and axonal loss in the brain(Kolb *et al.*, 2021). Although it is challenging to disentangle the contribution of these factors in acquired qT1, it has been shown that qT1 correlates well with myelin content in NAWM and MS lesions(Mottershead *et al.*, 2003; Seewann *et al.*, 2009).

Magnetization transfer (MT) imaging measures the magnetization exchange

between proton in free water and the protons coupled with macromolecules, which has been related to myelin integrity and content(Moccia *et al.*, 2020). MT saturation (MTsat) is developed to improve the MT ratio by decoupling the MTR from R1 by compensating for T1-relaxation and flip angle inhomogeneities, thus overcoming some limitations of previous MT-based methodologies (Helms *et al.*, 2008b).

In my doctoral work, I have investigated the interplay of myelin and axonal damage in MS using quantitative MRIs or to compare sensitivity of qMRIs to MS pathology.

1.4. Genetic susceptibility to MS

MS is a multifactorial disease which is influenced by genetic as well as environmental factors (Baranzini *et al.*, 2009; Patsopoulos, 2018). Formal genetic studies have emphasized the role of genetic factors to disease susceptibility, the heritability has been estimated between 0.48-0.64 (Patsopoulos, 2018) . The Major Histocompatibility (MHC) locus was the first susceptibility locus that has been identified with high probability of association with MS in numerous studies and previous work has also shown that MHC region harbors many independent SNPs (Parnell and Booth, 2017; International Multiple Sclerosis Genetics, 2019). specifically, the MHC locus contain the HLA-DRB1 gene, whose variant HLA-DRB1*15:01 elevates the risk of developing MS of about threefold (Goodin *et al.*, 2021). To date, more than 200 genomic loci outside the MHC (major histocompatibility complex) region were discovered. Interestingly, all genomic loci harboring a risk to develop MS were located in the vicinity of immune genes and no genetic loci have been directly related to components of the CNS tissue (De Jager *et al.*, 2009; International Multiple Sclerosis Genetics *et al.*, 2010; International Multiple Sclerosis Genetics *et al.*, 2013). Besides, up to the present time, most of the genetic variations that have been identified in MS patients were correlated with MS risk susceptibility rather than MS clinical and radiological phenotypes. In fact, only few studies correlated genetic variations with sub-clinical, MRI and cerebrospinal fluid (CSF) measures. One study showed that HLA-

DRB1*15:01 was correlated with age at onset, response to therapy and MRI parameters as WM lesion volume, reduction in brain parenchymal volume (BPV) (Masterman *et al.*, 2000; Liguori *et al.*, 2011). Another study provided evidence that HLA-B*44:02, a protective allele for MS, was conversely associated with these MRI parameters. An additional work revealed that the cumulative HLA risk was associated with younger age at onset of MS and atrophy of subcortical gray matter (Isobe *et al.*, 2016). In addition to these HLA genes-MS phenotypes associations, some studies tried to investigate genome-wide association with MS phenotypes, an attempt to find out new genetic loci related to disease severity and characteristics. Another large study found more than 60 SNPs associated with age at onset, disease clinical severity, T2 lesion load and BPV(Baranzini *et al.*, 2009).

So far, a handful of studies investigated the association of MS genotype with advanced MRI-derived phenotypes. One study showed lower concentration of magnetic resonance spectroscopy (MRS)-measured N-acetyl-aspartate (NAA) in NAWM of HLA DRB1 1501 carriers(Okuda *et al.*, 2009). In the other, a genome wide association study with glutamate concentration as a quantitative phenotypic trait was done to find out SNPs related to higher glutamate concentration in MS(Baranzini *et al.*, 2010).

As explained above, damage to myelin sheath and axons is the cardinal feature of MS and, therefore, exploring genetic loci with destructive/protective effects might shed light into the pathogenic mechanisms underlying myelin/axonal pathology.

To date, however, there are no studies linking genetic susceptibility to the extent of brain axon and myelin damage in MS patients.

2. Results

The overall aims of this doctoral thesis were to: i) study the interplay between myelin and axonal damage/repair in various MS lesion types using state-of-the-art quantitative magnetic resonance imaging (qMRIs) ii) to propose a new approach to distinguish MS lesion types in a clinically applicable way using qMRI iii) to evaluate the reproducibility of the applied qMRIs and their deferential sensitivity to MS pathology iv) to study the relationship between genetic risk factors and myelin/axonal alteration in MS measured by qMRIs.

This doctoral work has been developed thanks to a longitudinal cohort of MS patients that underwent a complex advanced MRI protocol, standardized clinical examination and blood sampling at the University Hospital Basel, Basel, Switzerland.

2.1. Manuscript 1

Myelin and axon pathology in multiple sclerosis assessed by myelin water and multi-shell diffusion imaging

The goal of this work was to exploit MWI and multi-shell diffusion imaging to investigate the relative distribution of myelin and axonal damage (i) in distinct lesion types – as identified with the help of magnetization-prepared 2 rapid acquisition gradient echoes (MP2RAGE) and QSM; (ii) in normal appearing white and grey matter (NAWM, NAGM) and (iii) across different disease phenotypes, as compared to healthy controls. Further, we have then assessed the relationship between NDI/MWF measures and neurofilament light chain, to determine whether those measures are related to global biological measures of neuroaxonal damage in living patients.

Myelin and axon pathology in multiple sclerosis assessed by myelin water and multi-shell diffusion imaging

Reza Rahmanzadeh[1,2], Po-Jui Lu[1,2], Muhamed Barakovic[1,2], Matthias Weigel[1,2,10], Pietro Maggi[3,12], Thanh D. Nguyen[4], Simona Schiavi[5], Alessandro Daducci[5], Francesco La Rosa[6,7], Sabine Schaedelin[1], Martina Absinta[8,11], Daniel S. Reich[8], Pascal Sati[8,9], Yi Wang[4], Meritxell Bach Cuadra[6,7], Ernst-Wilhelm Radue[1], Jens Kuhle[2], Ludwig Kappos[2], Cristina Granziera[1,2]

[1]*Translational Imaging in Neurology Basel, Department of Medicine and Biomedical Engineering, University Hospital Basel and University of Basel, Basel, Switzerland.*

[2]*Neurologic Clinic and Policlinic, Switzerland, Departments of Medicine, Clinical Research and Biomedical Engineering, University Hospital Basel and University of Basel, Basel, Switzerland.*

[3]*Department of Neurology, Lausanne University Hospital, Lausanne, Switzerland.*

[4]*Department of Radiology, Weill Cornell Medical College, New York, New York, USA.*

[5]*Department of Computer Science, University of Verona, Verona, Italy.*

[6]*Signal Processing Laboratory (LTS5), Ecole Polytechnique Fédérale de Lausanne (EPFL), Lausanne, Switzerland.*

[7]*Radiology Department, Center for Biomedical Imaging (CIBM), Lausanne University and University Hospital, Lausanne, Switzerland.*

[8]*Translational Neuroradiology Section, National Institute of Neurological Disorders and Stroke, NIH, 10 Center Drive MSC 1400, Building 10 Room 5C103, Bethesda, Maryland, USA.*

[9]*Department of Neurology, Cedars-Sinai Medical Center, Los Angeles, CA.*

[10]*Division of Radiological Physics, Department of Radiology, University Hospital Basel, Basel, Switzerland.*

[11]*Department of Neurology, Johns Hopkins School of Medicine, Baltimore, Maryland, USA.*

[12]*Cliniques universitaires Saint Luc, Université catholique de Louvain, Brussel, Belgium.*

Abstract

Damage to the myelin sheath and the neuroaxonal unit is a cardinal feature of multiple sclerosis; however, a detailed characterization of the interaction between myelin and axon damage in vivo remains challenging.

We applied myelin water and multi-shell diffusion imaging to quantify the relative damage to myelin and axons (i) among different lesion types; (ii) in normal-appearing tissue; and (iii) across multiple sclerosis clinical subtypes and healthy controls. We also assessed the relation of focal myelin/axon damage with disability and serum neurofilament light chain as a global biological measure of neuroaxonal damage.

Ninety-one multiple sclerosis patients (62 relapsing-remitting, 29 progressive) and 72 healthy controls were enrolled in the study. Differences in myelin water fraction and neurite density index were substantial when lesions were compared to healthy controls and normal-appearing MS tissue: both white matter and cortical lesions exhibited a decreased myelin water fraction and neurite density index compared with healthy ($P < 0.0001$) and peri-plaque white matter ($P < 0.0001$). Periventricular lesions showed decreased myelin water fraction and neurite density index compared with lesions in the juxtacortical region ($P < 0.0001$ and $P < 0.05$). Similarly, lesions with paramagnetic rims showed decreased myelin water fraction and neurite density index relative to lesions without a rim ($P < 0.0001$). Also, in 75% of white matter lesions, the reduction in neurite density index was higher than the reduction in the myelin water fraction.
Besides, normal-appearing white and grey matter revealed diffuse reduction of myelin water fraction and neurite density index in multiple sclerosis compared to healthy controls ($P < 0.01$). Further, a more extensive reduction in myelin water fraction and neurite density index in normal-appearing cortex was observed in progressive versus relapsing-remitting participants. Neurite density index in white matter lesions correlated with disability in patients with clinical deficits ($P<0.01$, beta=-10.00); and neurite density index and myelin water fraction in white matter lesions were associated to serum neurofilament light chain in the entire patients cohort ($P<0.01$, beta=-3.60 and $P<0.01$, beta=0.13, respectively).

These findings suggest that (i) myelin and axon pathology in multiple sclerosis is extensive in both lesions and normal-appearing tissue; (ii) particular types of lesions exhibit more damage to myelin and axons than others; (iii) progressive patients differ from relapsing-remitting because of more extensive axon/myelin damage in the cortex; and (iv) myelin and axon pathology in lesions is related to disability in patients with clinical deficits and global measures of neuroaxonal damage.

Keywords

multiple sclerosis; myelin water imaging; diffusion microstructural modeling; neurodegeneration; demyelination.

1.Introduction

The presence of myelin and axon damage - and the interaction between them - are major pathological drivers of neurological disability in multiple sclerosis (MS) (Lassmann, 2018b). Still, up to the present time, the investigation of myelin and axon properties in MS patients in vivo has been challenging, owing to the heterogeneity of the disease but also to the lack of appropriate methodologies to study the complex interplay between the pathological changes occurring to the myelin sheet and the neuroaxonal unit.

MS lesions are heterogeneous in terms of cellular composition of the inflammatory infiltrate, target of injury and degree of demyelination and axonal loss (Lucchinetti *et al.*, 2000). In neuropathological studies, lesion-wise variation has been observed intra- and inter-individually and among lesions in different locations and at different stages of development (Barnett and Prineas, 2004; Metz *et al.*, 2014). In fact, periventricular lesions exhibit much more pronounced myelin and axon loss than juxtacortical lesions (Patrikios *et al.*, 2006; Patani *et al.*, 2007). On the other hand, chronic active lesions show a more pronounced axon loss in their inactive center compared to other lesions (eg. acute and inactive), and a surrounding rim with myelin-phagocyting macrophages and axon end-bulbs (Kuhlmann *et al.*, 2017). Also, previous pathological and imaging studies revealed that axon/myelin damage is not limited to the plaque area, but rather extend to the tissue surrounding it (Lieury *et al.*, 2014; Mustafi *et al.*, 2019).

The pathological characteristics of WM lesions seem to be similar between plaques found in relapsing remitting MS (RRMS) and progressive MS (PMS) patients (Lucchinetti *et al.*, 2000). Nevertheless, the low efficacy of immunomodulatory therapeutics and higher disability in PMS patients suggest that there is more extensive diffuse pathology in PMS compared to RRMS. This damage encompasses pronounced myelin loss, axon transection/degeneration, and clusters of activated microglia in normal-appearing (NA) white and grey matter (Kutzelnigg *et al.*, 2005; Marik *et al.*, 2007).

Magnetic resonance imaging has provided a precious window into the neuropathological features of MS in living patients. Magnetization transfer imaging (MTI) and diffusion tensor imaging (DTI) showed the presence and extent of focal and diffuse changes in both RRMS and PMS patients by

exploiting measures such as magnetization transfer ratio, median diffusivity and fractional anisotropy (Enzinger *et al.*, 2015). Yet, despite the applied measures demonstrate good sensitivity to pathological changes in MS patients, those measures lack specificity for both myelin and axon damage.

Myelin water imaging (MWI) (Laule and Moore, 2018) and biophysical models of diffusion MRI (Cercignani and Gandini Wheeler-Kingshott, 2019) provide more specific surrogate measures of myelin and axon integrity than DTI and MTI. MWI quantifies the water between myelin layers by distinguishing multiple water components in T2 relaxometry data and supports with measures (eg. myelin water fraction, MWF), which have been validated postmortem (Moore *et al.*, 2000; Kozlowski *et al.*, 2014). Neurite orientation dispersion and density imaging mathematically models multi-shell diffusion data to estimate axon and dendrite density (neurite density index, NDI) and the orientation of tissue components in the central nervous system (Zhang *et al.*, 2012). The advantage of NODDI over DTI is that NODDI does not assume a Gaussian distribution of diffusion processes and, hence, models non-Gaussian diffusion in biological tissue providing more specific measures of tissue microstructure (Colgan *et al.*, 2016; Grussu *et al.*, 2017). Multi-compartment microscopic diffusion imaging (MCMDI) is an alternative technique to the NODDI model that provides estimates of intra- and extra-neurite compartments in the brain, which has also been applied to MS patients (Kaden *et al.*, 2016; Bagnato *et al.*, 2018).

Thanks to MRI hardware and software developments, it is nowadays possible to acquire MWI and multi-shell diffusion data in clinically compatible protocols, which allow to simultaneously assess the presence, extent and interplay between myelin and axon damage in living MS patients. Besides, MWI and multi-shell diffusion may be combined with other pulse sequences - such as inversion-contrast magnetization-prepared 2 rapid gradient echo sequence (MP2RAGE) (Marques *et al.*, 2010) and 3D segmented Echo-Planar-Imaging (3D-EPI) (Sati *et al.*, 2012) - that permit to identify specific lesion subtypes such as cortical lesions (CLs) and chronic active lesions.

The goal of the current work was to exploit MWI and multi-shell diffusion imaging to investigate the relative distribution of myelin and axonal damage (i) in distinct lesion types – as identified with the help of MP2RAGE and 3D EPI; (ii) in normal appearing white and grey matter (NAWM, NAGM) and (iii) across different disease phenotypes, as compared to healthy controls. Further, we have then assessed the relationship between NDI/MWF measures and neurofilament light

chain, to determine whether those measures are related to global biological measures of neuroaxonal damage in living patients.

2. Materials and methods

2.1. Participants

We enrolled 91 MS patients (62 RRMS and 29 PMS) and 72 healthy controls (Table 1). The inclusion criteria were: (i) MS diagnosis according to McDonald criteria 2018 (Thompson *et al.*, 2018) and diagnosis of active RRMS or inactive PMS as defined by Lublin et al. (Lublin *et al.*, 2014); (ii) absence of any concomitant psychiatric or neurological disease (excluding headache); (iii) absence of contraindication to MRI. The ethical review committee of the University Hospital Basel (IRB of Northwest Switzerland) approved the study, and all participants entered the study following written consent.

	Multiple sclerosis subjects	**Healthy control subjects**
Sex, n (male/female)	91 (35/56)	72 (29/43)
Age (years), mean ± SD	46 ± 14	36 ± 12
EDSS score, median (range)	2.5 (0–8)	-
Disease course (RR/PMS)	62/29	-
Disease-modifying therapy (n)	Untreated (10) Interferon-beta (1) Glatiramer acetate (1) Dimethyl fumarate (13) Fingolimod (5) Natalizumab (2) Rituximab (10) Ocrelizumab (49)	

Table 1. Patients and healthy controls demographics.

2.2. Clinical assessment

MS disability was assessed using Neurostatus-EDSS (www.neurostatus.net) (Kurtzke, 1983) by certified neurologists at Basel University Hospital. There were only 9 patients with EDSS 0 and 8 with EDSS 1 in our cohort: those patients showed various levels of mean MWF and NDI in lesions despite the absence of measurable clinical disability. Because this absence of a clinical correlate of focal damage in those patients might be due to several factors encompassing functional reserve and compensatory mechanisms, we have decided to focus on patients with clinical disability, where the relationship between focal damage and clinical deficits might be less confounded.

2.3. MR acquisition and metrics computation

MRI was performed on a 3T whole-body MR system (Magnetom Prisma, Siemens Healthcare, Erlangen, Germany) using a 64-channel phased-array head and neck coil for radio frequency reception. The MRI protocols included: (i) 3D FLAIR (TR/TE/TI=5000/386/1800 ms) and MP2RAGE (TR/TI1/TI2=5000/700/2500 ms) both with 1 mm^3 isotropic spatial resolution; (ii) Fast Acquisition with Spiral Trajectory and adiabatic T2prep (FAST-T2) (spiral TR/TE = 7.5/0.5 ms, six T2prep times = 0 (T2prep turned off), 7.5, 17.5, 67.5, 147.5, 307.5 ms, voxel size = 1.25x1.25x5 mm^3, scan time = 4.5 min, as described in (Nguyen *et al.*, 2016); (iii) multi-shell diffusion (TR/TE/δ/Δ/resolution = 4.5 s / 75 ms / 19 ms / 36 ms / 1.8 mm^3 isotropic with b-values 0 / 700 / 1000 / 2000 / 3000 s/mm^2 with 12/6/20/45/66 measurements, respectively, per shell and a diffusion acquisition with 12 measurements of b-value 0 s/mm^2 with reversed phase encoding as well as (iv) 3D segmented EPI with submillimeter isotropic resolution (TR/TE/resolution=64 ms/35 ms/0.67x0.67x0.67 mm^3), providing both T2* magnitude and phase contrast.

In FAST-T2, the robustness of the MWF map against noise propagation is achieved by judiciously sampling the T2 signal at a very short TE (0.5 ms) to maximize sensitivity to the fast-decaying myelin water component, and also by utilizing a local spatial smoothing constraint in the multi-exponential data fitting (Nguyen *et al.*, 2016), Fig. 1. As in Nguyen et al. (Nguyen *et al.*, 2016), we used an adiabatic T2prep design based on a 0° modified BIR-4 pulse (De Graaf *et al.*, 1997). This symmetric pulse consisted of a reverse half passage, a full passage, and a half passage adiabatic pulse separated by two equal time delays of length TE/2. A previously proposed spatially

local smoothness constraint (Kumar *et al.*, 2012) was incorporated in the three-pool nonlinear fitting by jointly solving the minimization problem over all brain voxels at once. The regularization parameter λ was determined by calculating MWF maps for different λ values in a healthy subject and selecting the one that provided an MWF map with the best visual quality. This optimized value was then fixed for all of the subjects enrolled in this study.

Diffusion images were denoised (Veraart *et al.*, 2016) and corrected for motion and eddy-currents (Andersson and Sotiropoulos, 2016). Two different diffusion models were used. NODDI (Zhang *et al.*, 2012), which is a state-of-the-art model aiming at characterizing the neurite orientation dispersion, Fig.1. However, NODDI has two strong assumptions: (1) fixed diffusivity for all the voxels in the brain tissue whole-brain voxels; and (2) applicability to single-bundle voxels (very few locations in the brain). Due to these limitations we investigated a second advanced diffusion model, Multi-Compartment Microscopic Diffusion Imaging (MCDMI) (Kaden *et al.*, 2016). MCDMI integrates the spherical mean technique to handle orientation dispersion and fiber crossing populations, allowing more accurate estimations in whole-brain voxels. From both models, we estimated the neurite density index, which corresponds putatively to the intra-axonal volume fraction. The results are termed NODDI-NDI and MCMDI-NDI.

Phase images collected with a 0.67 mm isotropic 3D-EPI acquisition (Sati *et al.*, 2012) were recently shown to provide high sensitivity at 3T for detecting chronic active lesions with paramagnetic rims (Absinta *et al.*, 2018). These phase images are interpreted after an automatic analytical phase unwrapping procedure and removal of large background gradients with Gaussian filtering (Fig. 1).

Quantitative susceptibility mapping (QSM) is a field-to-source inversion method to map the local susceptibility sources in the tissue from the shift in the magnetic field created by these sources which can be measured from gradient echo data. In this study, QSM were reconstructed from 3D EPI data by unwrapping phase, removing the background field through Projection onto Dipole Fields algorithm, and using the morphology-enabled dipole inversion algorithm to compute the susceptibility from the local field as in Liu *et al.*(Liu *et al.*, 2012) (Fig. 1).

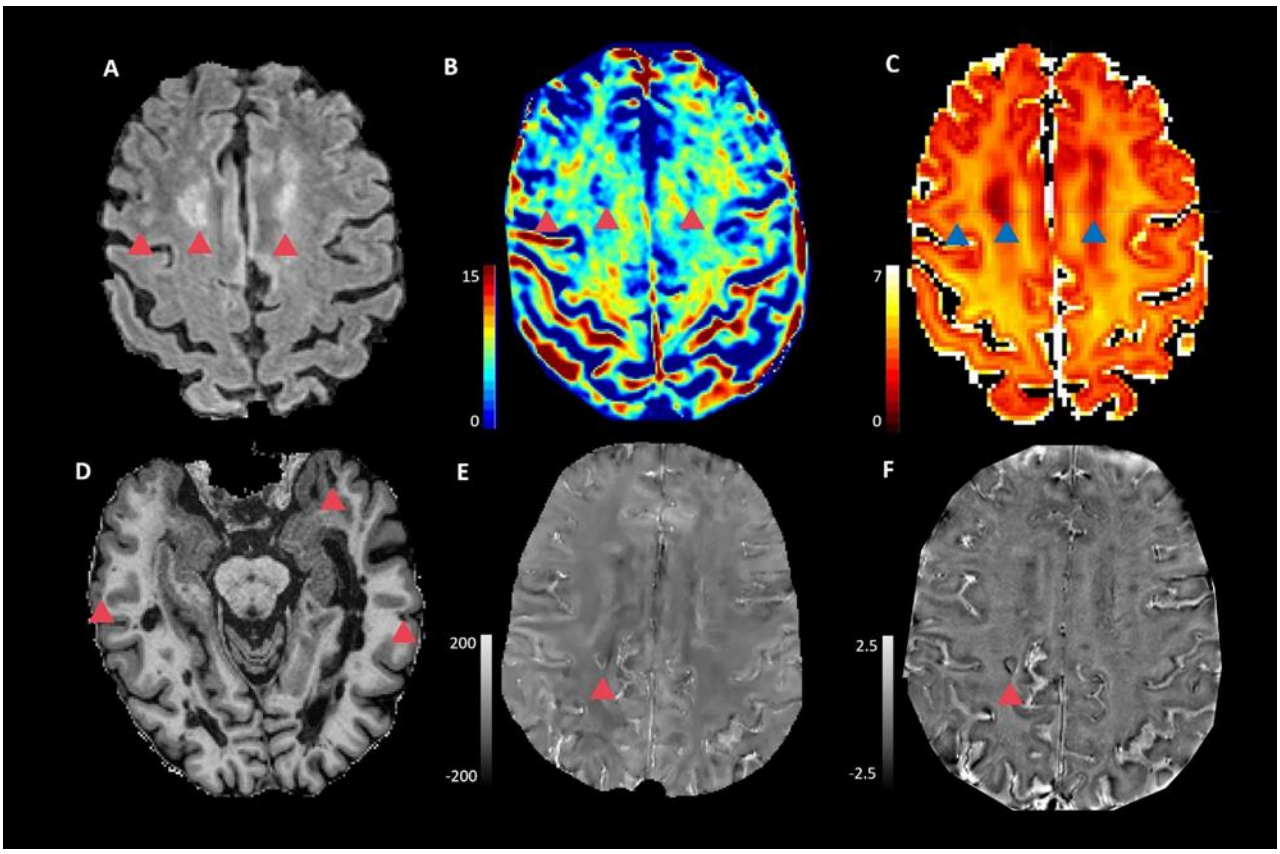

Figure 1. Axial images in one exemplary MS patient: A) FLAIR B) MWF map C) NODDI-NDI map D) MP2RAGE E) 3D-EPI QSM F) 3D-EPI unwrapped phase. Red/Blue triangles show WM lesions (A, B, C), Cortical lesions (D) and lesions with paramagnetic rim (E, F).

2.4. Lesion identification and segmentation

Automatic segmentation of WM lesions was performed by using an in-house deep-learning based method (La Rosa *et al.*, 2020). This approach consists of a cascade of two convolutional neural networks and was adapted to take as input FLAIR and MP2RAGE MRI contrasts. Manual correction of automatic WM lesion masks was performed on FLAIR (by RR and CG). Manual detection of cortical lesions on MP2RAGE was done by two experienced readers by consensus (RR and CG), and CLs were divided into ICLs and LCLs according to Guerts et al. (Geurts *et al.*, 2011).

Lesions with a paramagnetic rim (Rim+) on both 3D-EPI unwrapped phase and 3D-EPI QSM images were identified by two raters (PM and MA for phase and RR and CG for QSM) and were then manually refined by separating confluent Rim+ and Rim- lesions in original WM lesion masks on FLAIR. Of 265 lesions on unwrapped phase and 183 lesions on EPI QSM were Rim+, 159 lesions exhibited paramagnetic rims on both sequences.

To estimate the relative proportion of myelin and axonal damage in WMLs, we calculated the %MWF and %NDI reduction in WMLs as follows: (mean MWF/NDI in the mirror region of interest (ROI) in the contralateral hemisphere - mean MWF/NDI in lesion) x100/the value in the mirror ROI in contralateral hemisphere. For this purpose, all lesions exhibiting contralateral NA mirror areas were selected in the lesion masks. In total, 85 lesions were selected and the mirror ROIs were then manually contoured.

2.5. WM and cortex segmentation

To segment the brain into whole WM, cortex, deep grey matter structures, and ventricles we used the imaging software package FreeSurfer (v.6.0, surfer.nmr.mgh.harvard.edu) (Fischl, 2012). NAWM and NAGM masks were obtained by subtracting WM and cortical lesion masks from WM and cortical masks. An in-house algorithm was used to automatically produce two 2-voxel layers of NAWM surrounding the lesions; herein after denoted peri-plaque-1st (PP-1st) and peri-plaque-2nd (PP-2nd). WM masks were divided into three regions: periventricular (PV, i.e. area within 3 mm from ventricle wall), juxtacortical (JC, i.e. area in 3 mm from the boundary between WM and cortex), and deep white matter (DW, i.e. area between PV and JC).

2.6. Voxel-Based Analyses for NAWM

NAWM maps were co-registered patient-wise to a reference brain (standard MNI152 space) using a rigid-body registration in FMRIB Software Library (FSL) (Jenkinson *et al.*, 2012). As previously performed (Vrenken *et al.*, 2006a), in NAWM we excluded voxels that were not present in at least 50 percent of subjects, and (2) filled missing data with the group mean value of those voxels present in group subjects. We then performed a voxel-wise comparison of MWF, NODDI-NDI, MCMDI-NDI maps between patients and controls by using the randomize tool of FSL with

Threshold-Free Cluster Enhancement clustering. *P* values less than 0.01 were considered statistically significant.

2.7. Vertex-wise analysis for NAGM

A customized volume-to-surface mapping algorithm was applied to voxels assigned to the grey matter ribbon by Free Surfer - i.e., voxels with voxel centers located between the white and pial surfaces were registered and scattered into a standard surface. A smoothing kernel of 10-mm full-width at half-maximum was used. The whole-depth NAGM of MWF, NODDI-NDI, and MCMDI-NDI maps was resampled on inflated cortex, and a generalized linear model (GLM) analysis was conducted for comparison among groups with age and sex as covariates. *P* values less than 0.01 were considered statistically significant.

2.8. Serum Neurofilaments Quantification

Neurofilaments were quantified in serum collected within 1 month of the MRI (serum neurofilaments, sNfL) using a Single-Molecule-Array-Assay (Disanto *et al.*, 2017).

2.9. Statistical analysis

Based on previous histopathology and imaging findings, we hypothesized that: (1) cortical/white matter lesions (CLs, WMLs) and NAWM and NAGM are damaged compared to healthy tissue in HC and show different extents of myelin and axonal damage; (2) chronic active lesions exhibit more axonal and myelin damage compared to other WM lesions; (3) PP tissue is abnormal, and the extent of pathology is proportional to lesion pathology and decreases with distance from lesions; (4) myelin damage outweighs axon damage in MS lesions; (5) the extent of damage differs between RRMS and PMS patients; (6) clinical disability and sNFL levels are associated with myelin and axonal damage.

Statistical analysis was performed using R-project (www.r-project.org) and GraphPad Prism version 8.0.0 for Windows, GraphPad Software, San Diego, California USA. Kolmogorov-Smirnov's test was used to assess the normality of data. Paired t-test, non-parametric Mann-Whitney test, and Kruskal-Wallis test with Dunn's test for multiple comparisons correction, were

used for paired two-group analysis, unpaired two-group analysis, and more-than-three group analysis, respectively. All values, including intra-lesional, homogeneous non-lesional NA tissue and PP tissues, were automatically extracted in both lesion-wise and average patient-wise manners.

For sNfL measures, a logarithmic transformation was applied to comply with normality assumption. Correlation studies between MRI measures, sNfL and EDSS were performed using a general linear model, with age and gender as covariates. The GLM were performed for the whole sample and for patients with clinical deficits only (EDSS >1). A two-tailed $P < 0.05$ was considered statistically significant.

To model the respective contribution of NDI and MWF to the separation of WML/CL vs the corresponding normal appearing-tissue and the relative normal tissue in healthy controls, we have used multinomial logistic regression and a penalized (Firth, 1993) logistic regression as sensitivity analysis.

2.10. Data availability

The data that support the findings of this study are available upon reasonable request.

3. Results

3.1. Cortical and White Matter Lesions

The number, volume, and regional distribution of WML and CL are detailed in Table 2. WMLs were found in all MS patients: PV lesions in 89/91 (98%) patients, JC lesions in 91/91 (100%) patients. CLs were found in 41/91 (45%) MS patients, LCLs in 38/91 (42%), and ICLs in 16/91 (18%). Cortical lesions were more common in PMS than in RRMS (P = 0.017). The quantity of lesions with paramagnetic rims detectable in both EPI phase and EPI QSM images was not different in PMS when compared to RRMS (all P > 0.05).

Lesion Location	**Median (range)**	**Mean ± SD**
Cortical lesion count	0 (0–113)	6.5 ± 17
Cortical lesion volume (mm^3)	0 (0–1783)	195 ± 439
IC lesion count	0 (0–25)	0.6 ± 2.7
IC lesion volume (mm^3)	0 (0–236)	8.1 ± 30
LC lesion count	0 (0–88)	4.9 ± 13
LC lesion volume (mm^3)	0 (0–1718)	178 ± 406
White matter lesion count	47 (1–201)	54 ± 42
White matter lesion volume (mm^3)	5115 (23-64,359)	8602 ± 10,881
PV lesion count	8 (0–27)	10 ± 7
PV lesion volume (mm^3)	285 (0–6650)	913 ± 1381
JC lesion count	31 (1–152)	40 ± 34
JC lesion volume (mm^3)	1847 (7–36,435)	3885 ± 5623

Table 2. Lesion count and volume in WM and CLs. IC: Intra-cortical; LC: Leuko-cortical; PV: Periventricular; JC: Juxta-cortical.

3.2. Axon and myelin in distinct MS lesions types

In WMLs, the average MWF and NODDI-NDI were lower compared to NAWM in patients and WM of HCs (all P < 0.0001, Fig. 2A-B). The average MCMDI-NDI was also lower compared to

NAWM and WM of HCs (both $P < 0.0001$, Supplementary data, Figure 1.). In CLs, the average NODDI-NDI and MWF were lower compared to NAGM in patients and GM of HCs (both $P < 0.0001$, Fig. 1D-E). Also, the average MCMDI-NDI was lower compared to NAGM and GM of HCs ($P = 0.014$ and $P = 0.018$, respectively Supplementary data, Figure 1.).

Figure 1C shows that myelin and axon content in WML were proportional to each other (Spearman's r= 0.4901, p<0.0001) and there was a large variation in MWF and NODDI-NDI in WMLs. PV lesions exhibited lower MWF and NODDI-NDI compared to JC lesions (Fig. 2G-I, $P < 0.0001$ and $P = 0.024$, respectively). MCMDI-NDI was also lower in PV lesions compared to JC lesions ($P < 0.0001$, Supplementary data, Figure 1.). Although there was no difference in MWF between PV and JC regions in HCs ($P = 0.0741$), NODDI-NDI and MCMDI-NDI were lower in PV region compared to JC region in HCs (both $P < 0.0001$). Like WMLs, CLs exhibited proportional myelin and axon content (Spearman's r= 0.4372, p<0.0001, Fig. 2F), yet there was large variation in MWF and NODDI-NDI across CLs. Rim+ lesions exhibited lower NODDI-NDI and MWF compared to Rim- lesions (both $P < 0.001$, Fig. 2J-L). MCMDI-NDI was also lower in Rim+ lesions compared to Rim- lesions ($P = 0.001$, Supplementary data, Figure 1).

We have modeled NDI with MWF by using a multinomial logistic regression with (i) MWF and NDI as independent variables and (ii) tissue-types (i.e. lesions, normal appearing tissue and healthy tissue) as dependent variables. By doing this for both WM and cortical lesions, we have determined that both MWF and NDI explain to a certain extent the differences between the 3 tissue-types, but NDI appears to separate the 3 tissue types better than MWF (Table 3 & Supplementary data, Figure 2.) in WM; for the model related to cortical lesions neither NDI nor MWF could significantly explain the separation of the tissue-types. To address the separation between lesions vs healthy tissue and lesions vs normal-appearing tissue, we further estimated two penalized logistic regression models as suggested by (Firth, 1993) as sensitivity analysis. These analyses confirm the superior role of NDI in separating tissue type for WM lesions, show a trend for NDI also for separating cortical lesions from normal-appearing tissue and a very small but significant contribution of MWF in separating cortical lesions from healthy tissue.

A) White matter regions

Multinominal logistic regression

Comparison	Var	OR	Cl	p
WMLs vs NAWM	(Intercept)	12030141.99		
WMLs vs NAWM	NDI	0.00	[0.00;0.00]	<0.01
WMLs vs NAWM	MWF	2.46	[1.14;5.29]	0.0214
WMLs vs WM-HC	(Intercept)	27040504475680.04		
WMLs vs WM-HC	NDI	0.00	[0.00;0.00]	<0.01
WMLs vs WM-HC	MWF	2.59	[1.03;6.52]	0.0425

Penalized logistic regression: WMLs vs WM-HC

Comparison	Var	OR	Cl	p
WMLs vs WM-HC	(Intercept)	2508712324254-3737302965603-5328.00		
WMLs vs WM-HC	NDI	0.00	[0.00;0.00]	<0.01
WMLs vs WM-HC	MWF	0.47	[0.13;2.97]	0.343

Penalized logistic regression: WMLs vs NAWM

Comparison	Var	OR	Cl	p
WMLs vs NAWM	(Intercept)	3106304.83		
WMLs vs NAWM	NDI	0.00	[0.00;0.00]	<0.01
WMLs vs NAWM	MWF	2.22	[1.11;4.76]	0.0234

B) Cortical regions

Multinominal logistic regression

Comparison	Var	OR	Cl	p
CLs vs NAGM	(Intercept)	16.82		
CLs vs NAGM	NDI	0.00	[0.00;3.15]	0.0643
CLs vs NAGM	MWF	1.19	[0.48;2.94]	0.7104
CLs vs GM-HC	(Intercept)	956307.92		
CLs vs GM-HC	NDI	0.02	[0.00;759768339-0.68]	0.767
CLs vs GM-HC	MWF	0.04	[0.01;0.14]	<0.01

Logistic regression: CLs vs GM-HC

Comparison	Var	OR	Cl	p
CLs vs GM-HC	(Intercept)	917.72		
CLs vs GM-HC	NDI	0.02	[0.00;6283872.23]	0.686
CLs vs GM-HC	MWF	0.21	[0.09;0.48]	<0.01

Logistic regression: CLs vs NAGM

Comparison	Var	OR	Cl	p
CLs vs NAGM	(Intercept)	8.88		
CLs vs NAGM	NDI	0.00	[0.00;8.57]	0.0849
CLs vs NAGM	MWF	1.11	[0.51;2.43]	0.7870

Table 3. Multinomial and penalized (Firth's) logistic regression for white matter (A) and cortical (B) brain regions.

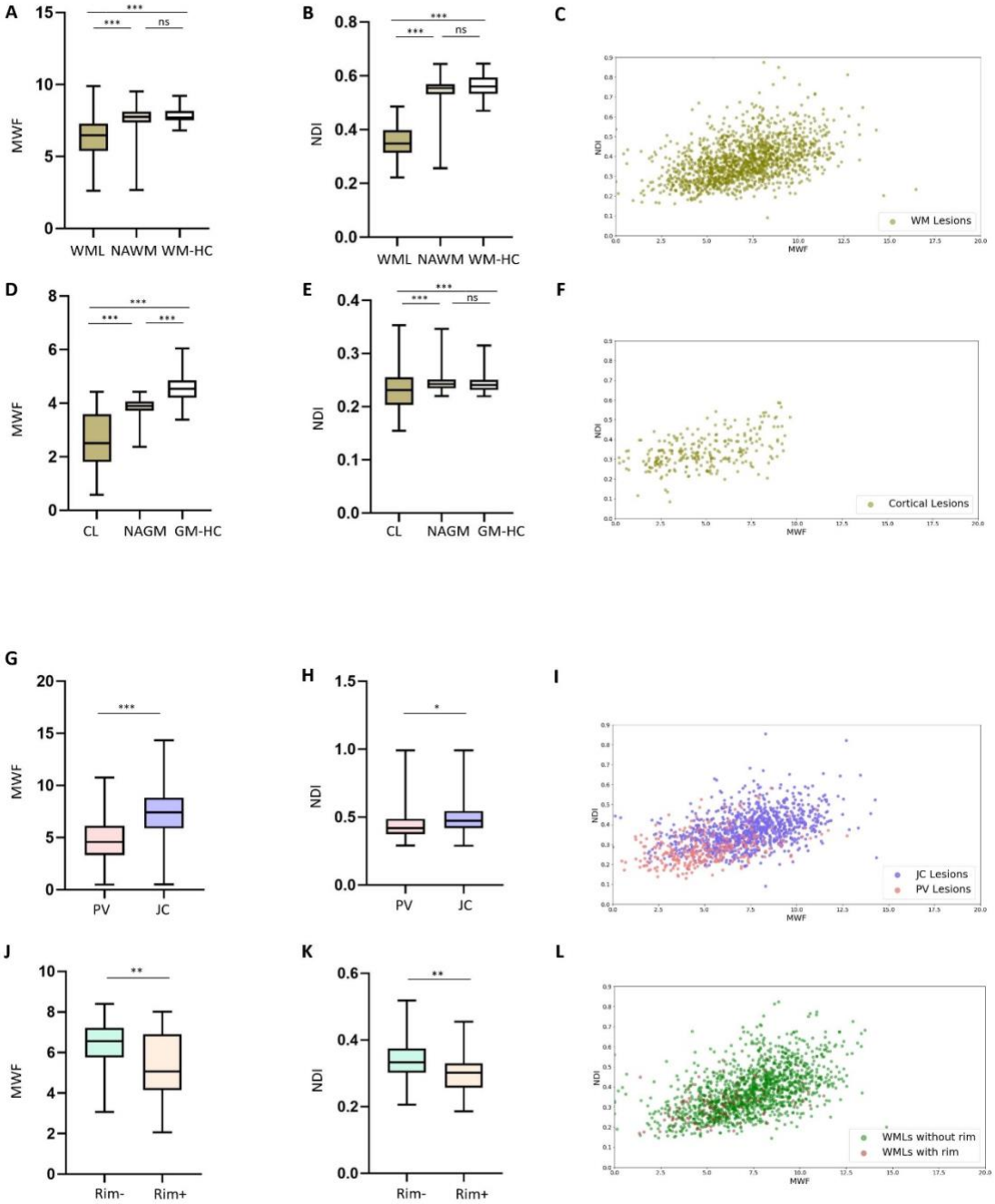
A
MWF
WML NAWM WM-HC
B
NDI
WML NAWM WM-HC
C
WM Lesions
D
MWF
CL NAGM GM-HC
E
NDI
CL NAGM GM-HC
F
Cortical Lesions
G
MWF
PV JC
H
NDI
PV JC
I
JC Lesions
PV Lesions
J
MWF
Rim- Rim+
K
NDI
Rim- Rim+
L
WMLs without rim
WMLs with rim

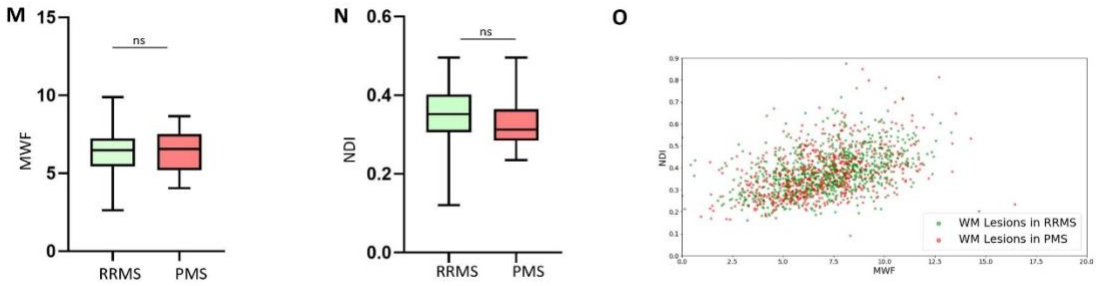

Figure 2. MWF and NODDI-NDI in different types of MS lesions. A) and B) Box plots showing that MWF and NDI in WMLs is lower than MWF and NDI in NAWM and WM-HC. C) NDI-MWF scatter plots in WM lesions. D) and E) Box plots showing that MWF and NDI in CLs is lower than in NAGM and GM-HC. F) NDI-MWF scatter plots in CLs. G) and H) MWF and NDI are lower in PV lesions than in JC lesions. I) NDI-MWF scatter plot in PV and JC lesions. J) and K) MWF and NDI are lower in Rim+ lesions than in Rim- lesions. L) NDI-MWF scatter plot for WM lesions with and without paramagnetic phase rim on both 3D EPI unwrapped phase and 3D EPI QSM images. M) and N) MWF and NDI were not different between RRMS and PMS. O) NDI-MWF scatter plots for WM lesions in RRMS versus PMS. NDI; NODDI-NDI. $^{***}P < 0.0001$; $^{**}P < 0.001$; $^{*}P < 0.05$.

3.3. Pathology around MS lesions

3.3.1. Peri-plaque tissue in WM and cortical lesions (PPWM and PPGM)

MWF and NODDI-NDI increased from the WML to PP-1st and from PP-1st to PP-2nd ((Fig. 3A-C); MWF: all $P < 0.0001$, NODDI-NDI: all $P < 0.0001$). In addition, MCMDI-NDI increased from WML to PP-1st and from PP-1st to PP-2nd (all $P < 0.0001$, Supplementary data, Figure 1.). However, MWF, NODDI-NDI, and MCMDI-NDI were not significantly different among WM-HC, PP-1st, and PP-2nd (all $P > 0.05$,).

Cortical lesions had lower MWF compared to PP-1st and PP-2nd (both $P < 0.001$). Cortical lesions also had lower NODDI-NDI compared to PP-1st and PP-2nd ($P = 0.03$, $P < 0.001$, respectively). However, the average NODDI-NDI and MWF in PP-1st and PP-2nd were similar (Fig. 3D-E). MCDMI-NDI is significantly lower in CLs compared to PP-1st and PP-2nd (both $P<0.05$, Supplementary data, Figure 1). However, MWF, NODDI-NDI, and MCMDI-NDI were not different among GM-HC, PP-1st, and PP-2nd (all $P > 0.05$).

3.3.2. Peri-plaque tissue in lesions with and without a paramagnetic rim

NODDI-NDI, MCMDI-NDI, and MWF were not different in PP-1st and PP-2nd around the Rim+ lesions compared to Rim- lesions (all $P > 0.05$).

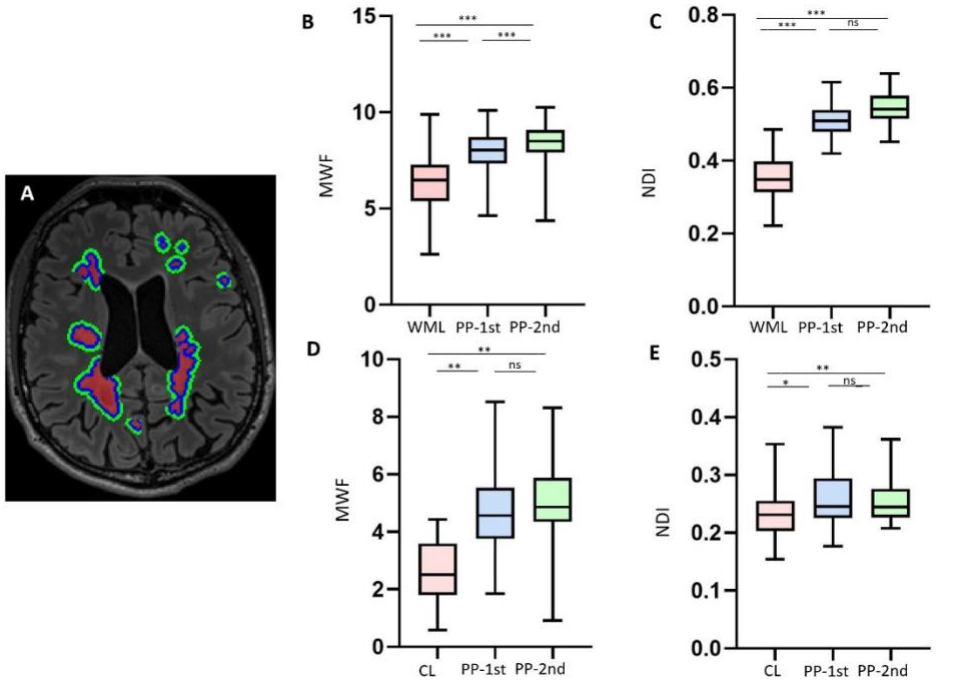

Figure 3. Peri-plaque WM around MS lesions. A) Axial 3D FLAIR image (with segmentation of WMLs (red), 1st PPWM (blue) and 2nd PPWM (green)). B), C) Box plots showing that MWF and NDI gradually increase from WML to PP-1st and PP-2nd. D), E) Box plots showing that MWF

and NDI in CLs are less than in PP-1st and PP-2nd. NDI; NODDI-NDI. $^{***}P < 0.0001$; $^{**}P < 0.001$; $^{*}P < 0.05$.

3.4. Normal-appearing brain tissue

3.4.1. NAWM

The average MWF and NODDI-NDI values in NAWM was not significantly different from that in WM of healthy controls (Fig. 2). However, voxel-wise analysis using TFCE randomized clustering showed that (i) both MWF and NODDI-NDI were diffusely reduced in some clusters of NAWM voxels compared to WM of controls (Fig. 4, $P < 0.01$) and (ii) the area of NDI reduction exceeded the area of MWF reduction. The voxel-wise analysis performed with MCDMI-NDI maps showed similar results to that obtained with NODDI-NDI.

3.4.2. NAGM

The average MWF value in NAGM was lower compared to GM of healthy controls ($P < 0.0001$). The average NODDI-NDI value in NAGM was not significantly different from GM of healthy controls (Fig.1). Yet, vertex-wise cortical surface analysis of MWF and NODDI-NDI showed areas in which MWF and NODDI-NDI were reduced in MS NAGM compared to GM of healthy controls (Fig. 4, $P < 0.01$). Vertex-wise analysis performed with MCDMI-NDI maps showed similar results to that obtained with NODDI-NDI.

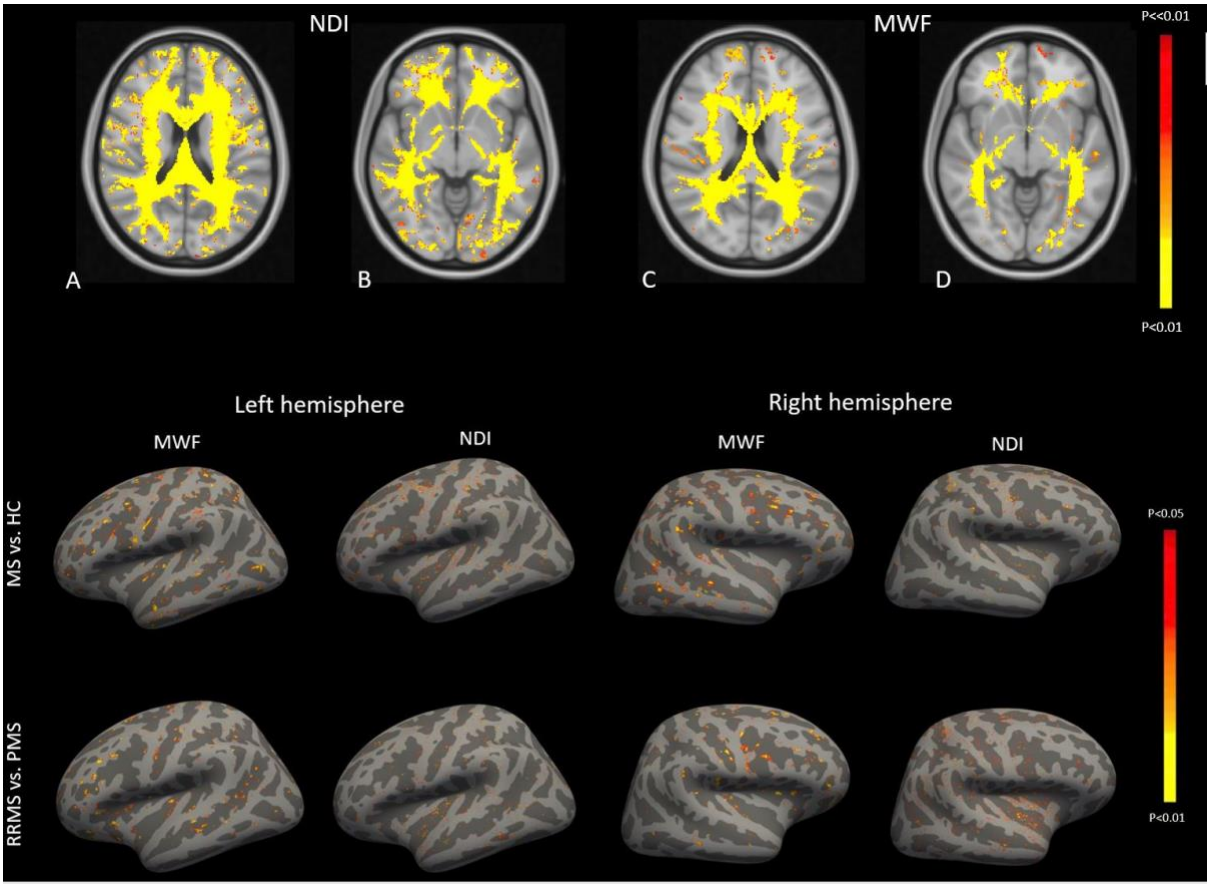

Figure 4. Comparison of NDI and MWF in NA brain tissue between patients and controls. A), B) MS patients show a widespread NODDI-NDI reduction compared to healthy subjects; C), D) MS patients show a widespread MWF reduction compared to healthy subjects. Bottom: There are patchy reductions in MWF and NODDI-NDI in the normal-appearing cortical surface of MS patients vs HC and in PMS vs RRMS patients.

3.5. Axon vs. myelin pathology

WMLs showed a variable reduction in MWF and NODDI-NDI (0.4–80 %MWF; 6–72 %NODDI-NDI) compared to contralateral mirror ROI in NAWM (Fig. 5A, Supplementary data, Figure 2). %MWF reduction was less than %NODDI-NDI reduction in WMLs ($P < 0.0001$) (Fig. 5B). In

26% of lesions the %MWF reduction was more than the %NODDI-NDI reduction, and in 74% of lesions the %NODDI-NDI was more than the %MWF reduction. There was no difference in %MWF and %NODDI-NDI among PV, DW, and JC lesions or between RRMS and PMS (all $P > 0.05$).

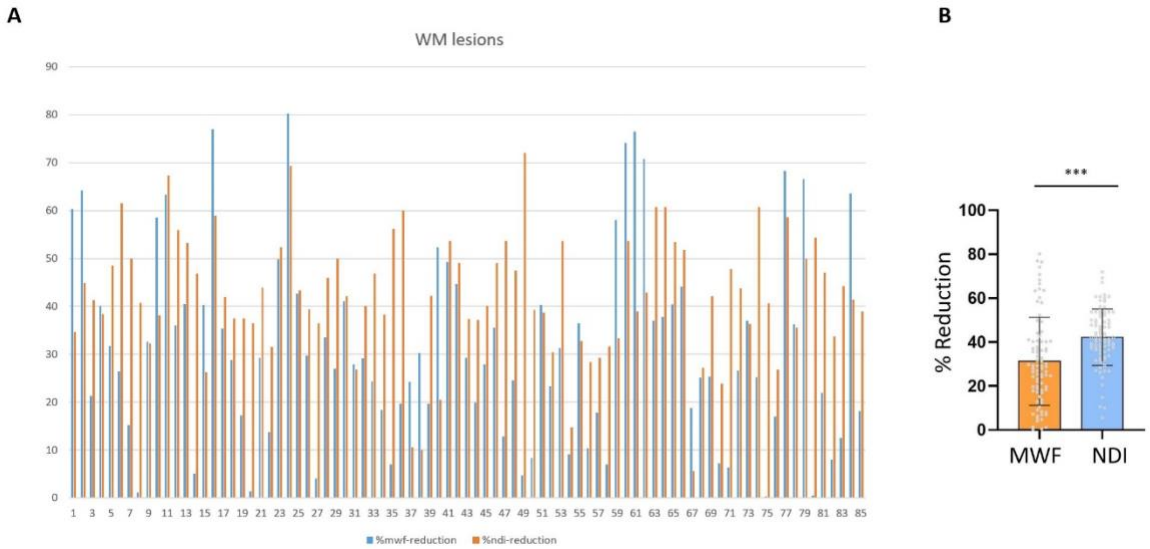

Figure 5. Alteration in MWF vs. NDI in MS WMLs. A) Percentage of MWF and NODDI-NDI decline for individual WMLs relative to mirror ROI in contralateral hemisphere (individual MS WMLs are shown with numbers). B) Graph-bar shows that NODDI-NDI decreases more than MWF in MS lesions ($^{***}P < 0.0001$).

3.6. Relapsing-remitting vs progressive MS patients

The average NODDI-NDI and MWF in WMLs were not different between RRMS and PMS patients (both $P > 0.05$). In accordance, lesion-wise analysis revealed a similar pattern of NDI and MWF distribution in PMS and RRMS lesions (Fig. 2M-O).

There was no difference in voxel-wise analysis in NODDI-NDI and MWF across NAWM voxels between RRMS and PMS. However, vertex-wise analysis showed areas across NAGM in which MWF and NODDI-NDI were lower in PMS compared to RRMS (Fig. 4, $P < 0.01$).

3.7. Correlation analysis between advanced MRI measures, disability and sNFL.

MWF and NDI in WML did not correlate with EDSS when the entire cohort of patients was considered. However, a post-hoc sensitivity analysis found that - in patients with clinical deficits (EDSS>1) - NDI in WMLs was associated with EDSS (NDI: P<0.01, beta=-10.00; N=74).
We also found that MWF and NDI in WMLs were related to sNfL (MWF: P<0.01, beta=0.13; NDI: P<0.01, beta=-3.60) when the entire cohort of patients was considered, but this correlation was not significant after adjusting for T2 lesion volume. However, when only patients with EDSS> 1 were considered, WML MWF correlated with sNfL (beta= 0.12 and P <0.05) also after covariating for T2 lesion volume.

4. DISCUSSION

In this study, we simultaneously measured myelin water fraction and neurite density index to explore the interplay between myelin and axonal damage in different categories of focal lesions, in normal-appearing tissue, and across MS subtypes compared to healthy subjects.

By leveraging MWI, multi-shell diffusion and MR contrasts that are sensitive to both WMLs and CLs, we studied focal axon and myelin pathology in both WM and the cortex.
Myelin water fraction and axonal density were markedly decreased in both WMLs and CLs compared to NAWM/NAGM and healthy tissue, hereby confirming previous neuropathological studies (Lassmann, 2018b; Reich *et al.*, 2018). Besides, axon and myelin pathology centrifugally decreased with distance from the lesions core as shown in prior pathological and imaging works (Kutzelnigg *et al.*, 2005; Androdias *et al.*, 2010; Ingram *et al.*, 2014). Additionally, MWF and NDI in WMLs and CLs were proportional to each other– across all lesions in WM and in the cortex - suggesting that axon and myelin damage are synchronized and/or driven by a common pathological event (Frischer *et al.*, 2009; Stys *et al.*, 2012).

However, as showed in previous neuropathology studies (Grussu *et al.*, 2017), NDI is also sensitive to myelin content. Our study provides new evidence in living subjects, that NDI

contributes more than MWF to the differentiate lesions from normal-appearing tissue and lesions from healthy tissue in WM. This suggests that the reported differentiation is not driven by the myelin sensitivity of NDI, but rather by its sensitivity to the intra-axonal water compartment.

Still, neuropathological works reported that there is a substantial variability in the extent of myelin and axonal damage across MS lesions due to the dynamic interplay between acute and chronic inflammatory demyelination, remyelination and loss of chronically damaged axons (Lucchinetti *et al.*, 1999; Bruck, 2005; Goldschmidt *et al.*, 2009).

Indeed, we have shown that PV lesions exhibited more myelin damage than did JC lesions, suggesting a higher rate of myelin loss and/or lower repair capacity. These findings confirm previous neuropathological and positron emission tomography studies suggesting lower remyelinating capacity and higher tissue damage in PV compared to JC lesions (Patrikios *et al.*, 2006; Goldschmidt *et al.*, 2009; Bodini *et al.*, 2016). JC regions are in fact characterized by more numerous and more efficacious oligodendrocytes precursor cells (OPC), compared to PV regions (Boyd *et al.*, 2013; Lurbke *et al.*, 2013; Schultz *et al.*, 2017); likewise, PV regions are more prone to damage due to diffusion of demyelinating antibodies and myelin-reactive immune cells from ventricles than other brain areas (Magliozzi *et al.*, 2007; Winges *et al.*, 2007).

We have also characterized the profiles of axon and myelin damage in chronic active lesions: those are plaques characterized by activated microglia/macrophages at the lesion border, which exhibit a paramagnetic rim on susceptibility weighted images (Dal-Bianco *et al.*, 2017b; Absinta *et al.*, 2019). Neuropathological studies showed that those lesions are characterized by extensive and ongoing damage to both myelin and axons (Dal-Bianco *et al.*, 2017b); as well, a recent imaging study revealed that their presence is associated to higher disability in patients (Absinta *et al.*, 2019). Extending those works, we showed in vivo that chronic active lesions contain substantially lower amounts of myelin and axons than other MS lesions, hereby shedding light into the mechanisms driving increased disability in MS patients with this type of lesions compared to patients without.

Furthermore, when we compared the relative myelin and axonal content among WMLs, it appeared that - in a large majority of lesions - axonal damage outweighed myelin damage. Interestingly, this finding did not seem to be influenced by the anatomical location of WMLs, since we did not observe differences between PV, JC and DW lesions. Higher axon than myelin damage in WMLs

may be caused by differences in lesion age and remyelinating capacity (Lucchinetti *et al.*, 1999; Solanky *et al.*, 2001; Patrikios *et al.*, 2006). In alternative or in addition, it may be due to a primary axonal pathology, as previously suggested (Trapp and Nave, 2008; Stadelmann, 2011; Stys *et al.*, 2012). On the other hand, since we normalized the axon/myelin content by the corresponding NAWM in the contralateral hemisphere, the variability in NAWM damage may have in part influenced our assessment; similarly, our measurements may have been influenced by a different degree of sensitivity to myelin and axonal damage of MWF and NDI respectively, although previous MRI-pathological studies suggest that it is similar (Laule *et al.*, 2006; Zhang *et al.*, 2012; Colgan *et al.*, 2016).

In NAWM, we measured a widespread MWF and NDI reduction compared to the corresponding areas in healthy subjects, with a prevalent decrease in NDI. Remarkably, we did not find any difference in myelin or axonal content in NAWM between RRMS and PMS patients. Numerous previous imaging studies showed alterations in NAWM in MS patients (Enzinger *et al.*, 2015). Reduced magnetization transfer ratio, increased T2 and T1 relaxation times, or altered mean diffusivity were reported in NAWM, suggesting various degrees of WM microstructural alterations outside MS lesions (Schmierer *et al.*, 2004; Inglese and Bester, 2010; Bonnier *et al.*, 2014; Filippi, 2015). Adding to previous knowledge, we have now shown a broader decrease in axonal density than in myelin content in NAWM. Consistent with our results, neuropathological investigations of NAWM have shown that primary demyelination, in contrast to microglial activation and axonal transection, is not a frequent finding in NAWM (Bjartmar *et al.*, 2001; Kutzelnigg *et al.*, 2005; Marik *et al.*, 2007).

With respect to the cortex, our vertex-wise analysis showed focal areas of myelin and axon damage throughout the NAGM, which were more extensive in PMS than in RRMS. Neuropathology studies also showed widespread neuronal loss and demyelination in NAGM, which might be associated with meningeal inflammatory infiltrates that are particularly evident in PMS (Kutzelnigg *et al.*, 2005; Marik *et al.*, 2007). In accordance, MTI (Ge *et al.*, 2002; Samson *et al.*, 2014) and DTI (Rovaris *et al.*, 2002; Ceccarelli *et al.*, 2007) showed lower magnetization transfer ratio, lower fractional anisotropy, and higher mean diffusivity in NAGM of MS patients, with a more robust change in PMS compared to RRMS.

A pivotal finding of this study is the presence of axonal damage independent of demyelination in both focal WML and in NAWM. These findings are also in line with previous spectroscopy studies showing a very early diffuse reduction of a N-acetylaspartate in NAWM in RRMS patients (Narayana *et al.*, 1998) and an increase in lipid levels at the site of future MS lesions (Filippi *et al.*, 1998). Pathologically, this may be related to primary oligodendrocytopathy leading to axonal damage via disruption of oligodendrocyte-neuron cross-talk (Ozawa *et al.*, 1994; Howell *et al.*, 2010; Cui *et al.*, 2017) or to direct damage to the neuroaxonal unit (Bitsch *et al.*, 2000; Srivastava *et al.*, 2012; Yan *et al.*, 2014).

It is still unclear whether RRMS and PMS are different entities or different presentations of the same entity. Our data show that distribution of axon and myelin pathology in both focal lesions and in NAWM is similar between RRMS and PMS, which is coherent with neuropathological studies suggesting that lesions in PMS and RRMS are qualitatively similar (Lucchinetti *et al.*, 2000; Antel *et al.*, 2012). Nonetheless, we also found remarkably widespread reductions in myelin and axonal content in NAGM in PMS compared to RRMS patients, which may explain the different clinical phenotype.

Last, we found that imaging surrogate markers of myelin and axon pathology in WML – and not in normal-appearing tissues – are correlated with disability and sNfL. This is in line with previous reports by showing that Magnetization Transfer Ratio (MTR) – another surrogate measure of both myelin and axonal damage – is mostly related to disability when measured in lesions and not in the normal-appearing tissue (Amann *et al.*, 2015) but apparently contradicts other works showing that NAWM/NAGM abnormalities are related to disability (Ramio-Torrenta *et al.*, 2006; Manfredonia *et al.*, 2007). These latter, however, were mostly univariate studies, which focused solely on the contribution of normal-appearing-tissue abnormalities to disability, without taking lesion properties into account.

Interestingly, the associations between those imaging markers and disability/sNFL were evident and stronger in patients with clinical deficits only compared to patients with no disability. Those patients exhibited very heterogeneous damage in lesions but overall shorter disease duration than patients with EDSS >1 (median disease duration 2.4 vs 7.7 years; $P<0.01$). Hence, it may well be that those patients experience a higher functional reserve and more effective mechanisms

compensating for structural damages, which is often the case at early disease stages (Lopez-Gongora *et al.*, 2015).

Methodologically, we have applied MWF and NDI, which provide surrogate – not direct - markers of myelin and axon characteristics. Despite their sensitivity and specificity has been already separately assessed in postmortem studies (Grussu *et al.*, 2017; Laule and Moore, 2018), future work should focus on providing knowledge on their sensitivity/specificity in relationship to each other. Also, the study of MWF suffers from the limitation of non-isotropic voxel acquisitions, which may have decreased the sensitivity to myelin damage. On the other hand, NODDI suffers from the limitation of assuming a fixed diffusivity for all the voxels in the brain tissue, which may hamper its sensitivity and specificity. Because of this, we confirmed the results obtained with NODDI-NDI by using MCDMI-NDI, another model applicable to multi-shell diffusion data that estimates the diffusivity voxel-wise. Last, we did not acquire diffusion data with multiple echo times (Gong, *et al.*, 2020) which would have helped to minimize the influence of myelin-water on NDI estimation: however, we have statistically modeled the contribution of both NDI and MWF to the separation of lesion, normal-appearing and healthy tissue, hereby showing that NDI is providing statistical independent information from MWF to achieve an optimal separation of tissue-types in WM. Future work should further expand the current findings by attempting at achieving a better specificity of NDI maps, through targeted data acquisition schemes.

In conclusion, by applying advanced MRI measures we have further characterized the complex interplay between myelin and axon damage in vivo in MS patients. Our data extend existing knowledge from previous imaging studies and are compatible with concepts derived from neuropathology. Longitudinal studies are warranted to explore the temporal dynamics of pathological changes in brain microstructure in MS.

2.2. Manuscript 2

A new advanced MRI biomarker identifies fully remyelinated lesions in Multiple Sclerosis: An *in vivo* cross-sectional and longitudinal study with double-blind *postmortem* validation.

In this work, we classified neuropathological MS lesion types according to their visual appearance in QSM maps. Further, we studied myelin and axonal content among QSM lesion types using MWF and NDI, both cross-sectionally and longitudinally. Last, we performed a combined histopathology-QSM evaluation in three post-mortem MS brains to assess the histopathological correlates of the *in vivo* QSM classification of MS lesions.

A new advanced MRI biomarker identifies fully remyelinated lesions in Multiple Sclerosis: An *in vivo* cross-sectional and longitudinal study with double-blind *postmortem* validation.

Reza Rahmanzadeh[1,2,3]; MD, Riccardo Galbusera[1,2,3]; MD, Po-Jui Lu[1,2,3] MSc; PhD, Erik Bahn[4]; MD, Matthias Weigel[1,2,3,5]; PhD, Muhamed Barakovic[1,2,3]; PhD, Jonas Franz[4,6,7]; MD, Thanh D. Nguyen[8]; PhD, Pascal Spincemaille[8]; PhD, Simona Schiavi[9]; PhD, Alessandro Daducci[9]; PhD, Francesco La Rosa[10,11]; PhD, Martina Absinta[12,13]; MD, Pascal Sati[14,15]; PhD, Meritxell Bach Cuadra[10,11]; PhD, Ernst-Wilhelm Radue[1,2]; MD, David Leppert[1,3]; MD, Jens Kuhle[1,3]; MD, Ludwig Kappos[1,3]; MD, Wolfgang Brück[4]; MD, Daniel S. Reich[14]; MD, Christine Stadelmann[4]; MD, Yi Wang[8]; MD, Cristina Granziera[1,2,3]; MD.

[1]*Neurology Clinic and Policlinic, Departments of Medicine, Clinical Research and Biomedical Engineering, University Hospital Basel and University of Basel, Basel, Switzerland.*

[2]*Translational Imaging in Neurology (ThINk) Basel, Department of Biomedical Engineering, University Hospital Basel and University of Basel, Basel, Switzerland.*

[3]*Research Center for Clinical Neuroimmunology and Neuroscience Basel (RC2NB), University Hospital Basel and University of Basel, Basel, Switzerland.*

[4]*Institute of Neuropathology, University Medical Center, Göttingen, Germany.*

[5]*Division of Radiological Physics, Department of Radiology, University Hospital Basel, Basel, Switzerland.*

[6]*Max Planck Institute for Experimental Medicine, Göttingen, Germany.*

[7]*Campus Institute for Dynamics of Biological Networks, University of Göttingen, Göttingen, Germany.*

[8]*Department of Radiology, Weill Cornell Medical College, New York, New York, USA.*

[9]*Department of Computer Science, University of Verona, Verona, Italy.*

[10]*Signal Processing Laboratory (LTS5), Ecole Polytechnique Fédérale de Lausanne (EPFL), Lausanne, Switzerland.*

[11]*Medical Image Analysis Laboratory (MIAL), Center for Biomedical Imaging (CIBM), Lausanne, Switzerland.*

[12]*Department of Neurology, Johns Hopkins University School of Medicine, Baltimore, MD, USA.*

[13]*Department of Neurology, IRCCS San Raffaele Hospital and Vita-Salute San Raffaele University, Milan, Italy*

[14]*Translational Neuroradiology Section, National Institute of Neurological Disorders and Stroke, NIH, 10 Center Drive MSC 1400, Building 10 Room 5C103, Bethesda, Maryland, USA.*

[15]*Department of Neurology, Cedars-Sinai Medical Center, Los Angeles, CA.*

Abstract

Neuropathological studies have shown that multiple sclerosis (MS) lesions are heterogeneous in terms of myelin/axon damage and repair, as well as iron content. However, it remains a challenge to identify specific chronic lesion types in vivo in MS patients, especially remyelinated lesions.

In this work, we have investigated whether white matter (WM) lesions – as classified based on their appearance in quantitative susceptibility maps (QSM) - represent distinct MS neuropathological lesion types.

To achieve this goal, we performed 3 studies: (i) a cross-sectional study in a prospective cohort of 115 MS patients and 76 healthy controls (age mean, sex (male/female); 46 [14] years, 48/67; 35 [13] years, 32/45, respectively), who underwent 3T MRI for QSM, myelin water fraction (MWF), neurite density index (NDI) maps. In this work, we performed the classification of WM lesions in QSM into five QSM lesion types (isointense, hypointense, hyperintense, lesions with hypointense rims, and lesions with paramagnetic rims (PRL) and comparison of QSM lesion types through MWF and NDI characteristics at baseline (ii) A prospective longitudinal MRI study on 40 MS patients to study the evolution of lesions over 2 years. (iii) A double-blind postmortem histopathology- QSM validation study in three MS brains to assess the accuracy of QSM classification to identify neuropathological lesion types (remyelinated, chronic active and chronic inactive lesions) in 63 postmortem WM lesions.

In 29% WMLs, we found a negative relative susceptibility and in 71% WMLs a positive relative susceptibility. At baseline, Hypo- and isointense lesions showed higher mean MWF and NDI values compared to other QSM lesion types ($P<0.0001$). Hyperintense lesions and PRL showed an extensive MWF and NDI decline compared to other QSM lesion types ($P<0.0001$). Hypo-/ iso-intense lesions at 2-year follow-up showed an increase in MWF. There was no difference in the average susceptibility between lesions with predominant damage to axon or myelin (4.06±17.67, 7.76±21.80, respectively; $P > 0.05$). Post-mortem analyses revealed that QSM highly accurately identifies (i) fully remyelinated areas as hypo-/iso-intense (sensitivity: 88.89%, specificity: 100%) (ii) chronic inactive lesions as hyperintense (sensitivity: 71.43%, specificity:

92.00%) and (iii) chronic active/smoldering lesions as PRLs (sensitivity: 92.86%, specificity: 86.36%).

These results provide first evidence that it is possible to distinguish MS remyelinated, chronic active and chronic inactive lesions in a clinical setting, hereby providing new biomarkers to develop and assess neuroprotective and remyelinating treatments.

1.Introduction

Quantitative susceptibility mapping (QSM) quantifies the spatial distribution of magnetic susceptibility within biological tissues (Wang *et al.*, 2017) and provides a measure that is sensitive to both iron accumulation and myelin content in the brain. QSM has been used to identify white matter (WM) lesions with a rim of iron-laden macrophages/activated microglia in multiple sclerosis (MS) patients (paramagnetic rim lesions-PRLs), which histopathologically correspond to chronic active and smoldering lesions (Bagnato *et al.*, 2011; Stephenson *et al.*, 2014; Absinta *et al.*, 2016; Dal-Bianco *et al.*, 2017b). In addition, QSM has also been applied to assess the longitudinal evolution of acute MS lesions over time (Chen *et al.*, 2014). Nevertheless, to date, QSM has not been exploited for the classification of MS lesion type heterogeneity reported in neuropathological studies.

Indeed, MS patients exhibit a variety of lesion types which are characterized by a variable extent of myelin/axon damage and repair and iron content (Lassmann, 2018a). In fact, MS lesions undergo multiple waves of de- and re-myelination, which lead to the final lesion phenotype of either demyelinated, partly remyelinated, or fully remyelinated (shadow plaques) (Kuhlmann *et al.*, 2017). Lesion location (i.e., periventricular vs juxtacortical) (Patrikios *et al.*, 2006), age (i.e., acute vs chronic lesions) (Goldschmidt *et al.*, 2009), cellular composition (i.e., presence of oligodendrocytes and macrophages/activated microglia) (Kuhlmann *et al.*, 2008), and clinical disease course (i.e., relapsing-remitting, RRMS vs progressive MS, PMS) (Patrikios *et al.*, 2006; Lassmann *et al.*, 2012) likely contribute to the heterogeneity of remyelination activity.

Axonal damage in MS lesions is largely heterogeneous as well. Acute axonal transection occurs more commonly in active demyelinating lesions, whereas inactive MS lesions show delayed degeneration of long-term demyelinated axons (Kuhlmann *et al.*, 2002), potentially owing to excitotoxic mechanisms and ongoing innate inflammation (Friese *et al.*, 2014). In chronic active and smoldering lesions, extensive axonal damage occurs mostly at the lesion border(Lassmann, 2018a).

Iron content is likewise extremely diverse across lesion types. Many, but not all, active MS lesions harbor iron-laden macrophages (Tham *et al.*, 2020). Shadow plaques contain higher amounts of iron compared to smoldering or inactive MS lesions (Popescu *et al.*, 2017). Furthermore, chronic

active lesions are also characterized by an iron-laden rim of macrophages/activated microglia (Bagnato *et al.*, 2011).

Currently, MS lesion types can be differentiated neuropathologically (Kuhlmann *et al.*, 2017), but the distinction of chronic MS lesion types *in vivo* (i.e., remyelinated vs chronic active/smoldering vs chronic inactive) remains challenging. For this study, we applied a multi-contrast quantitative MRI approach including QSM, myelin water imaging (MWI) and diffusion MRI, to disentangle lesion phenotypes *in vivo* in MS patients.

MWI (Nguyen *et al.*, 2016; Laule and Moore, 2018) and biophysical models applied to multi-shell diffusion MRI (Cercignani and Gandini Wheeler-Kingshott, 2019) offer more specific surrogate measures of myelin and axon content than other advanced MRI techniques. MWI quantifies the water between myelin layers by distinguishing multiple water compartments in T2 relaxometry data. Moreover, this measure (e.g. myelin water fraction, MWF) has been validated postmortem (Moore *et al.*, 2000; Kozlowski *et al.*, 2014).

Multi-compartment microscopic diffusion imaging (MCMDI) is a technique that quantitates the neurite density index (NDI) of the intra-neurite compartment and the extra-neurite compartments in the brain, which has also been applied to MS patients (Kaden *et al.*, 2016; Bagnato *et al.*, 2018). The advantage of MCMDI over diffusion tensor imaging (DTI) is that MCMDI does not assume a Gaussian distribution of the diffusion process and hence models non-Gaussian diffusion in biological tissue, providing more specific measures of tissue microstructure (Colgan *et al.*, 2016; Grussu *et al.*, 2017).

In order to distinguish chronic MS lesion types *in vivo*, we classified MS lesions according to their visual appearance in the QSM maps and studied myelin and axonal content among QSM lesion types using MWF and NDI, both cross-sectionally and longitudinally. Further, we performed a combined histopathology-QSM evaluation in three post-mortem MS brains to assess the histopathological correlates of the *in vivo* QSM classification of MS lesions.

2. Materials and methods

2.1. In vivo cross-sectional and longitudinal study

2.1.1 Participants

We enrolled 115 MS patients (76 RRMS and 39 PMS) and 76 healthy controls (HC), and demographic and clinical characteristics are reported in Table 1.

Table 1: Clinical characteristics of patients and healthy subjects

	Multiple sclerosis patients	Healthy subjects
Sex, n (male/female)	115 (48/67)	76 (32/45)
Age (years), mean ± SD	46 ± 14	35 ± 13
EDSS score, median (range)	3.14 (0–8)	-
Disease course (RR/PMS)	76/39	-
Disease-modifying therapy (n)	Untreated (13) Interferon-beta (1) Glatiramer acetate (1) Dimethyl fumarate (15) Fingolimod (9) Natalizumab (4) Rituximab (13) Ocrelizumab (55) Siponimod (2) Teriflunomide (2)	

Inclusion criteria were: (i) MS diagnosis according to McDonald criteria from 2017, (Thompson *et al.*, 2018) and diagnosis of active RRMS or inactive progressive MS (PMS) as defined by Lublin et al. (Lublin *et al.*, 2014); (ii) absence of any concomitant psychiatric or neurological disease

(excluding headache); (iii) absence of contraindication to MRI. All patients (n=115) enrolled in this study also underwent a conventional MRI (cMRI) during the three months before the study. All Gd enhancing lesions in cMRI were excluded from the following analyses. Eleven patients were excluded because of motion artifacts in QSM images.

All patients had a baseline MRI and n=40 patients had also an MRI at follow-up with the same protocol (Figure 1).

The study was approved by the ethics review committee of the University Hospital Basel (IRB of Northwest Switzerland) and all participants gave written consent prior to the study.

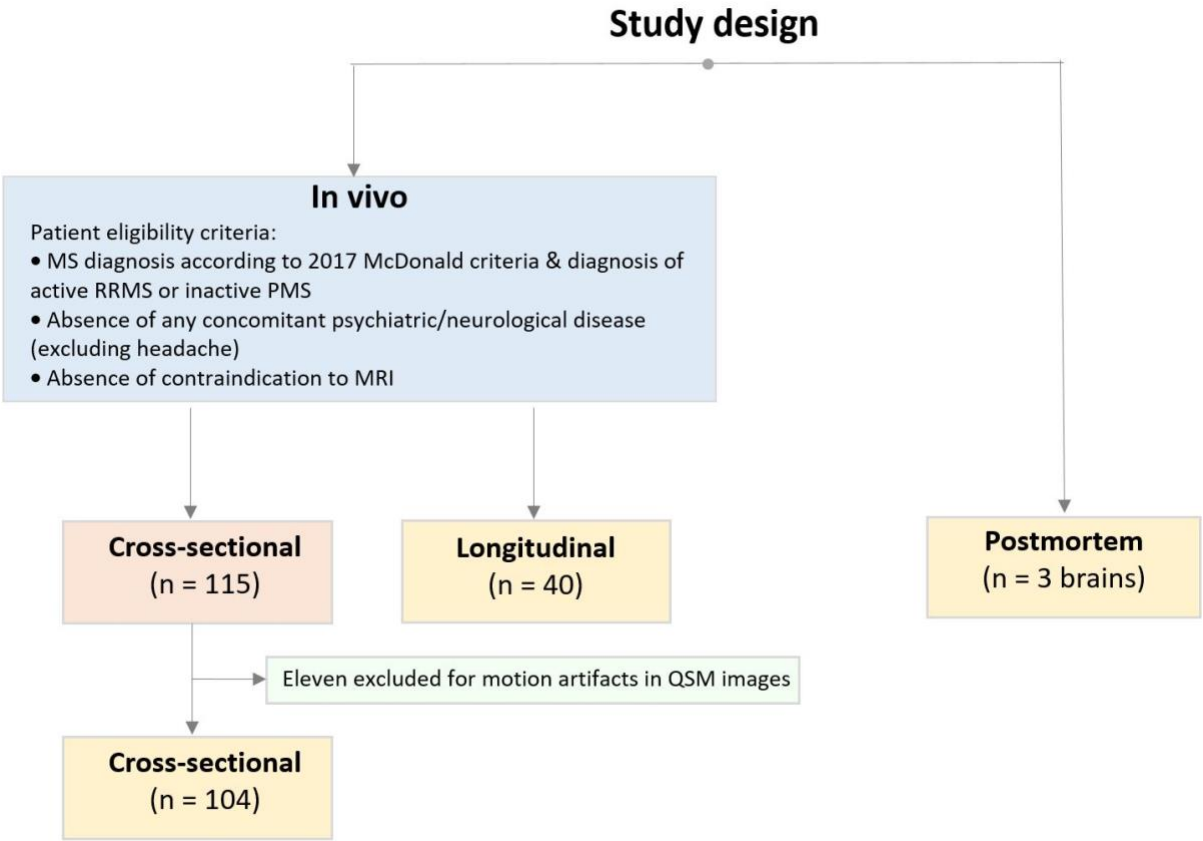

Figure 1. Design of the in vivo and post-mortem parts of the study.

2.1.2 MR acquisition

MRI was performed on a 3T whole-body MR system (Prisma, Siemens Healthcare, Erlangen, Germany) using a 64-channel phased-array head and neck coil. The MRI protocols included: (i) 3D FLAIR (TR/TE/TI=5000/386/1800 ms) with 1 mm^3 isotropic spatial resolution; (ii) Fast acquisition with spiral trajectory and adiabatic T2prep (FAST-T2) (spiral TR/TE = 7.5/0.5 ms, six T2prep times = 0 (T2prep turned off), 7.5, 17.5, 67.5, 147.5, 307.5 ms, voxel size = 1.25x1.25x5 mm^3, scan time = 4.5 min, as described in (Nguyen *et al.*, 2016); (iii) multi-shell diffusion (TR/TE/δ/Δ/resolution = 4.5 s / 75 ms / 19 ms / 36 ms / 1.8 mm^3 isotropic with b-values 0 / 700 / 1000 / 2000 / 3000 s/mm^2 with 12/6/20/45/66 measurements, respectively, per shell and a diffusion acquisition with 12 measurements of b-value 0 s/mm^2 with reversed phase encoding as well as (iv) 3D segmented EPI with submillimeter isotropic resolution (TR/TE/resolution=64 ms/35 ms/0.67x0.67x0.67 mm^3).

Diffusion images were denoised and corrected for motion and eddy-currents (Andersson and Sotiropoulos, 2016). The multi-compartment microscopic diffusion imaging (MCDMI) diffusion model was used, which is a state-of-the-art model that integrates the spherical mean technique to handle orientation dispersion and fiber crossing populations, allowing more accurate estimations in whole-brain voxels. From this model we estimated the neurite density index (NDI), which corresponds putatively to the intra-axonal volume fraction.

Quantitative susceptibility mapping (QSM) is a field-to-source inversion method to map the local susceptibility sources in the tissue from the shift in the magnetic field created by these sources which can be measured from gradient echo data. In this study, QSM were reconstructed from 3D EPI data by unwrapping phase, removing the background field through us of the projection onto dipole fields algorithm, and using the morphology-enabled dipole inversion algorithm to compute the susceptibility from the local field as in Liu *et al* (Liu *et al.*, 2012).

2.1.3 Lesion identification and segmentation

Segmentation of WM lesions (WMLs) was performed automatically by using a deep-learning based method (La Rosa *et al.*, 2020). Manual correction of automatic WML masks on FLAIR was a consensus of results from two experienced readers (RR and CG).

QSM lesion types were classified as follows: First, a map of MS lesions was obtained through automatic detection and segmentation as detailed above; then (ii) the FLAIR lesion map was registered to the QSM map using a boundary-based registration from the FMRIB software library (FSL) (Jenkinson *et al.*, 2012) so that MS lesions could then be identified in the QSM map; afterwards, (iii) MS lesions were classified according to their appearance on QSM at intensity range ±200 parts per billion (ppb): i) iso-intense (i.e. lesions that showed no intensity difference in QSM maps compared to the surrounding tissue) ii) hypointense lesions iii) hyperintense lesions iv) lesions with hypointense rim relative to the lesion center v) paramagnetic rim lesions-PRL (lesions with hyperintense rim in QSM maps) (Figure 2).

To identify dominantly myelin-damaged and dominantly axon-damaged WM lesions (i.e. lesions with a larger % change in MWF and NDI, respectively), we calculated the proportion of myelin and axonal damage in WMLs relative to the respective values in the contralateral hemisphere (%MWF and %NDI reduction) as follows (Rahmanzadeh *et al.*, 2021): [(mean MWF or NDI in the mirror region of interest (ROI) in the contralateral hemisphere) – (mean MWF or NDI in lesion)] x100/the value in the mirror ROI in contralateral hemisphere. For this purpose, all lesions exhibiting contralateral NA mirror areas were selected in the lesion masks. In total, 85 lesions out of 2,852 WMLs were selected and the mirror ROIs were then manually contoured.

2.1.4 WM and cortex segmentation

Using FreeSurfer (v.6.0, surfer.nmr.mgh.harvard.edu) (Fischl, 2012) , the brain was segmented into whole WM, cortex, deep grey matter structures, and ventricles. NAWM mask was produced by subtracting WM lesion mask from WM mask.

An in-house algorithm was used to automatically identify a 2-voxel layer of NAWM surrounding the lesions on FLAIR; herein after denoted as peri-plaque WM (PPWM). The relative susceptibility for individual WMLs was calculated as follows: $\text{Susceptibility}_{\text{lesion}} - \text{Susceptibility}_{\text{PPWM}}$.

WM masks were automatically divided into periventricular (PV, i.e. area within 3 mm from ventricular wall), juxtacortical (JC, i.e. area in 3 mm from the interface between WM and cortex), and deep white matter (DW, i.e. area between PV and JC).

All values, including intra-lesional, PP tissue and homogeneous non-lesional NA tissue, were automatically extracted both in lesion-wise and average patient-wise manners.

2.1.5 Clustering of Iso-/Hypo-intense lesions vs PRLs

To confirm that the qualitative appearance of QSM lesion types represents lesions with different MWF, NDI and susceptibility, we applied a Gaussian Mixture Model (GMM) to the lesion groups exhibiting the highest and lowest MWF/NDI/susceptibility mean content and assumed the presence of two clusters. Finally, we calculated the percentages of QSM lesion types (i.e. Iso-/Hypointense lesions vs PRLs) falling into two distinct clusters that were identified.

2.1.6 Longitudinal analysis

In the 40 patients who benefitted from a follow-up MRI at 2 years, we performed automatic WM lesion segmentation and manual correction as performed for baseline MRIs (n = 325 lesions).

WM lesions were then classified in the follow-up QSM as described above. 18/325 lesions (5.53%) exhibited iso- & hypointensity in QSM and had a corresponding lesion with a distinct QSM lesion type at baseline.

2.1.7. Statistical analysis

Statistical analysis was performed using GraphPad Prism version 8.0.0 for Windows, GraphPad Software, San Diego, California, USA.
A Kolmogorov-Smirnov's test was used to assess the normality of data. Paired t-test, non-parametric Mann-Whitney test, and Kruskal-Wallis test with Dunn's test for multiple comparisons correction were used for the paired two-group analysis, the unpaired two-group analysis, and the more-than-three group analysis, respectively.

2.2. Post-mortem imaging and histopathology

Postmortem MS brains from three MS patients (MS clinical type and age (years): secondary progressive, 59; secondary progressive, 65; primary progressive, 66) were imaged on a 3T whole-body MR system (Prisma^{Fit}, Siemens Healthcare, Erlangen, Germany) using a 20-channel head and neck coil and a dome-shaped brain container filled with perfluoropolyether. The brains were fixed directly in 4% neutral buffered formaldehyde solution (formalin) within 24 hours after death and for about 4-6 months before MRI. Post-mortem QSM images were reconstructed using 3D-EPI (330 µm isotropic, TR=65 ms, TE=35 ms, ETL=13, bandwidth 394Hz/pixel). We then designed and 3D-printed an individualized cutting box for each brain, as reported previously (Absinta *et al.*, 2014). Additional manual registration between the digitized brain slab surfaces and the corresponding MRI slices was performed to further refine the match between histopathological and MRI images. Regions of interest (ROI) including MS lesions were identified on 3D-EPI images and manually segmented using ITK-SNAP 3.6.0 (Yushkevich *et al.*, 2006).

2.2.1 Histopathological analysis

Three postmortem brains were provided by the MS Brain Bank of the German Competence Network Multiple Sclerosis (KKNMS).

Histopathologically, WM lesions and remyelinated areas were identified and then categorized as in (Kuhlmann *et al.*, 2017) by means of Luxol-Fast Blue staining (LFB, for myelin), anti-myelin basic protein (MBP, for myelin) immunohistochemistry (IHC), anti-CR3/43 (for MHCII-expressing macrophages/activated microglia) IHC, Turnbull's blue (TBB, for iron) staining and anti-breast carcinoma-amplified sequence 1 (BCAS1) IHC (for myelin and actively myelinating oligodendrocytes). Shadow plaques were characterized on Luxol fast blue (LFB)-stained slides. Digital processing of whole slide images was performed using an open microscopy OMERO server (version 5.6.3) (Allan *et al.*, 2012).

2.2.2 Lesion segmentation and QSM lesion classification

WM lesions were manually segmented in 3D EPI images and 3D FLAIR images (RR and RG).
The classification of WM lesions (n = 63) in postmortem QSM was performed by an experienced rater (RR) without prior knowledge of neuropathological lesion types, and the sensitivity and

specificity of QSM classification to detect remyelinated lesions, chronic inactive and chronic active MS lesions were reported.

2.2.3 QSM-Histopathology correlation

A double-blinded analysis was performed to correlate the classification of 63 WM lesions in postmortem QSM images with their respective histopathological types.

2.2. 4 Statistical Analysis

We used GraphPad Prism version 8.0.0 for Windows, GraphPad Software, San Diego, California, USA to assess the sensitivity and specificity of the QSM-classification to specific histopathological lesion groups.

2.3. Data availability

The data that support the findings of this study are available upon reasonable request.

3.Results

3.1. In vivo cross-sectional and longitudinal study

3.1.1 Classification of WMLs in MS patients on QSM maps

White matter lesions (WMLs; n= 1621) showed distinct characteristics within QSM maps and were classified as isointense lesions (n=476, 29.4%), hypointense lesions (n=69, 4.26%), hyperintense lesions (n=846, 52.2%), lesions with hypointense rims (hypo-rim) (n=20, 1.23%), and paramagnetic rim lesions (PRLs) (n=210, 13%) (Figure 2). A total of 1231 lesions were not included in this classification due to (i) the presence of a big vessel traversing the lesion area (75.62%), (ii) susceptibility artifacts (19.96%), and (iii) confluent lesions (4.42%) (Figure 3).

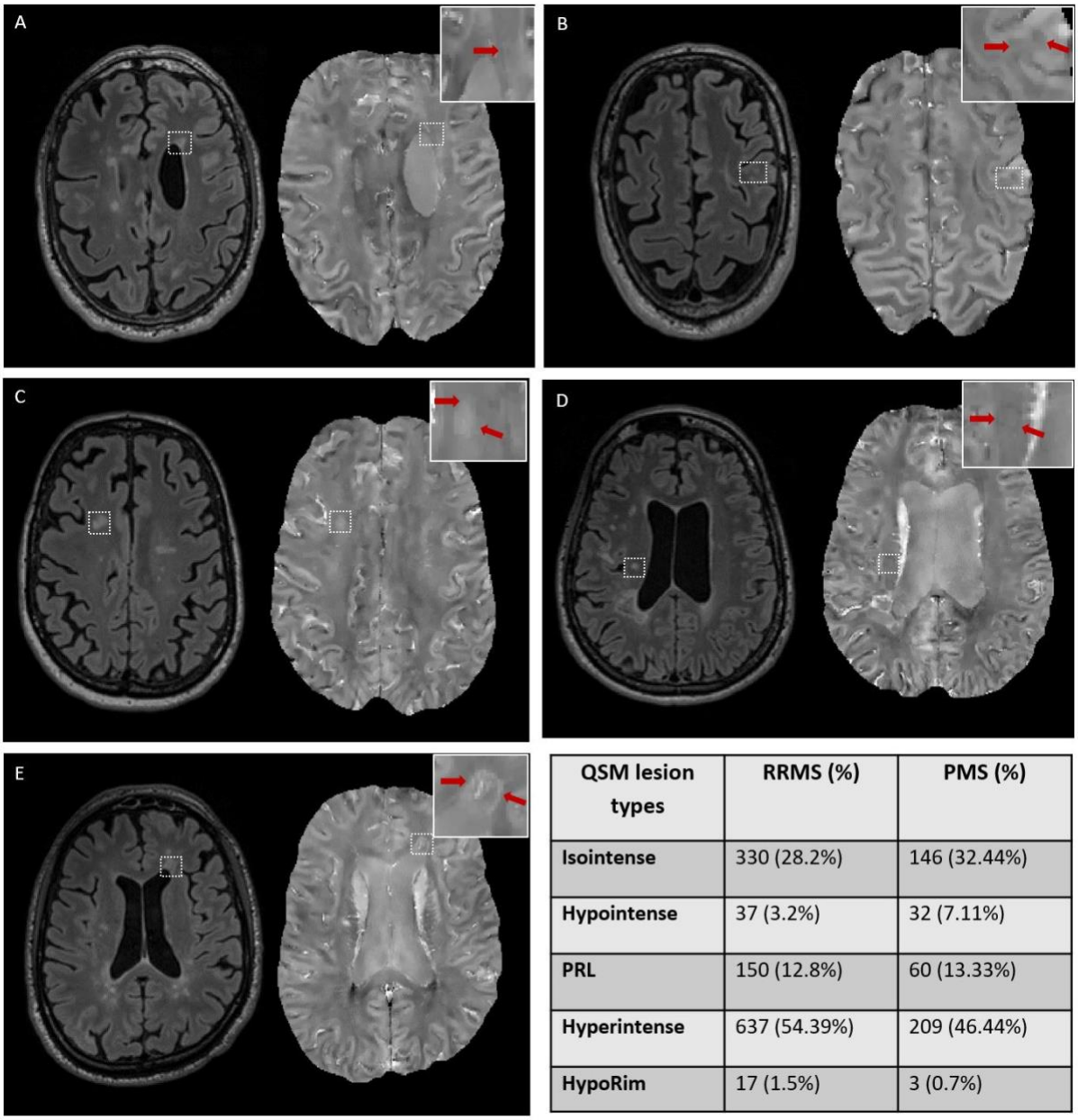

QSM lesion types	RRMS (%)	PMS (%)
Isointense	330 (28.2%)	146 (32.44%)
Hypointense	37 (3.2%)	32 (7.11%)
PRL	150 (12.8%)	60 (13.33%)
Hyperintense	637 (54.39%)	209 (46.44%)
HypoRim	17 (1.5%)	3 (0.7%)

Figure 2. QSM lesion types and their distribution in MS patients. A-E) Exemplary QSM lesion types (A: isointense, B: hypointense, C: hyperintense, D: hypo-rim, E: PRL); Table: distribution of the different QSM lesion types (%) in RRMS and PMS patients.

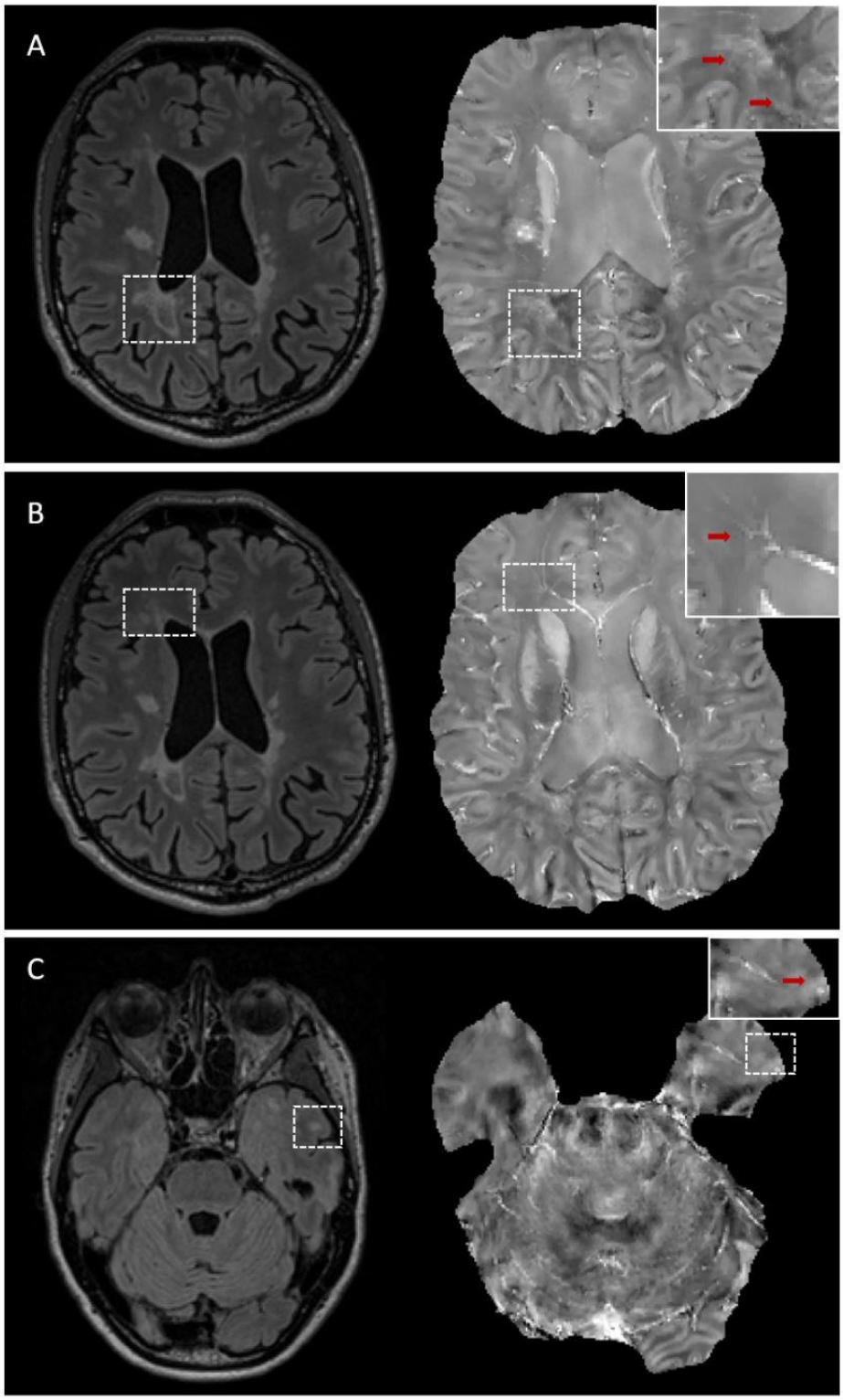

Figure 3. Lesions excluded from QSM classification. A, confluent lesions; B, lesions traversing with vessels; C, lesions in artifacts area. The lesion's area is shown by boxes and arrows.

3.1.2 Mean susceptibility in all WMLs

The patient-wise average of magnetic susceptibility in WMLs in MS patients (n = 104) was not different from the susceptibility in normal-appearing white matter (NAWM) nor from the white matter in healthy controls (WM-HC) ($P > 0.05$). However, the average susceptibility was lower in NAWM than in WM-HC ($P = 0.014$) (Figure 4A).

Lesion-wise analysis of 2,852 WMLs showed that the susceptibility in MS WMLs relative to PPWM exhibited values ranging from -163.7 ppb to +159.00 ppb (5.04 (0.99-13.52), median (interquartile range)). Moreover, 814/2,852 WMLs (28.54%) exhibited a negative relative susceptibility and 2,038/2,852 WMLs (71.46%) had a positive relative susceptibility (Figure 4B).

3.1.3 Mean susceptibility comparison across QSM lesion types

Comparison of relative susceptibility across groups revealed that hypointense lesions have lower relative magnetic susceptibility than isointense lesions ($P < 0.0001$), isointense lesions exhibit lower relative magnetic susceptibility than hyperintense lesions ($P < 0.0001$), and hyperintense lesions show lower relative magnetic susceptibility than PRLs ($P < 0.0001$) (Figure 4C).

Further, hypointense lesions in QSM images show lower absolute magnetic susceptibility than isointense lesions ($P = 0.0081$), isointense lesions show lower absolute magnetic susceptibility than hyperintense lesions ($P < 0.0001$), and hyperintense lesions show lower absolute magnetic susceptibility than PRLs ($P = 0.014$, Figure 4D).

3.1.4 Comparison of mean susceptibility between lesions with predominant axon or myelin loss

WMLs (n = 85) exhibiting contralateral mirror areas without focal lesions were selected and categorized into lesions with dominant axon or myelin damage according to the relative MWF and NDI changes. However, there was no difference in the average susceptibility between lesions with predominant axon or myelin damage (4.06±17.67, 7.76±21.80, respectively; $P > 0.05$). In addition,

no difference was found when the mean NDI was compared between lesions with positive and negative relative susceptibility (0.36±0.11, 0.35±0.11, respectively; $P > 0.05$).

3.1.5 MWF and NDI in QSM lesion types

Isointense lesions exhibited higher NDIs ($P < 0.05$) and MWFs ($P < 0.0001$) compared to QSM-visible lesions. Isointense lesions also exhibited lower NDIs compared to that of NAWM and WM-HC ($P < 0.0001$). On the other hand, the MWF of isointense lesions was not different from that of NAWM or WM-HC ($P > 0.05$). Nevertheless, isointense lesions exhibited higher MWFs and NDIs than hyperintense lesions and PRLs ($P < 0.0001$, Figure 3E, F). Lastly, there was no difference in MWFs and NDIs between isointense and hypo-rim lesions (both $P > 0.05$, Figure 4 E, F).

Hypointense lesions exhibited lower NDIs compared to that of NAWM and WM-HC ($P < 0.0001$). On the other hand, the MWF of hypointense lesions was not different from that of NAWM or WM-HC ($P > 0.05$). In comparison to other QSM lesion types, hypointense lesions showed higher MWFs and NDIs than did hyperintense lesions and PRLs (both $P < 0.0001$, Figure 4 E, F). The MWF was lower in hypo-rim lesions than in hypointense lesions ($P < 0.05$, Figure 4 E, F), however the NDI did not differ ($P > 0.05$, Figure 4 E, F).

Hyperintense lesions exhibited lower MWFs and NDIs compared to that of NAWM and WM-HC ($P < 0.0001$), and higher MWFs ($P = 0.0029$, Figure 4 E, F) and NDIs compared to that of PRLs ($P < 0.001$, Figure 4E, F). In addition, PRLs showed lower MWFs and NDIs compared to WM-HC, NAWM, and all other QSM lesion types ($P<0.01$, Figure 4E, F).

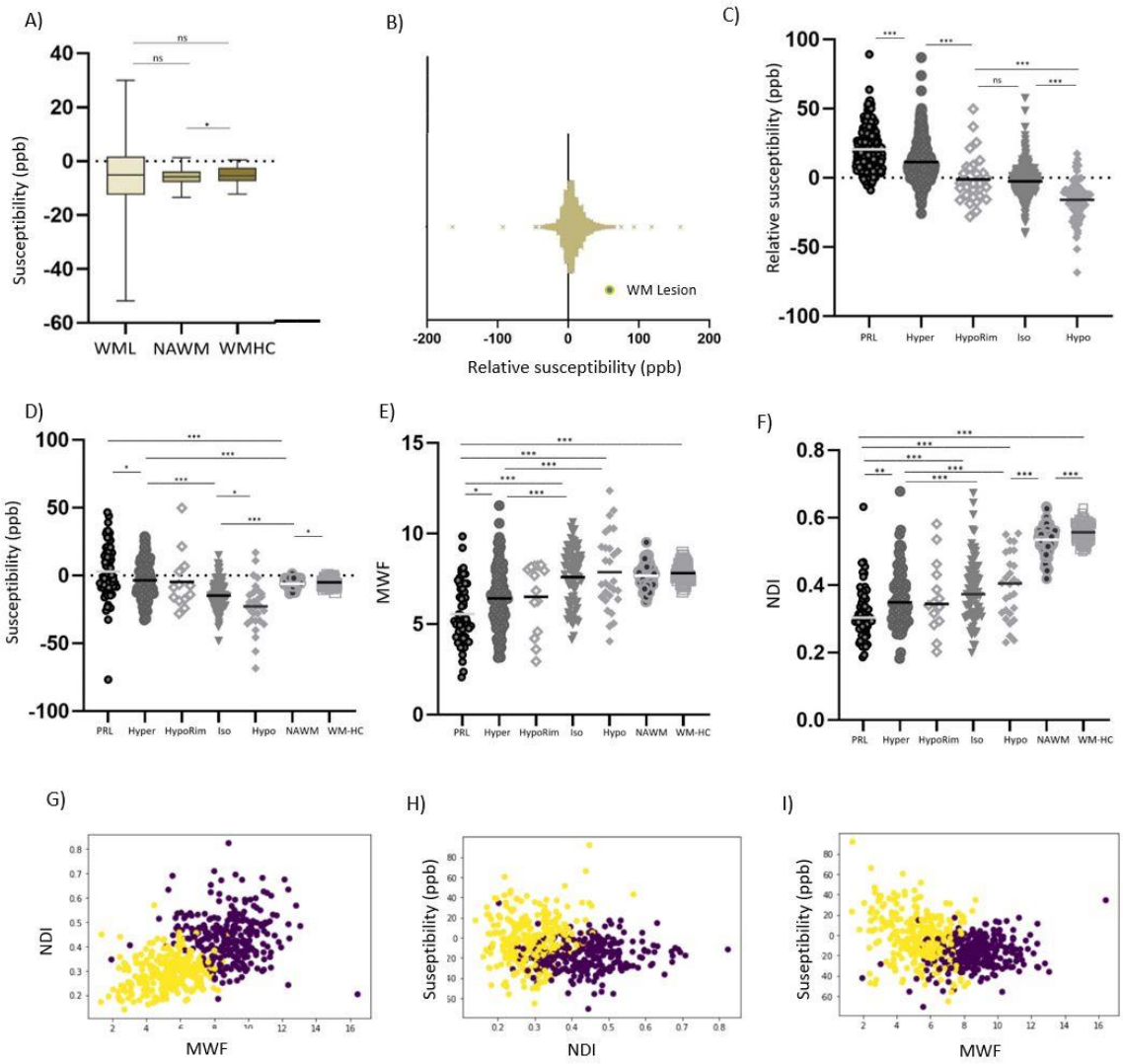

Figure 4. Quantitative susceptibility, myelin water fraction (MWF) and neurite density index (NDI) in QSM lesion types. A) Average susceptibility in WMLs, NAWM, and WM-HCs. B) Lesion-wise relative susceptibility of WMLs compared to PPWM. C) Comparison of mean relative susceptibility values among QSM lesion types. D-F) Comparison of susceptibility, myelin water fraction (MWF), and neurite density index (NDI) values among QSM lesion types. G-I) GMM clustering of WMLs using mean lesion MWF, NDI and susceptibility. * P<0.05 **P<0.001 ***P<0.0001

WMLs: white matter lesions; NAWM: normal-appearing WM; WM-HCs: white matter healthy controls; PPB: parts per billion; GMM: Gaussian mixture model.

3.1.6 Comparison of lesion size across QSM lesion types

Hypointense lesions and isointense lesions were smaller than hyperintense lesions (both $P < 0.0001$), which in turn was smaller than PRLs ($P < 0.05$) (Figure 5).

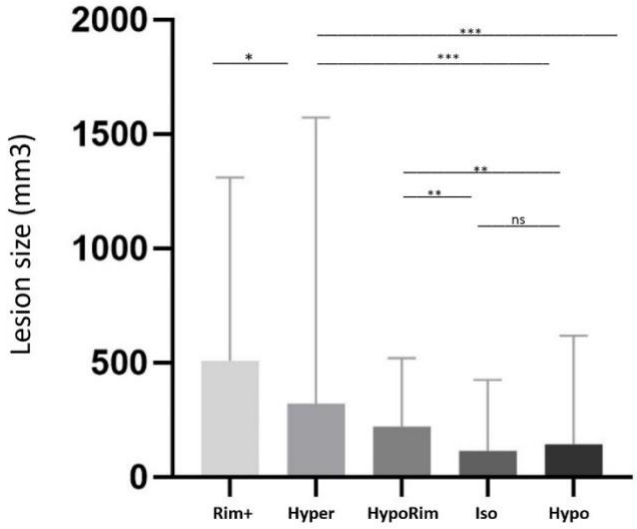

Figure 5. Lesion size comparison across QSM lesion types. * P<0.05 **P<0.001 ***P<0.0001.

3.1.7 Comparison of QSM lesion type frequency between RRMS and PMS and between different anatomical locations

There was no difference in the frequency of QSM lesion types between RRMS and PMS patients (Figure1; all $P > 0.05$). PRLs were predominantly located in PV regions ($P < 0.05$) and hypointense lesions mainly in JC areas ($P < 0.001$). Isointense and hyperintense lesions were evenly distributed across PV, DW, and JC regions.

3.1.8 Longitudinal evaluation of iso- & hypo- intense lesions

To confirm our cross-sectional observations suggesting that iso- and hypo-intense lesions are remyelinated lesions, we performed a longitudinal study in 40 patients. Specifically, we assessed how MWF changed between baseline MRI and follow-up MRI in lesions that appear iso- & hypo-intense in QSM maps at follow-up.

Out of 325 WM lesions in follow-up QSM, 18 lesions were iso- & hypointense and had a corresponding lesion in baseline QSM images.

Of those, 8/18 hypo- and iso-intense lesions at follow-up were iso- or hypo-intense, respectively, at baseline. In these lesions, MWF remained overall stable over time (average increase of 3.61%, mean MWF baseline: 8.15, TP2: follow-up: 8.47), Figure 6.

However, 10/18 hypo/iso-intense lesions at follow-up were hyperintense at baseline: those lesions showed an average increase of 33.55% in MWF (Mean MWF baseline: 7.39, follow-up: 8.45).

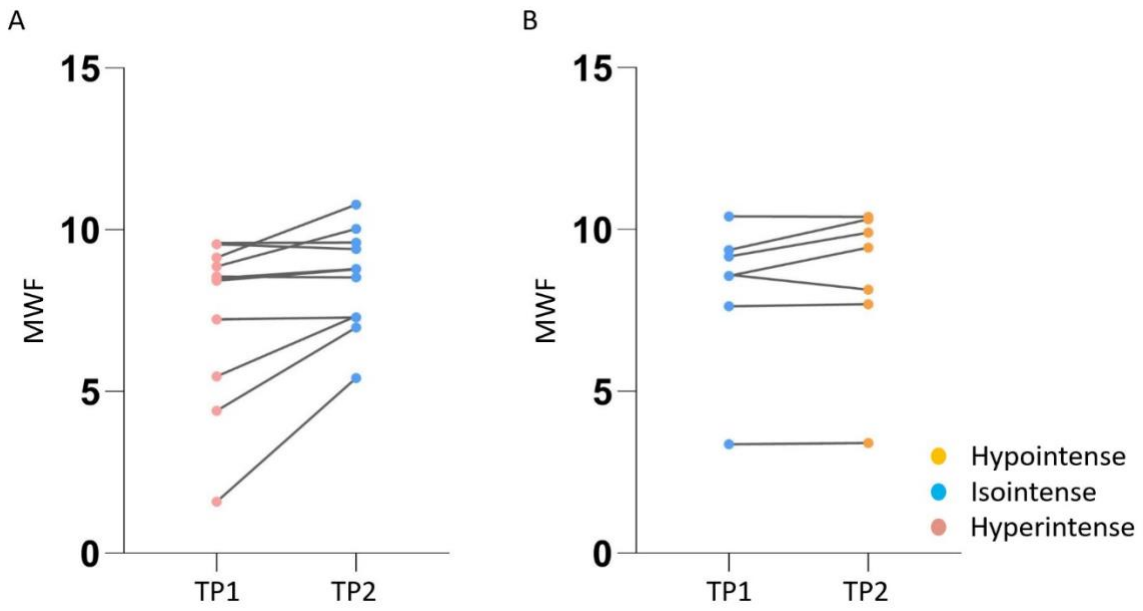

Figure 6. MWF changes in iso- & hypo-intense lesions at follow-up (timepoint2- TP2) compared to baseline (timepoint1- TP1). A) MWF increases in the majority of lesions that are hyperintense at TP1 and isointense at TP2. B) MWF is stable in lesions that are isointense at TP1 and hypointense at TP2.

3.1.9 Clustering of Iso-/Hypo-intense lesions vs PRLs

To confirm that the qualitative appearance of QSM lesion types represents lesions with different MWFs, NDIs and susceptibility, a GMM was applied to the lesion groups exhibiting the highest and lowest MWF and NDI mean content.

When PRLs and hypointense/isointense lesions were considered, the GMM identified two clusters: 80.23% of PRLs clustered in the area with low MWF and NDI values (yellow cluster, Figure 4G-I), while 72.55% of hypointense and 68.15% of isointense lesions clustered in the area with high MWF and NDI values (purple cluster, Figure 4G-I).

3.2. A double-blind coupled histopathology and QSM study

To further investigate the relationship between QSM lesion types and histopathological lesion categories, we performed a double-blind histopathology-QSM study in three brains including 63 WM MS lesions.

8/9 (88.88%) remyelinated lesions/areas appeared iso- or hypointense in QSM maps. However, all lesions (8/8 - 100%) detected as iso and hypo-intense in QSM were remyelinated lesions/areas. The only remyelinated lesion not appearing iso- or hypointense was hyperintense (n=1) in QSM images. This hyperintense remyelinated lesion was characterized by iron-rich macrophages/activated microglia and incomplete remyelination (Figure 7A-D).

10/14 (71.43%) chronic inactive lesions/areas appeared hyperintense in QSM maps and the other 4 were PRLs (28.57%). 10/14 QSM hyperintense lesions were chronic inactive lesions/area without signs of lesion activity (Figure 6E-H) and the remaining 4 were chronic active (n=3) and remyelinated lesions (n=1) with iron-laden macrophages/microglia.

37/40 (92.5%) chronic active lesions/areas appeared as PRL in QSM maps and the remaining 3 as hyperintense lesions (7.5%). On the other hand, 39/42 (92.85%) QSM PRLs appeared as chronic active lesions/areas with iron-laden macrophages/microglia at lesion border (Figure 7G, H) and the remaining 3 were chronic inactive (n=3).

Table 2 summarizes the sensitivity and specificity of QSM classification to identify distinct neuropathological MS lesions types.

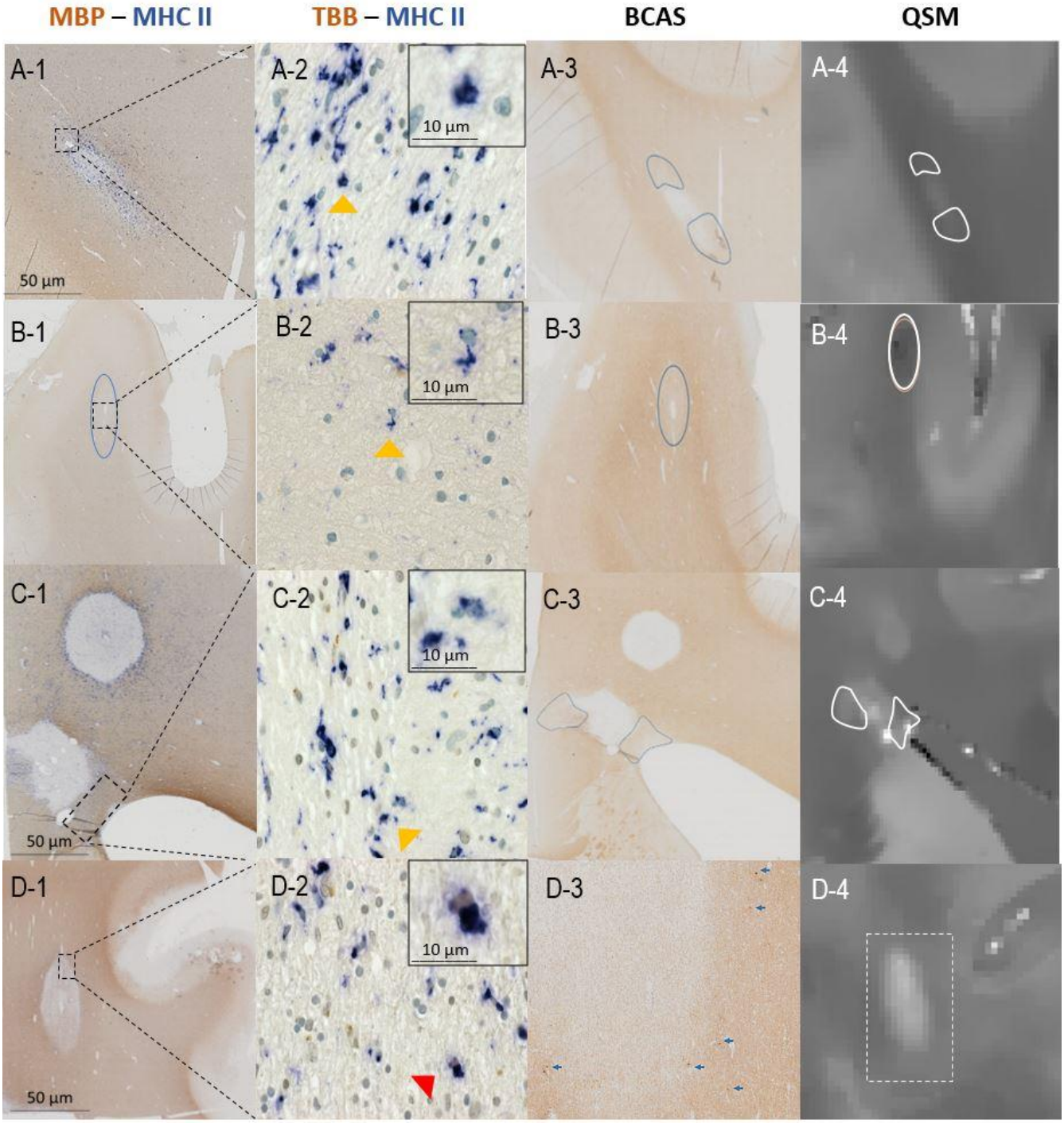
MBP – MHC II
TBB – MHC II
BCAS
QSM
A-1
A-2
A-3
A-4
B-1
B-2
B-3
B-4
C-1
C-2
C-3
C-4
D-1
D-2
D-3
D-4
50 µm
10 µm

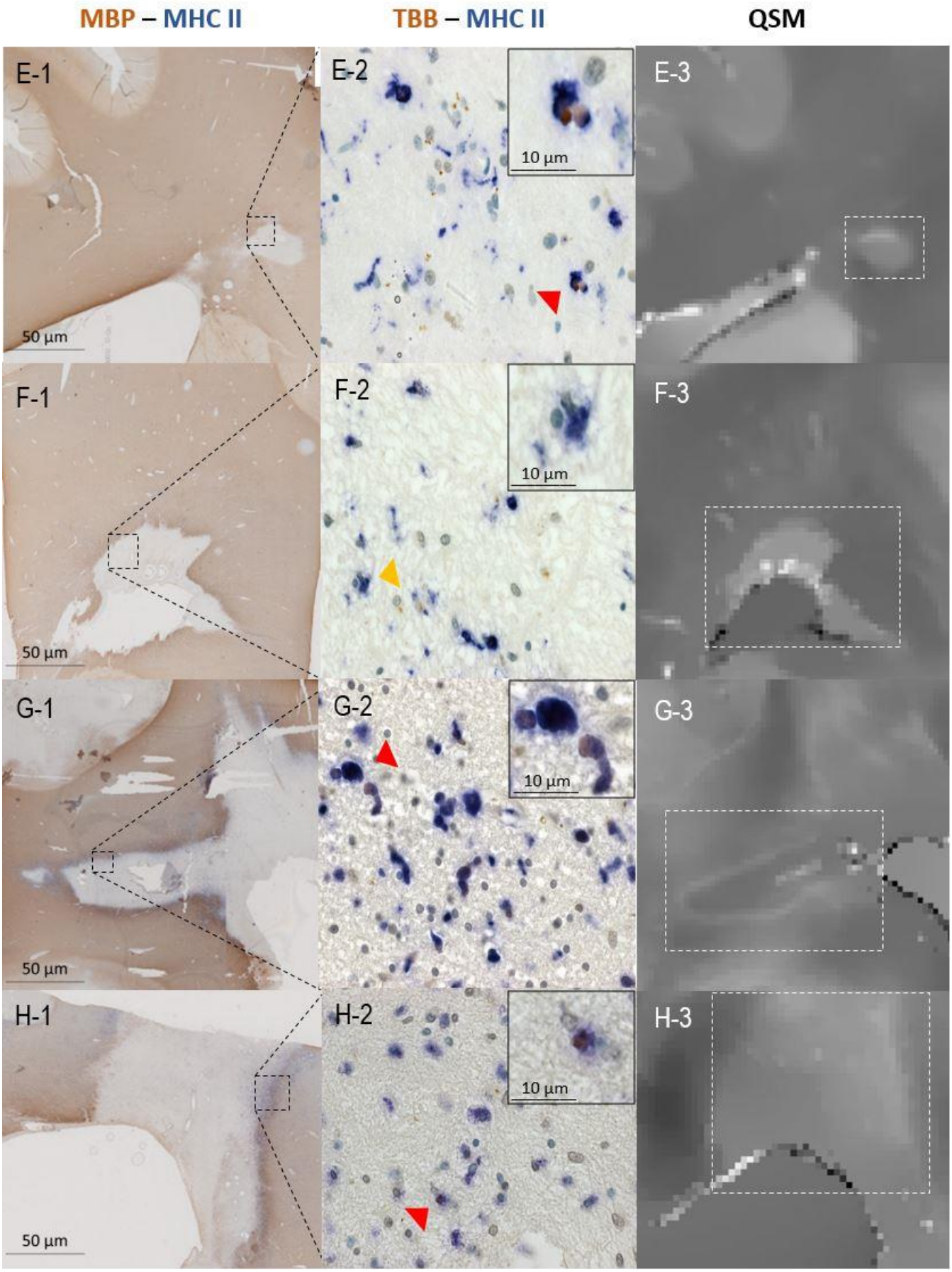
MBP – MHC II
TBB – MHC II
QSM
E-1
E-2
E-3
F-1
F-2
F-3
G-1
G-2
G-3
H-1
H-2
H-3
50 µm
10 µm

Figure 7. Histopathology and postmortem QSM of remyelinated, chronic inactive, and chronic active lesions.
A1-D1: MBP (brown)-MHC II (blue) double immunohistochemistry (IHC) in exemplary fully (B-1) or partially (A1, C1, D1) remyelinated lesions. **A2-D2:** DAB-enhanced Turnbull's blue (TBB) (brown)- MHC II (blue) staining showing macrophages/activated microglia containing (D1; red arrow) or lacking iron (A1-C1; yellow arrow); **A3-D3:** BCAS1 IHC showing non-compact myelin and, in D-3, newly formed myelinating oligodendrocytes; **A4-D4:** postmortem QSM showing fully (B-1) or partially (A1, C1, D1) remyelinated lesions. **E1-F1:** MBP- MHC II staining of chronic inactive lesions. **E2-F2:** TBB (brown)- MHC II (blue) staining of macrophages/activated microglia containing (E2; red arrow) or lacking iron (F2; yellow arrow). **E-3, F-3:** postmortem QSM showing a corresponding hyperintensity for chronic inactive lesions. **G1-H1:** MBP- MHC II IHC of chronic active lesions showing extensive demyelination. **G2-H2:** TBB (brown)- MHC II (blue) staining showing iron-laden macrophages/activated microglia at the lesion edge (red arrow). **G-3, H-3:** postmortem QSM revealing a hyperintense paramagnetic rim in chronic active lesions. MBP: myelin basic protein; MHC II: major histocompatibility complex II; TBB: DAB-enhanced Turnbull's blue.

Table 2: Sensitivity and specificity of QSM classification to distinct histopathological MS lesion types.

Histopathological MS lesion types	QSM Sensitivity	QSM Specificity
Remyelinated	88.89%	100%
Chronic inactive	71.43%	92.00%
Chronic active	92.86%	86.36%

4. Discussion

In this work, five MS lesions types were identified in QSM maps and their relative axon and myelin content was quantified using MWF and diffusion maps *in vivo* in MS patients. These five QSM lesion types exhibited imaging features (i.e., changes in susceptibility and surrogate markers of

myelin/axon characteristics) that were compatible with specific histopathological lesion subtypes, namely (i) remyelinated (iso and hypointense lesions) (ii) chronic inactive (hyperintense lesions) and (iii) chronic active/smoldering lesions (PRLs). An additional double-blind combined postmortem QSM-histopathology study confirmed these associations.

Previous studies related some characteristics of MS lesions on QSM maps to lesion age and to the presence of acute and chronic focal inflammation. Specifically, acute lesions were shown to exhibit susceptibility very close to that of surrounding NAWM(Chen *et al.*, 2014), whereas chronic active/smoldering lesions were described as areas with paramagnetic rims, which is associated with iron-rich macrophages and activated microglia (paramagnetic rim lesions-PRLs) (Chen *et al.*, 2014), (Hametner *et al.*, 2013; Absinta *et al.*, 2016).

In this study, several QSM lesion types that had been previously described (PRLs, hyperintense, and isointense lesions (Harrison *et al.*, 2016)) were identified and some other rarer types are reported here for the first time (hypointense and hypo-rim lesions). Furthermore, new evidence is presented that indicates QSM lesion types substantially differ in their myelin and axon content, as measured by MWF and NDI.

In accordance with previous neuropathological (Wisnieff *et al.*, 2015) and imaging studies (Bian *et al.*, 2016), the majority of WMLs in this cohort of MS patients showed a positive relative susceptibility on QSM maps, which is probably driven by iron accumulation in microglia, macrophages, and oligodendrocytes (Ropele *et al.*, 2017) (especially when the relative susceptibility is > 60 ppb (Li *et al.*, 2011)) and/or by loss of myelin integrity (Bagnato *et al.*, 2011; Li *et al.*, 2011; Yao *et al.*, 2012; Deh *et al.*, 2018). Interestingly, the range of relative magnetic susceptibility within each QSM lesion subtype was found to be quite broad suggesting that the pathological features within each lesion group are part of a spectrum and/or that the surrounding NAWM is variably affected in different patients.

Magnetic susceptibility across QSM lesion subtypes is inversely related to the MWF and NDI (as shown in Figure 2D-I). In fact, lesions with the highest relative susceptibility (i.e., PRLs and hyperintense lesions) also showed the lowest MWFs and NDIs, suggesting that iron deposition in lesions with higher susceptibility may lead to pro-inflammatory microglia-activation and to amplification of neurodegeneration (Stephenson *et al.*, 2014; Haider, 2015; Adamczyk and Adamczyk-Sowa, 2016).

PRLs have been previously described as QSM lesions characterized by a rim of activated and iron-rich microglia with accompanying smoldering demyelination and axonal loss (Absinta *et al.*, 2016; Dal-Bianco *et al.*, 2017a). Further, *in vivo* and post-mortem results of our study confirm that these plaques are characterized by extensive myelin and axon damage *in vivo* and that PRLs correspond to the histopathological subtypes of chronic active/smoldering lesions with a sensitivity of 92.86% and a specificity of 86.36% (Bagnato *et al.*, 2011; Hametner *et al.*, 2013; Absinta *et al.*, 2016; Dal-Bianco *et al.*, 2017b; Kaunzner *et al.*, 2019).

In this cohort of patients, hyperintense QSM lesions without a paramagnetic rim exhibited high susceptibility and low mean MWFs and NDIs, suggesting that those lesions are characterized by extensive myelin/axon loss (Wisnieff *et al.*, 2015). This was confirmed by our histopathological-MRI study, which showed that hyperintense lesions mostly correspond to demyelinated chronic inactive plaques [7]. Further, consistent with previous QSM studies performed *in vivo* (Chen *et al.*, 2014; Harrison *et al.*, 2016; Li *et al.*, 2016) and work focusing on chronic inactive lesions postmortem (Lassmann, 2018a), QSM hyperintense lesions were the most frequent QSM lesion type in our cohort of MS patients.

Hyperintense lesions exhibited a 92% specificity of being chronic inactive lesions in histopathology, which is explained by the fact that the extensive demyelination characterizing these lesions probably drives the QSM signal towards hyperintensity. Interestingly, 3/14 chronic inactive lesions exhibited a paramagnetic rim in QSM that was lacking in histopathological analysis, which may be due to pronounced demyelination at the lesion border in the absence of iron accumulation within microglia/macrophages.

We also identified a new QSM lesion type, hypointense QSM lesions, which showed the lowest susceptibility and the highest myelin and axon content compared to other QSM lesion types, suggesting that they may represent remyelinated plaques. In fact, the average MWF in these lesions was at the level of that measured in NAWM and in the WM of healthy controls. Moreover, it was higher than that of other QSM lesion types (PRLs, hypo-rim and hyperintense lesions). In line with this, fully remyelinated lesions with scarce macrophages/activated microglia and no signs of actively remyelinating oligodendrocytes (Todorich *et al.*, 2009) appeared hypointense in postmortem QSM.

It remains unclear why an MS lesion appears hypointense in QSM images. This may be due to the different diamagnetic properties of the remyelinated axons showing thinner myelin and shorter internodal lengths (Lubetzki *et al.*, 2020),(Lee *et al.*, 2017) and/or to their relatively low iron content compared to the peri-plaque region (Kirilina *et al.*, 2020). Supporting this latter explanation is the fact that hypointense lesions are predominant in the juxtacortical area, which is a region particularly rich in iron(Kirilina *et al.*, 2020). Thus, if myelin, but not iron, is restored in the lesion, remyelinated areas in this region may appear hypointense. Future studies focusing on this QSM lesion subtype may help to define the mechanisms driving this susceptibility change in QSM maps.

Isointense lesions have myelin content similar to that of hypointense lesions and higher than that of other QSM lesion types. However, isointense lesions exhibit higher susceptibility compared to that of hypointense lesions, probably due to higher iron content or incomplete remyelination as evidenced postmortem. Given that acute lesions show susceptibility that is very close to that of PPWM (Chen *et al.*, 2014), Gd-enhancing lesions detected within a 3-month window of this study were excluded to avoid the inclusion of acute lesions in the isointense QSM lesion group.

Iso- and hypo-intense lesions exhibited 100% specificity to histopathologically-defined remyelinated lesions. However, one remyelinated lesion appeared rather hyperintense leading to a sensitivity of ca 89% percent, probably due to the presence of iron-laden macrophages/microglia and incomplete remyelination. Hence, it appears that iso and hypo-intensity in QSM indicates complete focal remyelination with no active microglia and macrophages.

This interpretation is not only strongly suggested by our postmortem results but was also confirmed by the fact that baseline hyperintense lesions that converted to iso- and hypo-intense lesions at follow-up exhibited an average 33.55% increase in MWF.

Further supporting the fact that hypointense and isointense lesions are most probably fully remyelinated plaques is the observation that these lesions exhibited significantly less axon damage than other lesions (as measured by NDI), which was reported in previous neuropathological studies (Kornek *et al.*, 2000; Schultz *et al.*, 2017).

Lastly, MS lesions rarely appear with a hypointense rim around a relatively hyperintense center in QSM. We hypothesize that lower susceptibility at the edge of the lesions compared with the center

could signify destructive damage leading to tissue loss, probably in late stages of chronic active/smoldering lesions. Unfortunately, none of these lesions were identified in the two brains evaluated postmortem, which could be due to the rarity of this lesion type. Therefore, further studies will be needed to fully test this hypothesis.

It should be noted that although excessive iron accumulation may put demyelinated axons under devastating oxidative stresses (Friese *et al.*, 2014; Ropele *et al.*, 2017), our data showed that axonal damage did not differ between lesions with positive relative susceptibility and lesions with negative relative susceptibility. Further, susceptibility was not different between lesions with predominant-axonal damage and those with predominant-myelin damage. The contribution of both iron and myelin content to QSM susceptibility (Deh *et al.*, 2018) as well as the dual role of iron in oxidative damage (Friese *et al.*, 2014; Ropele *et al.*, 2017) and in fostering remyelination and repair (Lee *et al.*, 2019) may partly account for these findings.

Interestingly, PRLs were mainly located around the ventricles, a region characterized by plaques with a destructive nature that might be due to the release of immune cells and cytokines from the ventricles (Magliozzi *et al.*, 2007; Winges *et al.*, 2007). In contrast, hypointense lesions were mainly located in the juxta-cortical area, which is a region with potentially high remyelinating capacity thanks to the presence of more numerous and efficacious oligodendrocyte precursor cells (Patrikios *et al.*, 2006; Patani *et al.*, 2007).

Surprisingly, however, the distribution of QSM lesion types did not differ between RRMS and PMS patients in our cohort. This shows once more that differences in MS lesion types are not associated with different clinical phenotypes (Antel *et al.*, 2012).

One limitation of the current study is that contrast-agent was not used for the identification of acute lesions at the time of the MRI study; however, a conventional MRI with gadolinium injection was performed within three months of the advanced MRI performed in this study, which allowed reasonable exclusion of acute lesions from the classification. Another limitation of this work is that a histopathological correlate of hypointense rim lesions could not be identified due to their rarity. Future studies including a larger number of autoptic evaluations should clarify the nature of this type of lesion.

To date, numerous treatments are available that target the acute inflammatory component of MS; however, drugs fostering remyelination and repair are lacking. The identification of imaging biomarkers of axonal and myelin repair is fundamental to drive the development of targeted neuroprotective and reparative drugs. Further, this work provides new evidence that QSM maps may be used to identify fully remyelinated lesions *in vivo* in MS patients, providing a perspective to evaluate, at least in part, the repair capacity of existing and novel MS therapies using a single scan.

In summary, our findings show that QSM maps permit the classification of MS lesions with various extents of damage and repair to myelin and axons. In addition, our multiparametric cross-sectional and longitudinal data, together with our double-blinded postmortem analyses showed that QSM provide highly sensitive and specific biomarkers of completed remyelination.

2.3. Manuscript 3

A comparative assessment of sensitivity to multiple sclerosis pathology and intra-scanner reproducibility for myelin-sensitive MRI measures

In this work, we studied a large cohort of MS patients and healthy controls and performed a comprehensive evaluation of the sensitivity of myelin-sensitive qMRI measures to MS pathology, with regard to changes in both focal lesions and normal appearing (NA) tissue. Furthermore, we assessed and compared the intra-scanner reproducibility of myelin-sensitive qMRIs acquired within and across scanning sessions in a single 3T MR system.

A comparative assessment of sensitivity to multiple sclerosis pathology and intra-scanner reproducibility for myelin-sensitive MRI measures

Reza Rahmanzadeh[1,2], Matthias Weigel[1,2,3], Po-Jui Lu[1,2], Lester Melie-Garcia [1,2], Thanh D. Nguyen[4], Alessandro Cagol[1,2], Francesco La Rosa[5,6,7], Muhamed Barakovic[1,2], Yi Wang[4], Meritxell Bach Cuadra[5,6,7], Ernst-Wilhelm Radue[1], Laura Gaetano[8], Ludwig Kappos[2], Jens Kuhle[2], Stefano Magon[9], Cristina Granziera[1,2]

[1]*Translational Imaging in Neurology Basel, Department of Medicine and Biomedical Engineering, University Hospital Basel and University of Basel, Basel, Switzerland.*

[2]*Neurologic Clinic and Policlinic, MS Center and Research Center for Clinical Neuroimmunology and Neuroscience Basel (RC2NB), University Hospital Basel and University of Basel, Basel, Switzerland*

[3] *Division of Radiological Physics, Department of Radiology, University Hospital Basel, Basel, Switzerland.*

[4]*Department of Radiology, Weill Cornell Medical College, New York, New York, USA.*

[5]*Signal Processing Laboratory (LTS5), Ecole Polytechnique Fédérale de Lausanne (EPFL), Lausanne, Switzerland.*

[6] *CIBM Center for Biomedical Imaging, Lausanne, Switzerland.*

[7]*Radiology Department, Lausanne University and University Hospital, Lausanne, Switzerland.*

[8]*F. Hoffmann-La Roche Ltd., Basel, Switzerland*

[9]*Pharmaceutical Research and Early Development, Roche Innovation Center Basel, F. Hoffmann-La Roche Ltd., Basel, Switzerland*

Abstract

Introduction

Multiple Sclerosis (MS) is a common neurological disease primarily characterized by myelin damage in lesions and in normal - appearing white and gray matter (NAWM, NAGM).

Several quantitative MRIs (qMRIs) are sensitive to myelin characteristics by measuring specific tissue biophysical properties. However, there are currently few studies assessing the relative reproducibility and sensitivity of qMRI measures to MS pathology *in vivo* in patients.

Methods

In this work, we performed two studies. The first was the assessment of the sensitivity of qMRI measures to MS pathology; in this work, we recruited 150 MS and 100 healthy subjects, who underwent brain MR at 3T including quantitative T1 mapping (qT1), susceptibility-based imaging for quantitative susceptibility mapping (QSM), magnetization transfer saturation imaging (MTsat) and myelin water imaging for myelin water fraction (MWF). The sensitivity of qMRIs to MS focal pathology (MS lesions vs peri-plaque white/gray matter (PPWM/PPGM)) was studied lesion-wise; the sensitivity to diffuse normal appearing (NA) pathology was studied using voxel-wise threshold-free cluster enhancement (TFCE) in NAWM and vertex-wise inflated cortex analysis in NAGM. Furthermore, the sensitivity of qMRI to the identification of lesion tissue was assessed using a voxel-wise logistic regression analysis to distinguish MS lesion and PP voxels.

The second study assessed the reproducibility of myelin-sensitive qMRI measures. To assess intra-session and inter-session reproducibility of qMRI measures, we have investigated 10 healthy subjects, who underwent two brain 3T MRIs within the same day (without repositioning), and one after 1-week interval. Five region of interest (ROIs) in white and deep grey matter areas were segmented, and inter- and intra- session reproducibility was studied using the intra-class correlation coefficient (ICC). Further, we also investigated the voxel-wise reproducibility of qMRI measures in NAWM and NAGM.

Results

qT1 and QSM showed the highest sensitivity to distinguish MS focal WM and cortical pathology from peri-plaque WM ($P < 0.0001$). qT1 also showed the highest accuracy in identifying

FLAIR/MP2RAGE MS lesions in logistic regression analysis (0.86 for WMLs and 0.82 for CLs). MWF and MTsat exhibited the highest sensitivity to NAWM pathology ($P < 0.01$). On the other hand, qT1 appeared to be the most sensitive measure to NAGM pathology ($P < 0.01$). All studied qMRI measures exhibited high inter/intra sessional ICCs in various WM and deep GM ROIs, in NAWM and in NAGM (ICC 0.82 ± 0.12).

Conclusion

This work shows that all studied qMRIs are highly reproducible and exhibit differential sensitivity to focal and diffuse WM and GM pathology in MS patients.

1. Introduction

In the last decades, several myelin-sensitive quantitative magnetic resonance imaging (qMRI) techniques (e.g. myelin water imaging, magnetization transfer, T1 relaxometry, quantitative susceptibility imaging) have been developed, which provide more specific measures of demyelination and remyelination than conventional MRI in multiple sclerosis (MS) patients(Piredda *et al.*, 2021),(Granziera *et al.*, 2021). To date, however, it is unclear how all these measures compare to each other, both in terms of sensitivity to MS damage and of reproducibility across different acquisition sessions(van der Weijden *et al.*, 2021).

MS lesions contain variable amounts of inflammatory infiltrates, demyelination and axonal loss (Lucchinetti *et al.*, 2000). Also, the peri-plaque (PP) tissue around the MS lesion is not healthy and contains both myelin and axonal damage although to a lesser degree than the lesion itself(Lieury *et al.*, 2014). Furthermore, the normal-appearing tissue (i.e. white and gray matter areas that do not exhibit signs of focal pathology, NAWM and NAGM, respectively) is characterized by diffuse myelin and axonal damage and microglia clusters(Kutzelnigg *et al.*, 2005; Cui *et al.*, 2017; Granberg *et al.*, 2017; Lassmann, 2018a).

Myelin-sensitive techniques exploit different contrasts mechanisms to assess specific characteristics of the myelin sheets. Myelin water imaging (MWI) quantifies the water between myelin layers by distinguishing multiple water components in T2 relaxometry data, and provides with measures (e.g. myelin water fraction, MWF) that have been validated postmortem (Moore *et al.*, 2000; Kozlowski *et al.*, 2014). Quantitative susceptibility mapping (QSM) quantifies the spatial distribution of magnetic susceptibility in biological tissue(Liu *et al.*, 2012) and has been shown to be sensitive to iron content and to myelin integrity(Wisnieff *et al.*, 2015; Hametner *et al.*, 2018). Quantitative T1 mapping (qT1)(Taylor *et al.*, 2016) quantifies T1 relaxation times that are sensitive to water content and macro/micro molecules changes within a tissue, such as the one provoked by demyelination and axonal loss in the brain(Kolb *et al.*, 2021). Although it is challenging to disentangle the contribution of these factors in acquired qT1, it has been shown that qT1 correlates well with myelin content in NAWM and MS lesions(Mottershead *et al.*, 2003; Seewann *et al.*, 2009). Magnetization transfer (MT) imaging measures the magnetization exchange

between proton in free water and the protons coupled with macromolecules, which has been related to myelin integrity and content(Moccia *et al.*, 2020). MT saturation (MTsat) is developed to improve the MT ratio by decoupling the MTR from R1 by compensating for T1-relaxation and flip angle inhomogeneities, thus overcoming some limitations of previous MT-based methodologies(Helms *et al.*, 2008b). Combined MRI – neuropathology studies have shown that the MT ratio correlates to myelin content within the brain tissue but also to the presence of macrophages and astrocytes(Schmierer *et al.*, 2004; Moccia *et al.*, 2020).

In the current work, we studied a large cohort of MS patients and healthy controls and performed a comprehensive evaluation of the sensitivity of myelin-sensitive qMRI measures to MS pathology, with regard to changes in both focal lesions and normal appearing (NA) tissue. Furthermore, we assessed and compared the intra-scanner reproducibility of myelin-sensitive qMRIs acquired within and across scanning sessions in a single 3T MR system.

2. Materials and methods

2.1. Participants

2.1.1. Sensitivity study

We enrolled 150 MS patients (92 RRMS and 58 PMS) and 100 healthy controls. The inclusion criteria were: (i) MS diagnosis according to McDonald criteria 2018 (Thompson *et al.*, 2018) and diagnosis of active RRMS or inactive PMS as defined by Lublin et al. (Lublin *et al.*, 2014); (ii) absence of any concomitant psychiatric or neurological disease (excluding headache); (iii) absence of contraindication to MRI. The ethical review committee of the University Hospital Basel (IRB of Northwest Switzerland) approved the study, and all participants entered the study following written consent. All subjects underwent MRI at 3T.

2.1.2. Reproducibility study

We have enrolled 17 healthy subjects who underwent two scans conducted 1h apart without repositioning (time point 1 and 2, TP1 and TP2) and a third scan (TP3) was performed 1 week (±

3 days) later. Seven subjects were excluded from the study because of motion artefacts (n=4), technical issues leading to heavy artifacts (n =1) and impossibility to acquire MRI in time (n=2) (Figure 1.).

Figure 1. Reproducibility study design. Time points (TP) 1 & 2 were performed without repositioning and TP3 1w±3 later.

2.2. MR acquisition and qMRI maps reconstruction

2.2.1. MR acquisition

MRI was performed on a 3T whole-body MR system (Magnetom Prisma, Siemens Healthcare, Erlangen, Germany) using a 64-channel phased-array head and neck coil for radio frequency reception. The MRI protocols included: (i) 3D FLAIR (TR/TE/TI=5000/386/1800 ms) and MP2RAGE (TR/TI1/TI2=5000/700/2500 ms) both with 1 mm^3 isotropic spatial resolution; (ii) Fast Acquisition with Spiral Trajectory and adiabatic T2prep (FAST-T2) (TR/TE = 7.5/0.5 ms, six T2prep times = 0 (T2prep turned off), 7.5, 17.5, 67.5, 147.5, 307.5 ms, voxel size = 1.25x1.25x5 mm^3, scan time = 4.5 min, as described in; as well as (iii) 3D segmented EPI with submillimeter isotropic resolution (TR/TE/resolution=64 ms/35 ms/0.67x0.67x0.67 mm^3) (Sati *et al.*, 2012). Quantitative Magnetization Transfer saturation (MTsat) images were acquired using three 3D RF spoiled gradient echo acquisitions with predominantly Magnetization Transfer-weighted (MTw:

TR/α = 25 ms/5º), proton density-weighted (PDw: TR/α = 25 ms/5º) and T1-weighted (T1w: TR/α = 11 ms/15º) contrast(Helms *et al.*, 2008a; Helms and Dechent, 2009; Helms *et al.*, 2009) (Helms et al., 2009, 2008a, 2008b). The MT contrast was achieved by use of a Gaussian-shaped RF pulse prior to the excitation (12.8 ms duration, 520º nominal flip angle, 2.2 kHz frequency offset from water resonance). A single gradient echo was acquired with echo time TE = 4.92 ms. The image resolution was 1.33 mm^3 isotropic, the field of view was 256 x 248 x 160 mm and the matrix size 192 x 186 x 120. Parallel imaging was used along the phase-encoding direction (acceleration factor 2 GRAPPA reconstruction(Griswold *et al.*, 2002)), 6/8 partial Fourier was used in both phase-encoding directions. The acquisition times were 1:22 min (T1w) and 3:07 min (MTw, PDw). Data were acquired to calculate radio frequency (RF) transmit field $B1^+$ maps using the steady state free precession based B1-TRAP approach(Ganter *et al.*, 2013); and to correct for effects of RF transmit inhomogeneities on the quantitative maps(Helms and Dechent, 2009; Helms *et al.*, 2009; Wisnieff *et al.*, 2015). The image resolution of the B1-mapping data was 4 x 4 x 5 mm3, echo time TE = 1.76 ms, TR = 2300 ms and flip angle α=60 º. The acquisition time of the B1 mapping sequence was 2:09 min. The total acquisition time for the MTsat protocol was 9:45 min.

2.2.2. qMRI maps reconstruction

MWF maps were reconstructed using FAST-T2 data as previously proposed.

QSM maps were reconstructed from 3D EPI data by unwrapping phase, removing the background field through Projection onto Dipole Fields algorithm, and using the morphology-enabled dipole inversion algorithm to compute the susceptibility from the local field (MEDI reconstruction), as in Liu *et al.*(Liu *et al.*, 2012)

The calculation of the quantitative MTsat maps from the acquired data was implemented with the hMRI Toolbox (https://github.com/hMRI-group/hMRI-toolbox)(Kaunzner *et al.*, 2019; Tabelow *et al.*, 2019) running under SPM12 (Wellcome Trust Centre for Neuroimaging, London, UK; http://www.fil.ion.ucl.ac.uk/spm) and Matlab 9.9 (R2020b) (Mathworks, Natick, MA, USA). The MTsat maps were computed as described in Helms, Dathe, and Dechent(Helms *et al.*, 2008a) and Helms and Dechent(Helms and Dechent, 2009) using the MTw, PDw, and T1w images.

2.3. Lesion/ROIs identification and segmentation

For the sensitivity study, an automatic segmentation of WM lesions was performed by using an publicly available deep learning-based method(La Rosa *et al.*, 2020). This approach consists of a single convolutional neural network and was adapted to take as input FLAIR and MP2RAGE MRI contrasts. Manual correction of automatic WM and cortical lesion masks was performed on FLAIR and MP2RAGE images by consensus (WM: RR and CG, cortical: RR and AC). (Geurts *et al.*, 2011)

For the reproducibility study, five regions of interests (splenium of corpus callosum, genu of corpus callosum, putamen, head of caudate and thalamus) segmented automatically by imaging software package FreeSurfer (FS) (v.6.0, surfer.nmr.mgh.harvard.edu)(Fischl, 2012) were manual corrected on FLAIR and MP2RAGE. The ROIs mask were then registered to qMR spaces using a linear registration in FMRIB Software Library (FSL)(Jenkinson *et al.*, 2012).

2.4. WM and cortex segmentation

For both studies, to segment the brain into whole WM, cortex, deep grey matter structures, and ventricles we used the imaging software package FS. NAWM and NAGM masks were obtained by subtracting WM and cortical lesion masks from WM and cortical masks.

An in-house algorithm was used to automatically produce a 2-voxel layers of NAWM surrounding the lesions; herein after denoted peri-plaque (PP).

For the reproducibility study, FS was performed using MP2RAGE acquired at baseline and FS outputs were then registered to the other time-points using the linear registration.

2.5. Voxel-Based Analyses in NAWM

NAWM maps were co-registered patient-wise to a reference brain (standard MNI152 space) using a rigid-body registration in FSL (Jenkinson *et al.*, 2012). As previously performed (Vrenken *et al.*, 2006a), in NAWM we excluded voxels that were not present in at least 50 percent of subjects, and (2) filled missing data with the group mean value of those voxels present in group subjects. By using the randomize tool of FSL with Threshold-Free Cluster Enhancement (TFCE), we carried on a voxel-wise comparison of MWF, qT1, MTsat and QSM maps (i) between patients and

controls (sensitivity analysis); and (ii) between TP1-TP2 & TP1-TP3 (reproducibility analysis). *P* values less than 0.01 were considered statistically significant.

2.6. Vertex-wise analysis in NAGM

A customized volume-to-surface mapping algorithm was applied to voxels assigned to the grey matter ribbon by FreeSurfer - i.e., voxels with coordinates located between the white and pial surfaces were registered and projected into a standard surface. A smoothing kernel of 10-mm full-width at half-maximum was used. Then, generalized linear model (GLM) analysis was conducted to assess (i) the sensitivity of each map in NAGM to assess damage between patients and controls; and (ii) to assess the intra- and inter-scanner reproducibility of each qMRI measure in GM (TP1 vs TP2 & TP1vs TP3, respectively). *P* values less than 0.01 were considered statistically significant.

2.7. Voxel-wise logistic regression to assess the specificity and sensitivity of qMRI measures to focal FLAIR/MP2RAGE lesions

To assess the relative specificity and sensitivity of qMRI measures to focal lesions, as segmented in FLAIR/MP2RAGE images, we have performed a logistic regression. Parameter optimization was performed on training dataset (70% of sample) and the performance was reported using test dataset (remaining 30% of sample). True positives were estimated using the FLAIR/MP2RAGE lesion masks for WM and CL respectively. This voxel-based approach (300’000 voxels) was applied for the contrasts “WMLs vs surrounding PPWM” and “CLs vs surrounding PPGM” in MS subjects and used an equal number of voxels from both regions.

2.8. Intra-class correlation coefficient to assess intra and inter-session reproducibility

In five regions of interest (ROIs: genu and splenium of the corpus callosum, putamen, head of caudate and thalamus), we calculated the intra-class correlation coefficient (ICC) for each qMRI measure using a two-way model with consistency of agreement within and across sessions (TP1-TP2, TP1-TP3). The ICC analysis was performed in Stata 16 statistical package.

The $\Delta^{WML\text{-}PPWM}$ and $\Delta^{CL\text{-}PPGM}$ were calculated as relative changes in qMR measures in lesions compared with normal-appearing PP tissue. Due to the challenges in establishing an automatic procedure to assess the PP-tissue in i) small lesions (due to partial-volume effects) ii) lesions close to ventricle wall and WM-GM border iii) lesions located in dirty WM area, those MS plaques were excluded.

Statistical analysis was performed using GraphPad Prism version 8.0.0 for Windows, GraphPad Software, San Diego, California USA. Kolmogorov-Smirnov's test was used to assess the normality of data. Non-parametric Mann-Whitney test and Kruskal-Wallis test with Dunn's test for multiple comparisons correction, were used for unpaired two-group analysis and more-than-three group analysis, respectively.

For the independent two sample analysis, a Cohen's d effect size was calculated as Cohen's $d = (M_2 - M_1) / SD_{pooled}$, where M_1 and M_2 are the group means and $SD_{pooled} = \sqrt{((SD_1^2 + SD_2^2) / 2)}$.

3. Results

3.1. Sensitivity study (analysis pipeline is summarized in Figure 2.)

3.1.1. Sensitivity of qMRI measures to focal MS pathology

Lesion-wise analysis showed that mean $\Delta^{WML\text{-}PPWM}$ was the highest for QSM and the lowest for MTsat (Figure 3). The $\Delta^{WML\text{-}PPWM}$ was higher for QSM than for qT1 ($P<0.0001$; Cohen's *d* effect size = 0.69) and for qT1 than for MWF ($P<0.0001$; Cohen's *d* effect size = 0.69). Further, voxel-wise logistic regression analysis showed that qT1 had the highest accuracy in distinguishing lesional voxels vs PPWM voxels followed by MTsat, MWF and QSM (Table 1).

Lesion-wise analysis showed that mean $\Delta^{CL\text{-}PPGM}$ was the highest for QSM and the lowest for MTsat (Figure 3). The $\Delta^{CL\text{-}PPGM}$ was higher for QSM than for qT1 ($P<0.001$; Cohen's *d* effect size =0.75) and for qT1 than for MWF ($P<0.0001$) (Figure 1; Cohen's *d* effect size =1.46). In voxel-wise logistic regression analysis qT1, MTsat, QSM and MWF exhibited the highest accuracy in distinguishing lesional voxels vs PPWM voxels (Table 1).

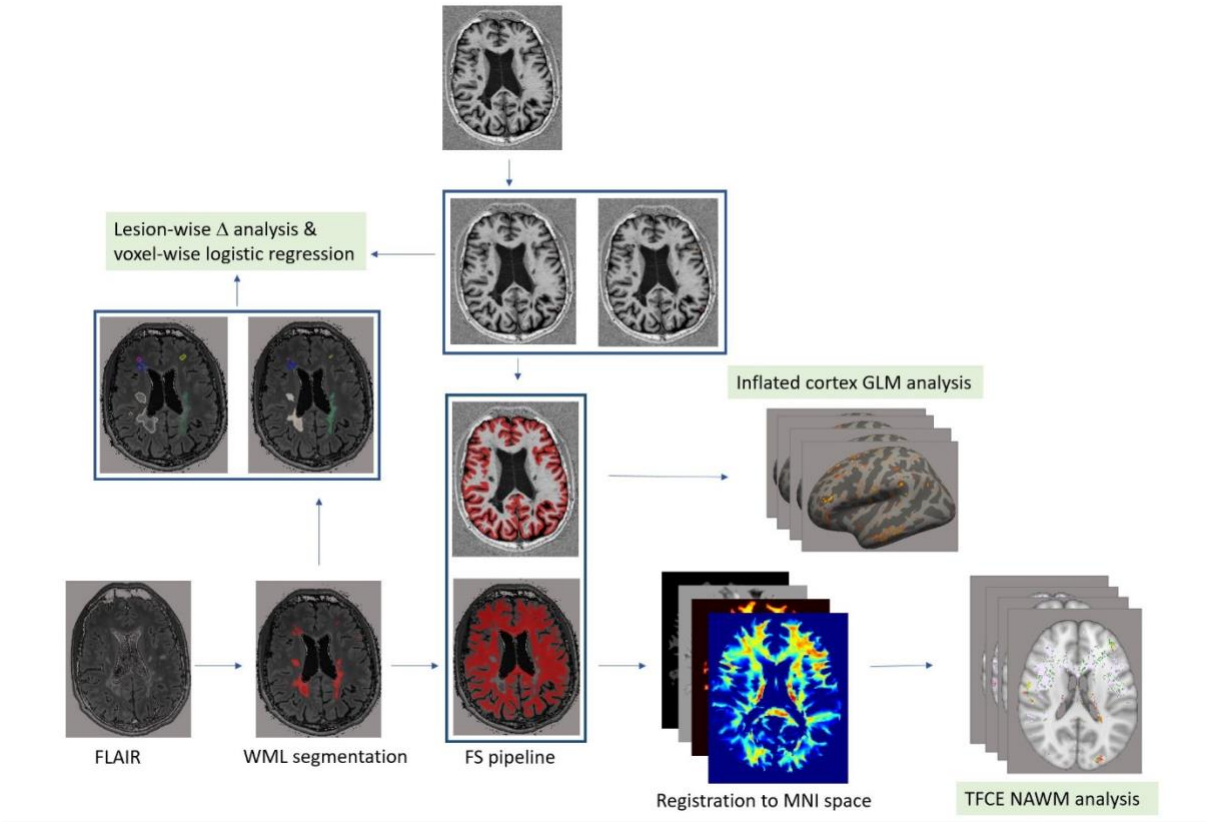

Figure 2. Analysis pipeline for sensitivity study. FLAIR: Fluid-attenuated inversion recovery, WML: white matter lesion, CL: cortical lesion, NAWM: normal-appearing white matter, NAGM: normal appearing gray matter, FS: FreeSurfer, GLM: general linear model, TFCE: threshold-free cluster enhancement.

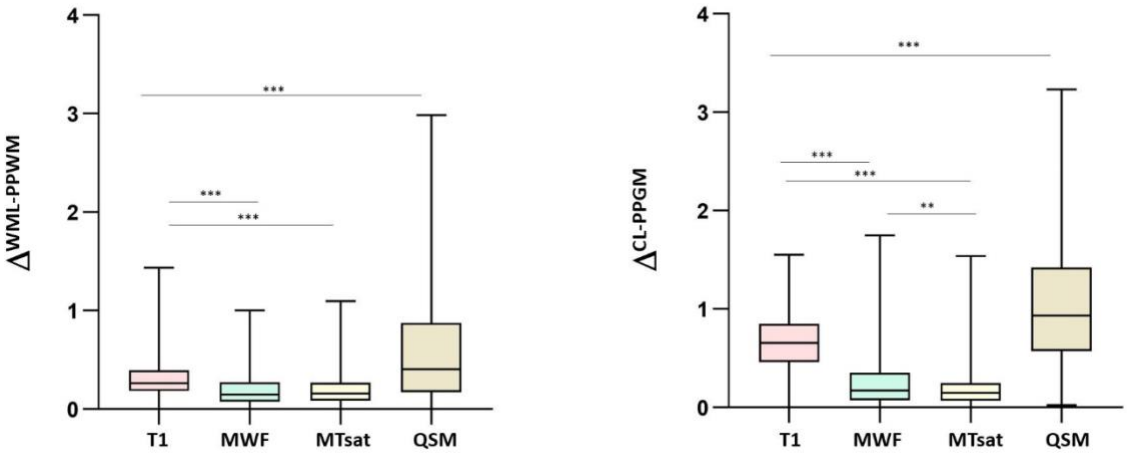

Figure 3. Comparison of the sensitivity of qMRI in distinguishing lesion vs peri-plaque tissue in WM and in the cortex.

qMRI	Comparison	Sensitivity	Specificity	Accuracy	AUC
MWF	WMLs	0.60	0.66	0.64	0.68
	CLs	0.46	0.53	0.50	0.50
qT1	WMLs	0.74	0.88	0.86	0.89
	CLs	0.74	0.83	0.82	0.85
MTsat	WMLs	0.67	0.74	0.72	0.75
	CLs	0.60	0.59	0.60	0.62
QSM	WMLs	0.52	0.59	0.55	0.57
	CLs	0.48	0.57	0.52	0.52

Table 1. Sensitivity, specificity, accuracy and area under the curve (AUC) for qMRIs in finding MS WMLs and CLs.

3.1.2. Sensitivity of qMRI measures to NAWM pathology in MS

Voxel-wise analysis showed that all qMRI measures were sensitive to changes in some clusters of NAWM voxels compared to WM in healthy controls. However, MTsat, MWF, QSM and qT1 appeared to show decreasing sensitivity to NAWM pathology in MS (Fig. 4, total clusters voxel number for MWF: 285820, MTsat: 340304, QSM (QSM1+QSM2): 132548, qT1: 36757; $P < 0.01$).

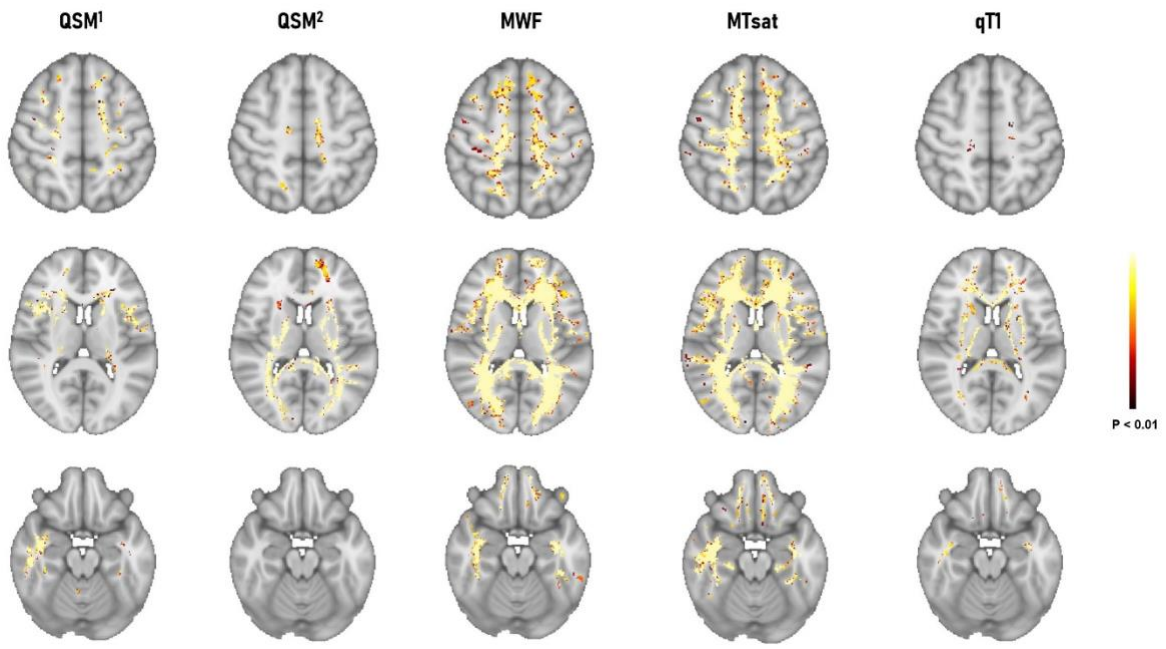

Figure 4. Voxel-wise TFCE comparison between MS patients and healthy subjects in NAWM and vertex-wise inflated cortex analysis in NAGM. QSM^1 shows areas where susceptibility values are higher in patients vs controls and QSM^2 shows areas in which susceptibility is lower in patients vs controls.

3.1.3. Sensitivity of qMRI measures to NAGM pathology in MS

Vertex-wise cortical surface analysis showed that all qMRI measures are sensitive to changes in some clusters of NAGM voxels compared to GM in healthy controls. However, qT1, QSM, MWF and MTsat appeared to show decreasing sensitivity to NAGM pathology in MS (Fig. 5, total clusters voxel number for qT1: 4223, QSM (QSM1+QSM2): 2678, MWF: 926, MTsat: 876; $P < 0.01$).

Figure 5. Vertex-wise inflated cortex analysis between MS patients and healthy subjects in NAGM. QSM^1 shows areas where susceptibility values are higher in patients vs controls and QSM^2 shows areas in which susceptibility is lower in patients vs controls.

3.2. Reproducibility study

3.2.1. ICC analysis

Intra-session (TP1-TP2) and inter-session (TP1-TP3) ICCs for qMRI measures are summarized in Table 2.

qT1 exhibited the highest intra-session and inter-session reproducibility (ICCs TP1 vs TP2: 0.83-0.98; ICC TP1 vs TP3: 0.77-0.95, respectively). MWF followed with an intra-session ICC of 0.81-0.98, and an inter-session ICC of 0.50-0.90, with lower ICCs in deep gray matter structures than CC parts (Table 2). Also MTsat and QSM exhibited relatively high ICC in most ROIs (MTsat: intra-session ICC 0.59-0.93 and inter-session ICC 0.67-0.88; QSM: intra-session ICC 0.57-0.93 and inter-session ICC 0.62-0.90, Table 2).

qMRI	Comparison	Splenium	Genu	Putamen	Caudate	Thalamus
MWF	Intra - session	0.94	0.8	0.81	0.89	0.98
	Inter - session	0.90	0.82	0.71	0.50	0.88
qT1	Intra - session	0.86	0.83	0.98	0.92	0.94
	Inter - session	0.95	0.92	0.93	0.77	0.84
MTsat	Intra - session	0.82	0.79	0.85	0.59	0.93
	Inter - session	0.68	0.73	0.77	0.67	0.88
QSM	Intra - session	0.77	0.57	0.91	0.93	0.91
	Inter - session	0.84	0.62	0.81	0.90	0.87

Table 2. ICCs comparison among qMRIs.

3.2.2. Voxel-wise WM reproducibility analysis

For all qMRI measures, WM voxel-wise analysis exhibited no clusters of significant intra- and inter-session differences ($P < 0.01$).

3.2.3. Vertex-wise GM reproducibility analysis

Vertex-wise cortical surface analysis showed very small areas of intra- and inter-session differences for all qMRI measures ($P < 0.01$).

4. Discussion

In this work, we performed a comprehensive assessment of the sensitivity to MS pathology of myelin-sensitive qMRI measures, and of their respective intra-scanner reproducibility.

There are a number of qMRI measures providing information about the integrity of the myelin sheet surrounding the axons in the central nervous system, and each of those exploits different contrast mechanisms to quantify myelin properties(Granziera *et al.*, 2021). Nevertheless, to date, head-to-head comparisons of the sensitivity of these different qMRI measures to focal and diffuse MS pathology are lacking.

Our results showed that qMRI measures such as MWF, MTsat, qT1, and QSM exhibit differential sensitivity to MS pathology in MS plaques and in WM and cortical regions outside areas of focal damage. qT1 showed the highest sensitivity to MS lesions pathology in both WM and cortical GM. This may be due to the broader sensitivity of qT1 to the tissue destruction in CNS encompassing demyelination, axonal degeneration, edema and tissue destruction (Lucchinetti *et al.*, 2000; Lassmann, 2018b), which are predominant within the core of the lesion and present to a smaller extent in the peri-plaque tissue(Rodriguez *et al.*, 1993; Vrenken *et al.*, 2006b; Mustafi *et al.*, 2019; Rahmanzadeh *et al.*, 2021).

Nevertheless, the sensitivity of qT1 to NAWM pathology was the lowest among all qMRI measures. In contrast, MTsat and MWF were the most sensitive to NAWM pathology.Indeed, MWF and MTsat exploit different contrast mechanisms allowing to detect subtle changes in myelin water and lipid/macromolecular content, which may be the consequence of diffuse microglia activation in NAMW as described in neuropathological studies (Rodriguez *et al.*, 1993; Rodriguez and Scheithauer, 1994; Cui *et al.*, 2017).

As to NAGM pathology, qT1 and QSM were the most sensitive measures to assess the consequences of neuroinflammatory and neurodegenerative processes occurring in the cortical ribbon of MS patients (Kutzelnigg *et al.*, 2005; Magliozzi *et al.*, 2007) .

All qMRI measured exhibited high intra and inter-session reproducibility. qT1 obtained with MP2RAGE(Marques *et al.*, 2010) exhibited good-to-excellent ICCs (0.77-0.98) in both WM (i.e.

splenium/genu of corpus callosum) and in deep gray matter structures. Similarly, qT1 showed the high reproducibility in voxel-wise and vertex-wise analyses. It is true that the reproducibility of qT1 measures is highly hardware-, software- and sequence-dependent(Bane *et al.*, 2018); nevertheless, the results obtained in this study by using MP2RAGE confirm the feasibility of reproducible measurements across sessions in a single 3T scanner, which were previously reported (Marques *et al.*, 2010).

Previous reproducibility studies for MTsat imaging using various acquisition/reconstruction methods has shown good to excellent ICC in inter-scanner and intra-scanner in single-center and multi-center studies(Barker *et al.*, 2005; Ropele *et al.*, 2005; Weiskopf *et al.*, 2013). Our results support and extend previous finding by showing an overall good reproducibility for MT in all ROIs except in the caudate (ICC intra-session: 0.59, inter-session: 0.67). Similarly, the voxel-wise WM and vertex-wise cortical analysis showed almost no intra-/inter-session changes in MTsat, a finding that highlights the robustness of MTsat for myelin imaging in a single-scanner and single-center setting.

As to QSM, our results confirm previous reports of high intra-scanner and inter-scanner reproducibility for the applied MEDI reconstruction method and acquisition protocol(Deh *et al.*, 2015). Interestingly, these results are also supported by a multi-center phantom study where the MEDI QSM reconstruction appeared to be highly reproducible (ICC >0.99) among different clinical and preclinical scanners(Deh *et al.*, 2019). Nevertheless, high reproducibility in QSM experiments seems not to be limited to the MEDI reconstruction method, as also other (i.e. the L2 regularization) have shown high intra-scanner reproducibility (Lin *et al.*, 2015; Santin *et al.*, 2017; Choi *et al.*, 2019), supporting the knowledge that QSM provide robust qMRI measures for longitudinal and multicentric studies.

Similarly, confirming one previous study(Nguyen *et al.*, 2016), our work shows that the reproducibility of FAST-T2 MWF maps is high when assessed both with a region of interest and with a voxel-wise or surface-wise approach in both WM and cortical GM. Previous works also showed a high reproducibility of myelin water fraction maps obtained with other acquisition methods such as GRASE and mcDESPOT (multi-component Driven Equilibrium Single Pulse

Observation of T1 and T2,)(Meyers *et al.*, 2009; Lee *et al.*, 2018; Levy *et al.*, 2018), although in this case no voxel-wise and surface-wise comparison was performed.

Our work is unique in that it compares different qMRI measures for both focal and diffuse sensitivity to MS pathology as well as for intra-session and inter-session reproducibility at 3T MRI. Moreover, our study applies qMR measures derived from sequences acquired in a clinically feasible time (acquisition time ranging from 4.5 min for MWF to 9.45 min for MTsat min), providing therefore a reference for future clinical trials or clinical applications of myelin-sensitive qMRI. Besides, this work is based on comprehensive evaluation applying multiple approaches to assess sensitivity and reproducibility in both white and cortical grey matter. On the other hand, our study suffers also from some limitations: out of 17 subjects enrolled in the reproducibility study, only 10 were finally assessed due to motion artifacts derived from the length of the protocol including multiple qMRI sequences. In addition, we did not perform a comparison of the reproducibility among different field strengths, scanners and vendors; future studies will expand our findings to a multi-center setting.

In summary, we demonstrated that myelin-sensitive qMRI measures exhibited differential sensitivity to MS pathology in various brain regions; qT1 and QSM appeared to be the most sensitive to focal MS pathology, while MWF and MTsat were the most sensitive to NAWM alterations and qT1 was most sensitive to NAGM damage. Our study also showed that qT1, MTsat, QSM and MWF exhibit high intra-scanner reproducibility in a single-scanner and in single-center setting, a finding that might facilitate the incorporation of the studied MR techniques in future clinical trials.

2.4. Manuscript 4:

Genetic susceptibility to myelin and axonal injury as measured by myelin water imaging and multi-shell diffusion in multiple sclerosis

In the current work, we studied a cohort of MS patients and healthy controls who benefitted of advanced MRI investigation in the context of the INsIDER study and performed GWAS using NDI and MWF as quantitative traits (QT). Further, a polygenic risk score study was performed to assess the association between (i) cumulative effect of non-MHC (major histocompatibility complex) SNPs showing genome-wide (GW) significance in large-scale MS GWAS (International Multiple Sclerosis Genetics, 2019) and (ii) MWF and NDI in white matter (WM) and WM lesions (WML).

Genetic susceptibility to myelin and axonal injury as measured by myelin water imaging and multi-shell diffusion in multiple sclerosis

Reza Rahmanzadeh[1,2], Stefan Herms[3], Bettina Burger[3], Po-Jui Lu[1,2], Muhamed Barakovic[1,2], Matthias Weigel[1,2], Thanh D. Nguyen[4], Francesco La Rosa[5,6], Yi Wang[4], Meritxell Bach Cuadra[5,6], Ernst-Wilhelm Radue[1], Jens Kuhle[2], Ludwig Kappos[2], Sven Cichon[7], Cristina Granziera[1,2]

[1]*Translational Imaging in Neurology Basel, Department of Medicine and Biomedical Engineering, University Hospital Basel and University of Basel, Basel, Switzerland.*

[2]*Neurologic Clinic and Policlinic, Switzerland, Departments of Medicine, Clinical Research and Biomedical Engineering, University Hospital Basel and University of Basel, Basel, Switzerland.*

[3]*Human Genomics Research Group, Department of Biomedicine, University Hospital and University of Basel, Basel, Switzerland.*

[4]*Department of Radiology, Weill Cornell Medical College, New York, New York, USA.*

[5]*Signal Processing Laboratory (LTS5), Ecole Polytechnique Fédérale de Lausanne (EPFL), Lausanne, Switzerland.*

[6]*Radiology Department, Center for Biomedical Imaging (CIBM), Lausanne University and University Hospital, Lausanne, Switzerland.*

[7]*Institute of Medical Genetics and Pathology, University Hospital Basel, Basel, Switzerland.*

Abstract

Despite several large-scale genome-wide association study (GWAS) for exploring single-nucleotide polymorphism (SNPs) that might increase susceptibility risk for multiple sclerosis (MS), there's no study attempting to explore the relationship between genetic risk factors for MS patients and the extend of myelin and axonal damage as measured by advanced MRI techniques. We applied myelin water and multi-shell diffusion imaging to quantify the relative damage to myelin and axons in MS white matter lesions (WMLs) and in WM in MS patients and healthy controls. We conducted quantitative GWASs (qGWAS) to explore SNPs related to myelin and axonal damage and repair in multiple sclerosis. Further, we calculated poly-genic risk scores (PRS) to assess the association of cumulative effect of known MS non-MHC (major immunohistochemistry complex) SNPs with myelin and axonal damage in MS. 176 multiple sclerosis patients and 104 healthy controls were enrolled in the study. GWASs revealed several SNPs showing association with qMRI measures below the suggestive level of significance ($P< 10^{-5}$), but no SNPs below the genome wide (GW) significance threshold ($P< 5 \times 10^{-8}$): rs3006496, rs1057920, rs9324461, rs9694042, rs4959030, rs3104391, rs3104373 and rs7829745. WM MWF in MS patients was higher in homozygotes for the minor allele of rs3006496 than in heterozygotes than in MS patients that were homozygotes for the major allele ($P<0.0001$). Also, WM NDI in MS patients was lower in homozygotes for the minor allele of rs1057920 & rs9324461than in patients who were homozygotes for the major allele ($P<0.001$, $P<0.01$, respectively). NDI in WML of MS patients was higher in heterozygotes/homozygotes for the minor allele of rs7829745 than in patients who are homozygotes for the major allele ($P<0.001$). PRS were not associated with MWF in WMLs in MS patients and with MWF and NDI in WM of patients and controls ($P>0.05$). On the other hand, PRS were associated with NDI in WMLs in MS patients (beta: -0.0018, $P<0.0001$). These findings (i) suggest novel genetic loci that might be involved in myelin and axonal pathology in MS (ii) provide support for previous evidence that interferon pathway and long non-coding RNAs are involved in MS pathology. Supportive evidence from independent studies is warranted before more firm conclusions can be drawn.

1.Introduction

Myelin and axon pathology are major drivers of neurological disability in multiple sclerosis (MS)(Granberg *et al.*, 2017; Rahmanzadeh *et al.*, 2021). Yet, to date, it is unclear to what extent genetic factors contribute to myelin and axonal damage in MS patients.

Several neuropathology and neuroimaging studies have shown the focal and diffuse damage to myelin and axonal structures in MS brains. MS lesions contain variable amounts of inflammatory infiltrates, myelin and axonal loss (Lucchinetti *et al.*, 2000). Also, the normal-appearing tissue (i.e. white and gray matter areas that do not exhibit signs of focal pathology, NAWM and NAGM) is not healthy and contains diffuse myelin and axonal damage and microglia clusters (Kutzelnigg *et al.*, 2005; Cui *et al.*, 2017; Granberg *et al.*, 2017; Lassmann, 2018a) although to a lesser degree than the lesion (Lieury *et al.*, 2014). The inter-individual heterogeneity in MS lesions and NA tissue has also been shown in neuropathological studies (Barnett and Prineas, 2004; Lassmann, 2018a).

MS is shown to be a poly-genic heritable autoimmune disease with complex interaction with environmental factors. Genome-wide association studies (GWAS) identified 200 genomic loci outside MHC (major histocompatibility complex) region that might increase the risk to develop MS (International Multiple Sclerosis Genetics *et al.*, 2007; International Multiple Sclerosis Genetics *et al.*, 2013; International Multiple Sclerosis Genetics, 2019). Almost all the genomic loci associated with MS susceptibly are located in the vicinity of immune genes and none has been so far related to components of the central nervous system (International Multiple Sclerosis Genetics, 2019). Several studies have summarized the cumulative effect of those SNPs in poly-genic risk score (PRS) and have shown association between PRS and quantitative MRI measures and CSF antibody production in MS subjects(Goris *et al.*, 2015; Smets *et al.*, 2021).

Myelin water imaging (MWI) quantifies the water between myelin layers by distinguishing multiple water components in T2 relaxometry data and maps MW fraction (WMF), which has been validated postmortem (Nguyen *et al.*, 2016) Neurite orientation dispersion and density imaging (NODDI) mathematically models multi-shell diffusion data to measure axon and dendrite density (neurite density index, NDI) in the CNS(Zhang *et al.*, 2012).

In the current work, we studied a large cohort of MS patients and healthy controls and performed GWAS with NDI and MWF in white matter (WM) and WM lesions (WMLs) as quantitative traits (QT). Further, a poly-genic risk score study was performed to assess the association of cumulative effect of non-MHC SNPs showing genome-wide (GW) significance level in MS large-scale GWAS(International Multiple Sclerosis Genetics, 2019) with MWF and NDI in WM and WMLs.

Keywords

multiple sclerosis; genome-wide association study; poly-genic risk score; myelin water imaging; diffusion microstructural modeling.

2. Materials & Methods

2.1. Participants

We enrolled 176 MS patients and 104 healthy controls. The inclusion criteria were: (i) MS diagnosis based on McDonald criteria 2018 (Thompson *et al.*, 2018) and diagnosis of active RRMS or inactive PMS as defined by Lublin et al. (Lublin *et al.*, 2014); (ii) lack of any concomitant psychiatric or neurological disease (excluding headache); (iii) lack of contraindication to MRI. The ethical review committee of the University Hospital Basel (IRB of Northwest Switzerland) approved the study, and all participants entered the study following written consent.

2.2. MR acquisition and metrics computation

MRI was performed on a 3T whole-body MR system (Magnetom Prisma, Siemens Healthcare, Erlangen, Germany) using a 64-channel phased-array head and neck coil for radio frequency reception. The MRI protocols included: (i) 3D FLAIR (TR/TE/TI=5000/386/1800 ms) and MP2RAGE (TR/TI1/TI2=5000/700/2500 ms) both with 1 mm^3 isotropic spatial resolution; (ii) Fast Acquisition with Spiral Trajectory and adiabatic T2prep (FAST-T2) (spiral TR/TE = 7.5/0.5 ms, six T2prep times = 0 (T2prep turned off), 7.5, 17.5, 67.5, 147.5, 307.5 ms, voxel size = 1.25x1.25x5 mm^3, scan time = 4.5 min, as described in (Nguyen *et al.*, 2016); (iii) multi-shell diffusion (TR/TE/δ/Δ/resolution = 4.5 s / 75 ms / 19 ms / 36 ms / 1.8 mm^3 isotropic with b-values 0 / 700 / 1000 / 2000 / 3000 s/mm^2 with 12/6/20/45/66 measurements, respectively, per shell and a diffusion acquisition with 12 measurements of b-value 0 s/mm^2 with reversed phase encoding.

MWF maps were reconstructed using FAST-T2 data as previously proposed. In FAST-T2, the robustness of the MWF map against noise propagation is achieved by judiciously sampling the T2 signal at a very short TE (0.5 ms) to maximize sensitivity to the fast-decaying myelin water component, and also by utilizing a local spatial smoothing constraint in the multi-exponential data fitting (Kumar *et al.*, 2012).

NODDI (Zhang *et al.*, 2012) is a state-of-the-art model aiming at characterizing the neurite density and orientation dispersion, thereby helping to characterize axonal integrity in the brain Diffusion images were denoised and corrected for motion and eddy-currents (Andersson and Sotiropoulos, 2016).

2.3. Lesion identification and segmentation

Automatic segmentation of WM lesions was performed by using an in-house deep-learning based method (La Rosa *et al.*, 2020). This approach consists of a cascade of two convolutional neural networks and was adapted to take as input FLAIR and MP2RAGE MRI contrasts. Manual correction of automatic WM lesion masks was performed on FLAIR (by RR and CG).

2.4. WM segmentation

To segment the brain into whole WM, cortex, deep grey matter structures, and ventricles we used the imaging software package FreeSurfer (v.6.0, surfer.nmr.mgh.harvard.edu) (Fischl, 2012).

2.5. Extraction of DNA and Microarray genotyping

Lymphocyte DNA from enrolled subjects were extracted from blood sample. DNA samples were genome-wide genotyped using Infinium GSA-24 v3.0 (Illumina, Inc., San Diego, CA, USA) and quality control of raw genotypes was performed as explained in (Caspers *et al.*, 2020),(Marees *et al.*, 2018).

2.6. GWAS and PRS studies

Nineteen subjects were excluded following GWAS QC (n = 4) or because of incomplete or artefactual genetic or MRI data (n = 15). Case-control GWAS and Quantitative GWAS (qGWAS) with age and sex as covariate was performed using PLINK 1.9 (Purcell *et al.*, 2007) . In total, we performed four qGWAS analyses where we used the following QTs (i) MWF in WM; (ii) NDI in WM; (iii) MWF in WML for MS patients and MWF in WM for controls; (iv) NDI in WML for MS subjects and NDI in WM for controls. The asymptomatic P values and odds ratio (OR) for SNPs association with disease/qMRI measures were reported.
Because we were interested to focus on loci with evidence of the highest probability of being associated with MS, we selected SNPs that provide genome-wide significance and evidence for replication in large-scale GWAS performed by International Multiple Sclerosis Genetics Consortium (IMSGC)(International Multiple Sclerosis Genetics, 2019). Poly-genic risk scores

(PRS) for those non-MHC SNPs (n = 127) were calculated in PLINK1.9 (Purcell *et al.*, 2007): the allele count for each SNPs was weighted by the log of odds ratio from large-scaled GWAS and summed across 127 non-MHC SNPs showing GW significance in(International Multiple Sclerosis Genetics, 2019).

Best-fit model PRS was performed in PRSice v2: poly-genic risk score software (https://www.prsice.info/) with the default settings (*i.e.*, SNPs were clumped in 250-kb windows on either side of target SNPs using clump-r2 and clump-p thresholds of 0.1 and 1, respectively)(Euesden *et al.*, 2015).

2.7. Statistical analysis

We studied the association of individual PRS score with MWF and NDI in WMLs and WM in MS subjects using linear regression models (with age and sex as covariates) in GraphPad Prism 8.0.0 for Windows, GraphPad Software, San Diego, California, USA. To further analyze the association of individual SNPs with myelin and axonal damage in MS, MRI measures in subjects with different genotypes regarding that particular SNP (i.e. different copy number of minor allele) were compared using a non-parametric Kruskal Wallis test with Dunn's test for multiple comparison correction. In addition, the average PRS was compared between patients and controls using non-parametric Mann-Whitney-Test.

3. Results:

3.1. GWAS analyses

3.1.1. Case-control GWAS

We did not find any SNPs showing an association with MS below the GW significance threshold ($P < 5 \times 10^{-8}$). However, case-control GWAS revealed 43 SNPs showing association below the suggestive level of significance ($P < 10^{-5}$). Out of those SNPs, 37 were on chromosome (CHR) 6 in MHC region and 6 were non-MHC SNPs (Table 1).

CHR	SNP	MA	OR	P	GENE
8	rs12681042	T	2.59	2.7E-06	LOC105375773 : Intron Variant
11	rs7938244	G	0.41	2.2E-06	TMEM45B-LINC01395
11	rs63702661	G	0.43	7.1E-06	TMEM45B-LINC01395
12	rs527118	T	0.34	1.2E-06	SLC6A13 : Intron Variant
14	rs12588287	C	0.41	9E-06	ATXN3 : Intron Variant
14	rs8020781	C	0.41	9E-06	ATXN3 : Intron Variant

Table 1. Non-MHC susceptibility SNPs that showed association with MS traits in our case-control GWAS. CHR: Chromosome, SNP: Single nucleotide polymorphism, MA: Minor allele, P: asymptomatic P value.

3.1.2. qGWAS analyses

QT (i): MWF in WM

We did not find any SNPs showing an association with MWF in WM below the GW significance threshold ($P < 5 \times 10^{-8}$). However, GWAS revealed that rs3006496 on CHR 10 shows association with MWF in WM below the suggestive level of significance (beta = 0.23, P = 3.95E-06; table 2).

QT (ii): NDI in WM

We did not find any SNPs showing an association with NDI in WM below the GW significance threshold ($P < 5 \times 10^{-8}$). However, GWASs revealed that rs1057920 on CHR 1 (beta = -0.0128, P = 2.94E-06) and rs9324461 on CHR 8 (beta = -0.0131, P = 3.7E-06) show association with NDI in WM below the suggestive level of significance (Table 2).

QT (iii): MWF in WMLs for MS patients and MWF in WM for controls

We did not find any SNPs showing an association with MWF in WMLs below the GW significance threshold ($P < 5 \times 10^{-8}$). However, GWAS revealed that rs9694042 on CHR 8 shows association with MWF in WMLs below the suggestive level of significance (beta = -0.5308, P = 5.46E-06; table 2).

QT (iv): NDI in WMLs for MS patients and NDI in WM for controls

We did not find any SNPs showing an association with NDI in WM below the GW significance threshold ($P < 5 \times 10^{-8}$). However, GWAS revealed that rs7829745 on CHR 8 (beta = 4.81, P = 2.52E-06) and rs4959030 on CHR 6 (beta = -4.65, P = 5.32E-06) shows association with NDI in WMLs below the suggestive level of significance (table 2).

CHR	SNP	MA	BETA	P	GENE
10	rs3006496	C	0.23	3.95E-06	LOC101929279-RNU6-598P
1	rs1057920	G	-0.0128	2.94E-06	IFI44L : 3 Prime UTR Variant
8	rs9324461	C	-0.0131	3.7E-06	LOC105375776 : 2KB Upstream Variant
8	rs9694042	G	-0.5308	5.46E-06	BNIP3L-DNAJB6P2
6	rs4959030	A	-4.65	5.32E-06	HLA-DRB1 – LOC107986589
6	rs3104391	T	-4.54	8.68E-06	LOC107987449 LOC107987459
6	rs3104373	T	-4.65	5.32E-06	LOC107987449 : Intron Variant LOC107987459 : Intron Variant
8	rs7829745	C	4.81	2.52E-06	C8orf37-AS1 : Intron Variant

Table 2. SNPs that showed association with quantitative traits in one of four qGWASs. CHR: Chromosome, SNP: Single nucleotide polymorphism, MA: Minor allele, P: asymptomatic P value.

3.2. Non-MHC PRS analysis

The average PRS made out of 127 non-MHC SNPs showing association below GW significance level in IMSGC GWAS was significantly higher in patients compared with healthy subjects (P<0.001; Figure 1.).

PRS were not associated with MWF in WMLs in MS patients and with MWF and NDI in WM of patients and controls (P>0.05). On the other hand, PRS were associated with NDI in WMLs in MS patients (beta: -0.0018, P<0.0001).

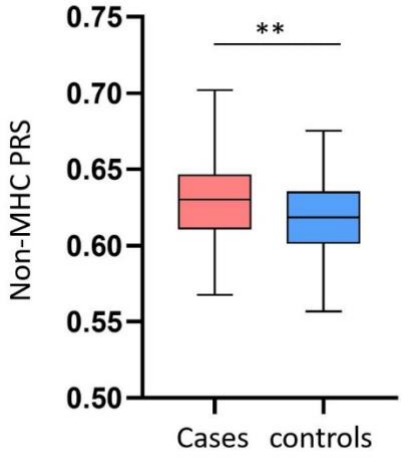

Figure 1. Non-MHC PRS that were significantly higher in patients vs controls (** P<0.001).

3.3. Association of risk allele carrier status and qMRI measures

Interestingly, WM MWF in MS patients was higher in homozygotes for the minor allele of rs3006496 than in heterozygotes (P<0.001) and in heterozygotes WM MWF was higher than in MS patients that were homozygotes for the major allele (P<0.01). Also, WM NDI in MS patients was lower in homozygotes for the minor allele of rs1057920 & rs9324461than in patients who were homozygotes for the major allele (P<0.001, P<0.01, respectively). NDI in WML of MS patients was higher in heterozygotes/homozygotes for the minor allele of rs7829745 than in patients who are homozygotes for the major allele (P<0.001) (Figure 2.).

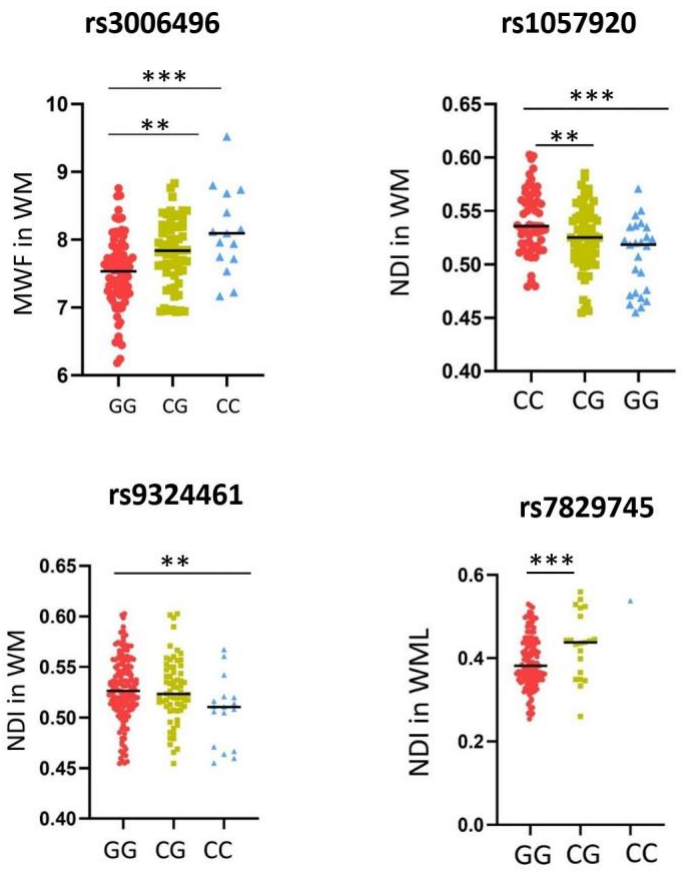

Figure 2. Association between SNPs carrier status and qMRI measures (**P<0.01; ***P<0.001).

3.4. Best-fit model PRS

The average PRS calculated using best-fit model approach implemented in PRSice v2 was significantly higher in patients compared with controls (P<0.0001; Figure 3.).

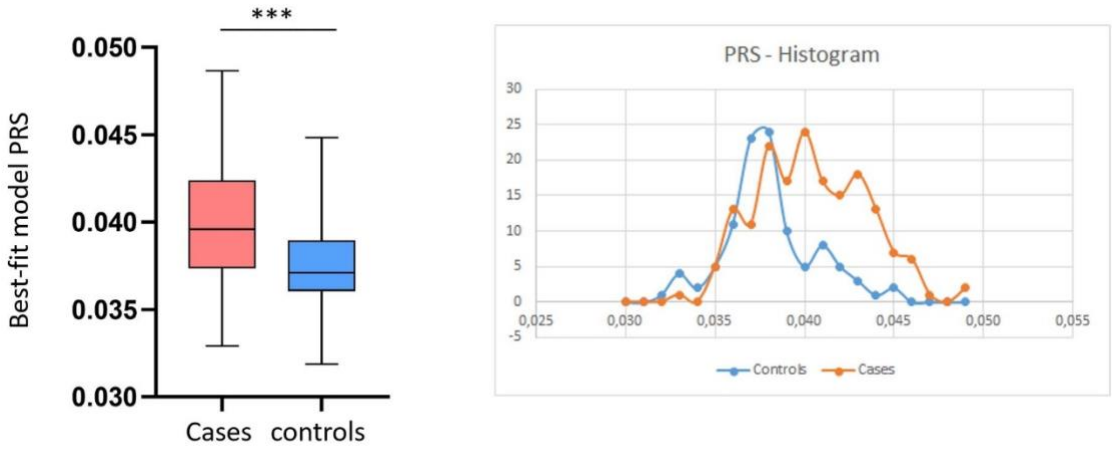

Figure 3. Best-fit PRS is significantly higher in patients vs controls (*** P<0.0001).

4. Discussion & Conclusion

In this study, we found evidence for novel genomic loci that may be associated with myelin and axonal damage measured using MWF and diffusion maps *in vivo* in MS patients. These genomic loci were located in vicinity of genes with strong evidence of involvement in MS pathology (e.g. interferon pathway). Further, we studied the cumulative effect of non-MHC SNPs by calculating PRS scores and have shown that non-MHC PRS are well correlated with NDI in WMLs in MS.

MHC was the susceptibility locus that has been first identified with high probability of association with MS and high evidence for replication and previous studies has shown that MHC region harbors many independent SNPs(Parnell and Booth, 2017). Particularly, it has been shown that an allele from the MHC class II HLA-DRB1 gene, HLA-DRB1*15:01 elevates MS risk about threefold(Goodin *et al.*, 2021). In accordance, 37/43 SNPs showing association below the suggestive significance level (P<10 -5) in our case-control GWAS were located in or in vicinity of MHC region.

In addition, previous large-scaled GWAS have identified 200 SNPs outside the MHC regions showing GW significance and were independently replicated e.g. IL2RA (CD25), CD58 (LFA3),

CLEC16A (KIAA0350) and EVI5(Alcina *et al.*, 2008; Hoppenbrouwers *et al.*, 2008; Weber *et al.*, 2008; Baranzini *et al.*, 2009; International Multiple Sclerosis Genetics, 2019). Gene function annotation and pathway enrichment analyses have shown that those non-MHC SNPs map to adaptive and innate immune systems and non is related to CNS (Baranzini *et al.*, 2009; International Multiple Sclerosis Genetics, 2019).

Our case-control GWAS has identified six non-MHC SNPs showing association with MS below the suggestive level of significance. Out of those non-MHC SNPs, rs527118 is located in SLC6A13 gene involved in GABA (gamma-Aminobutyric acid)-ergic signaling and is responsible for an autosomal recessive neurodegenerative disorder Cerebral Creatine Deficiency Syndrome 2 that is characterized by developmental delay and cognitive disturbance (Farr *et al.*, 2020). An impaired GABAergic signaling in MS has been previously suggested (De Stefano and Giorgio, 2015; Cao *et al.*, 2018; Gao *et al.*, 2018). Interestingly, it has been shown that the expression of GABA transported-2 (the protein coded by SLC6A13 gene) is altered in MS, which might also play a role in abnormal inflammatory response observed in MS (Paul *et al.*, 2014). In addition, our results found two other non-MHC SNPs rs12588287 & rs8020781 that are located in ATXN3 gene and are involved in Akt signaling pathway. ATXN3 mutation is responsible for Machado–Joseph disease, an autosomal dominant neurodegenerative disorder of late onset (Bettencourt *et al.*, 2010). Akt/mTOR signaling pathway is a major regulator of T cell response and its involvement has been shown in autoimmune disorders including MS (Jung *et al.*, 2018; Mammana *et al.*, 2018).

Our qGWAS analyses revealed several SNPs that exhibit an association with qMRI measures in MS WM lesions and in WM below the suggestive level of significance. Our results showed that rs1057920 – a SNP located in the IFI44L gene belonging to the interferon pathway – is associated with NDI in WM in MS patients, confirming previous evidence of the involvement of interferon pathway in MS pathology(Crow *et al.*, 2019). Interestingly, a previous study using DNA microarray technology has shown that the expression of IFI44L is increased in peripheral blood cells in MS subjects compared with healthy subjects(van Baarsen *et al.*, 2006). Previous studies have identified several long non-coding RNAs (lncRNAs) to be associated with MS(Yang *et al.*, 2018), which have mainly been over-expressed in microglia(Sun *et al.*, 2017) or Th1/Th17 cells(Zhang *et al.*, 2017), components of innate and adaptive immune system. In

accordance, the association between rs7829745 & rs9324461 and NDI in WML and in WM, respectively, in our study supports the increasing evidence of a role of lncRNAs in MS(Yang *et al.*, 2018) .

The average PRS made out of SNPs out of MHC region was higher in MS patients than in controls, a finding that confirms the enrichment of IMSGC non-MHC SNPs in MS patients versus healthy subjects.

The non-MHC susceptibility PRS was associated with NDI in MS WMLs. Indeed, the association of both rs4959030 – a SNP that is located close to the MHC region on CHR 6 - and the polygenic non-MHC risk scores for MS with lower surrogate measures of axonal damage (NDI) in WML might suggest a possible genetic substrate of axonal degeneration in MS and a similarity in pathogenetic pathways leading to MS emergence and axonal damage in MS.

In conclusion, our results suggest several SNPs with potential associations with myelin and axonal amount in MS brains, which might help us to better understand the processes driving myelin and axonal injury in MS. These data require further confirmation in different and larger cohorts of MS patients.

3. Discussion, future works & conclusion

Myelin and axon damage are major pathological drivers of neurological disability in multiple sclerosis (MS) (Lassmann, 2018b). Neuropathological postmortem studies have shown that the extent of myelin and axon damage is different among MS lesions, i.e. lesions in different locations and at different stages of development (Barnett and Prineas, 2004; Metz *et al.*, 2014). Confirmatory to that, previous in vivo qMRIs have revealed the extent of myelin and axonal focal/diffuse alterations in MS by exploiting measures such as T1 relaxometery, myelin water fraction, magnetization transfer ratio, median diffusivity and fractional anisotropy (Enzinger *et al.*, 2015). However, a comprehensive study of the interplay of myelin and axon damage in various MS brain regions in both WM and GM was still lacking.

In the first part of my doctoral work, I have concomitantly assessed MWF and NDI as measured by MWI and multi-shell diffusion MRI to explore the interplay between myelin and axonal damage in different types of focal lesions (in both WM and the cortex), in normal-appearing tissue, and across MS subtypes compared to healthy subjects. Adding to previous knowledge, our work showed a broader decrease in axonal density than in myelin content in NAWM. Consistent with our results, neuropathological investigations of NAWM have shown that primary demyelination, in contrast to microglial activation and axonal transection, is not a frequent finding in NAWM (Bjartmar *et al.*, 2001; Kutzelnigg *et al.*, 2005; Marik *et al.*, 2007). Furthermore, in a large majority of lesions the relative axonal damage outweighed myelin damage. Hence, a novel finding of the present work is the presence of axonal damage independent of demyelination in both focal WML and in NAWM (Lucchinetti *et al.*, 1999; Solanky *et al.*, 2001; Patrikios *et al.*, 2006). These findings are in line with previous studies showing a very early diffuse reduction of a N-acetylaspartate in NAWM in RRMS patients (Narayana *et al.*, 1998) and an increase in lipid levels at the site of future MS lesions (Filippi *et al.*, 1998), and suggest that surrogate measures of axon damage like the ones derived from models applied to multi-shell diffusion MRI are sensitive to capture subtle axon-related damage in MS patients. Further, this work confirmed the neuropathological findings that myelin/axonal structures are more damaged in PV lesions and paramagnetic rim lesions (PRL) than in JC lesions and in non-PRLs (Patani *et al.*, 2007; Absinta *et al.*,

2018). We found that MWF and NDI in WML – and not in normal-appearing tissues – are well associated with disability and sNfL, confirming previous reports by showing that MTR is mostly related to disability when measured in lesions (Amann *et al.*, 2015). Yet, despite the applied measures demonstrate good sensitivity to pathological changes in MS patients, those measures lack specificity for both myelin and axon damage. In this regard, we have statistically modeled the contribution of both NDI and MWF to the separation of lesion, normal-appearing and healthy tissue, hereby showing that NDI is providing statistically independent information from MWF to achieve an optimal separation of tissue-types in WM. In addition, the NODDI diffusion model suffers from several strong assumptions: fixed diffusivity for all the voxels in the brain tissue whole-brain voxels; and applicability to single-bundle voxels (very few locations in the brain). Because of this, we additionally reconstructed multi-shell diffusion data using the MCDMI model, which integrates the spherical mean technique to handle orientation dispersion and fiber crossing populations, allowing more accurate estimations in whole-brain voxels (Kaden *et al.*, 2016; Bagnato *et al.*, 2018). And the MCDMI model also confirmed our findings from NODDI model. Future studies should extend this approach to the data collected at two-year follow-up in this cohort of patients within the INsIDER study. In addition, it would be interesting to compare the two-year follow-up of lesions with predominant damage to myelin versus axon, and to study the evolution of myelin/axon alterations in NAWM areas with the diffuse axonal changes measured using the TFCE voxel-wise analysis.

MS lesions have been characterized by a variable extent of myelin/axon damage and repair and iron content (Lassmann, 2018a) and distinguished neuropathologically based on their characteristics (Kuhlmann *et al.*, 2017). Nevertheless, the distinction of chronic MS lesion types *in vivo* (i.e., remyelinated vs chronic active/smoldering vs chronic inactive) remains challenging. Several previous efforts to identify neuropathological MS lesion types in vivo, particularly the remyelinated lesions, failed to find an accurate in vivo MR surrogate (Lubetzki *et al.*, 2020). In the attempt to overcome the limitations of previous studies, we applied a multi-contrast quantitative MRI - including QSM, myelin

water imaging (MWI) and diffusion MRI - to disentangle lesion phenotypes *in vivo* in MS patients.

Our multi-parametric cross-sectional and longitudinal data, together with our double-blinded postmortem analyses showed that QSM maps permit the classification of neuropathological MS lesions with various extents of damage and repair to myelin and axons, hereby providing highly sensitive and specific biomarkers of completed remyelination in a clinical setting. Further, the proposed approach provided a perspective to evaluate the repair capacity of existing and novel MS therapies using a single scan. One limitation of this study was the high number of lesions excluded from the classification because of being affected by artifacts or containing multiple/big vessels, which are typically hyperintense in QSM images. Ongoing works aimed at improving QSM algorithms to reduce the effect of the streaking artifacts might allow inclusion of those lesions in future works. The other limitation of the study is the small sample size in longitudinal analysis to study the evolution of remyelinated lesions. Currently, in the context of INsIDER project almost 200 subjects have undergone follow-up MRI and hence the longitudinal analysis could be extended. Ongoing additional work in our group is also trying to disentangle the iron from the myelin contribution to the QSM signal by applying a very recent method developed by some collaborators i.e magnetic susceptibility source separation- 'chi-separation'(Shin *et al.*, 2021).

There are a number of qMRI measures providing information about the integrity of the myelin sheet surrounding the axons in CNS, and each of those exploit different contrast mechanisms to quantify myelin properties (Granziera *et al.*, 2021). Previous reproducibility studies have shown controversial reports and/or are limited by qMRIs that are not clinically applicable (Granziera *et al.*, 2021). In addition, there are few studies investigating how these measures compare to each other in terms of sensitivity to MS damage (van der Weijden *et al.*, 2021).

Therefore, another aspect of my work was to perform a comprehensive evaluation of the sensitivity of myelin-sensitive qMRI measures to MS pathology, with regard to changes in both focal lesions and NA tissue. Furthermore, I have assessed and compared the intra-

scanner reproducibility of myelin-sensitive qMRIs acquired within and across scanning sessions in a single 3T MR system.

In this study, we found that all qMRI measures such as MWF, MTsat, qT1, and QSM are highly reproducible and exhibit differential sensitivity to MS pathology in MS plaques and in WM and cortical regions outside areas of focal damage: MTsat and MWF were more sensitive to NAWM pathology, while qT1 and QSM are more sensitive to focal MS pathology. This finding showed that different qMRIs - by capturing different biophysical properties of tissue - are sensitive to different pathological mechanisms in MS.

One limitation of this work relies in its intra-scanner single-center design; studies should expand the current findings to other scanner types from the same or from other vendors.

MS is a multifactorial autoimmune disease which is likely the result of complex interactions between common genetic and environmental risk factors. Genome-wide association studies (GWAS) identified 200 genomic loci outside MHC (major histocompatibility complex) region that might increase the risk to develop MS (International Multiple Sclerosis Genetics *et al.*, 2007; International Multiple Sclerosis Genetics *et al.*, 2013; International Multiple Sclerosis Genetics, 2019). Almost all the genomic loci associated with MS susceptibly are located in the vicinity of immune genes, especially MHC region. Despite several large-scale GWAS for exploring SNPs that might increase susceptibility risk for MS, there was so far no study attempting to explore the relationship between genetic risk factors for MS patients and the extend of myelin and axonal damage within the brain, as measured by advanced MRI techniques. As a result, there's no information on the genetic factors associated with axonal and myelin pathology in MS.

We conducted quantitative GWASs to explore SNPs related to myelin and axonal damage and repair in MS patients. Further, we calculated poly-genic risk scores (PRS) to assess the association of cumulative effect of known MS non-MHC SNPs with brain myelin and axonal damage. Our study found several novel SNPs with association with MS disease or the damage/repair to myelin and axonal components, which – if confirmed in other cohorts -might help to shed light on the pathogenic mechanism involved in MS pathogenesis or myelin/axonal injury in MS.

As an example, our results show that rs1057920 – a SNP located in the IFI44L gene belonging to the interferon pathway – showed an association with axonal content in WM in MS patients, confirming previous evidence of the involvement of interferon pathway in MS pathology(Crow *et al.*, 2019). In addition, some SNPs such as rs7829745 & rs9324461 showed association with axonal content in WML and in WM, respectively, support the increasing evidence of a role of long non-coding RNAs in MS (Yang *et al.*, 2018) .The non-MHC susceptibility PRS was associated with axonal content in MS WMLs. Indeed, the association of both a SNP that is located close to the MHC region and the polygenic non-MHC risk scores for MS with lower surrogate measures of axonal damage in WML might suggest a possible genetic substrate of axonal degeneration in MS and a similarity in pathogenetic pathways leading to MS emergence and axonal damage in MS.

One major limitation of our study is the sample size that is relatively small for genome-wide studies. The incorporation of Swiss MS Cohort data and other MS cohorts with advance MRI data is necessary for confirmation and replication of our results.

As a conclusion of this multi-faceted doctoral investigation, we have generated new hypotheses about mechanisms leading to myelin and axonal damage in living patients suffering for MS. These results will pave the way for future investigations in multi-centric settings and in larger cohorts, which will further extend these finding with the final goal of elucidating what drives disability progression in a complex neurological disorder such as multiple sclerosis.

4. Contributions by the PhD student

During my PhD, I had the opportunity to acquire a number of essential experience and skills and explore my scientific way for future career. The collaborative nature in the ThINk group improved my project management and data analysis knowledge. Attendance to highly comprehensive courses improved my basic knowledge in a wide range of MR-related topics including principle of medical imaging, MR acquisition and MR physics, and image post-processing domains including segmentation and registration, and deep mathematical approaches e.g. optimization algorithms and deep learning models. Finally, I've been able to develop a unique insight into the basics of medical image development and post-processing. Further, the other courses improved my molecular/biological knowledge regarding genetic mechanisms and epigenetic modification and the state-of-the-art methods for genome-wide analyses and enabled me to perform genetic analyses using genetics software such as PLINK and PRSice for the qMRI GWAS study outlined above. I further improved my ability in performing statistical analyses with different statistical tools including STATA and SPSS, thereby I could perform statistical analyses of the studies outlined in this thesis. Working alongside colleagues with programming skills helped me a lot to retrieve my programming ability during my student Olympiad in Iran and learn how to write python/bash scripts.

Moreover, for the reproducibility study -that is reported above- I've been involved and highly engaged in all steps of the project from subject selection and enrollment, arranging MRI appointment in contact with radiology ward staff, quantitative MRI reconstruction, using advanced MRI toolboxes e.g. SPM MATLAB, FreeSurfer and FSL for neuroimaging analysis, performing statistical analysis and writing/revising the manuscript under supervision of my PhD supervisor. Therefore, I think I had the opportunity to experience a full project management during this work in my PhD.

My presentation skills have gradually improved along with my experience in the conferences and during my PhD, I had several oral presentations and talks in well-known MRI and MS congresses such as European Committee for Teaching and Research in Multiple Sclerosis 2020 (ECTRIMS), MS International Federation Symposium 2019, the International Society for Magnetic Resonance in Medicine 2021 (ISMRM). My ability to collaborate with people from different backgrounds also improved greatly due to the diverse

nature of the ThINk group, strong collaboration with labs in Italy, USA, Germany, South Korea and Australia. My ability for leadership was also developed by participating in the supervision of master projects, through that I have learned how to convey knowledge/expertise in an effective way.

5. Curriculum Vitae

5.1. Personal information

Name: Reza Rahmanzadeh, MD, PhD Candidate

Nationality: Iranian

Date of birth: 21 March 1992

Place of birth: Amol, Iran

Marital status: Married

Languages: English (TOEFL Certificate); German (Goethe B2 Certificate); Persian (Native language); Arabic (Basic)

5.2. Educational status

- 2003-2010 Secondary School at Shahid Beheshti High School (The National Organization for Development of Exceptional Talents), Amol, Iran.

- 2010-2016 Medical student at Iran University of Medical Sciences (IUMS), Tehran, Iran.

- 2016-2018 Medical internship at Iran University of Medical Sciences (IUMS), Tehran, Iran.

- 2018 Oct-Now PhD-Candidate, Department of Biomedical Engineering, Universität & Universitätsspital Basel, Switzerland

5.3. Honors & Awards

- **2021** "**Magna Caum Laude**", International Society for Magnetic Resonance in Medicine (ISMRM) Merit Award.
- **2021 The prize-winner for the best work in quantitative MRI SG**, International Society for Magnetic Resonance in Medicine (ISMRM).
- **2021** "**Swiss Government Excellence Scholarships"**, Extended.
- **2020** "**Magna Caum Laude**", International Society for Magnetic Resonance in Medicine (ISMRM) Merit Award.
- **2020&2021** "**Young Investigator Grant**", Joint American & European Committee for Treatment and Research in Multiple Sclerosis (ACTRIMS & ECTRIMS).
- **2020** "**Swiss Government Excellence Scholarships"**, Extended.
- **2020&2021** "**Educational Scholarship**", International Society for Magnetic Resonance in Medicine (ISMRM).
- **2019 McDonald Fellowship, Multiple Sclerosis International Federation (MSIF)**.
- **2019** "**Young Investigator Grant**", European Committee for Treatment and Research in Multiple Sclerosis (ECTRIMS).
- **2019 Swiss Government Excellence Scholarships**.
- **2016 Du Pre Grant, Multiple Sclerosis International Federation (MSIF)**.
- **2016 Best Young Investigator Reward**, Basic & Clinical Neuroscience Congress, Tehran, Iran.
- **2015 Bronze medal (Rank 3 nationwide)**, National Medicine Olympiad, Tehran, Iran.
- **2010 Rank 103** among 673919 participants in National University Entrance Exam in the Natural Sciences Group at the age of 16, June 2009.
- **2009 Silver medal (Rank 2 nationwide)** in the National Astronomy Olympiad, Tehran, Iran.
- **2008 Gold medal (Rank 1 nationwide)** in the National Mathematics Olympiad, Tehran, Iran.
- **2019-Now** Member of **European Academy of Neurology**.
- **2010-Now** Member of **Iran's National Elites Foundation**.
- **2003-Now** Member of **National Organization for Development of Exceptional Talents.**

5.4. Clinical & Research Experience in Neurology, Neuroradiology and Neuroscience

- **2020 Sep-2021 Jan (part-time)** Neurology training under supervision of Prof. Dr. Cristina Granziera, University Hospital Basel, Basel, Switzerland.
- **2019-2020** MRI evaluation for Swiss MS Cohort Study (SMSC), University Hospital Basel, Basel, Switzerland. I evaluated about 5000 conventional MRIs alongside Prof. Dr. Ernst-Wilhelm Radue and participated in research projects for cross-sectional and longitudinal magnetic resonance images (MRIs) analysis of MS lesions.
- **2018 Oct- now** PhD student ("Myelin/Axonal brain damage and genetic susceptibility in multiple sclerosis: a GWAS-advanced MRI coupled study" under supervision of Prof. Dr. Cristina Granziera, University of Basel, Basel, Switzerland).
- **2018 Feb-2018 Oct** Research assistant in neuroradiology at Biomedical Research & Training (BMRT), Universitätsspital Basel, Basel, Switzerland. I performed several neuroimaging research alongside Prof. Dr. Ernst-Wilhelm Radue.
- **2017 Mar-2017 Sep** Multiple Sclerosis International Federation (MSIF)-funded researcher under supervision of Prof. Dr. Wolfgang Brueck at the department of Neuropathology, Universitätsmedizin Göttingen, Göttingen, Germany. I investigated alongside Prof. Dr. Wolfgang Brueck the potential misfunction of mTOR signaling pathway in oligodendrocyte progenitor cells in active MS lesions in post-mortem samples of MS brain.
- **2016-2018** Internship at the neurological Policlinic, Rasoul- Akram Hospital, Tehran, Iran. I have visited 1000s of patients with neurological conditions including multiple sclerosis, stroke, movement disorders e.g., Parkinsonism's disease and Alzheimer's disease.
- **2016-2018 (part-time)** Neurology resident under supervision of Prof. Dr. Mohammad Ali Sahraian (vice-president of Iranian multiple sclerosis society). I have visited about 1000 patients with multiple sclerosis and 300 patients with neuromyelitis optica and evaluated many brain and spinal cord MRIs.
- **2016-2018 (part-time)** Neurology resident under supervision of Prof. Dr. Mansoure Toghae (president of Iranian headache society). I have visited about 500 patients with headache and performed several research projects on the therapy of patients with migraine and idiopathic intracranial hypertension.

- **2014-2018** Research assistant at Sina Multiple Sclerosis Center, Sina hospital, Tehran, Iran. I performed several neuroimaging research projects alongside Prof. Dr. Mohammad Ali Sahraian.
- **2011-2014** Research assistant at Cellular and Molecular Research Center, Iran University of Medical Sciences, Tehran, Iran. I performed several molecular research projects on excitatory GABA neurotransmitter in temporal lobe epilepsy and schizophrenia both in patients and in animal models alongside Prof. Dr. Mohammad Taghi Joghataei (president of Iranian Neuroscience society).

5.5. Publications

- Google Scholar link: https://scholar.google.com/citations?user=ryMkovIAAAAJ&hl=en
- ORCID link: https://orcid.org/0000-0002-5091-0585

1. Pietro Maggi, Jens Kuhle, Sabine Schaedelin, Franziska Van der Meer, Reza Rahmanzadeh, Pascal Benkert, Francesco La Rosa, Meritxell Bach cuadra, Pascal Sati, et al. **Chronic White Matter Inflammation and Serum Neurofilament Levels in Multiple Sclerosis.** Neurology: Neuroimmunology & Neuroinflammation (2021). August 10, 2021; 97 (6).
2. Oechtering J, Schaedelin S, Benkert P, Müller S, Achtnichts L, Vehoff J, Disanto G, Findling O, Fischer-Barnicol B, Orleth A, Chan A**. Intrathecal Immunoglobulin M synthesis is an independent biomarker for higher disease activity and severity in multiple sclerosis.** Annals of Neurology. ANN NEUROL 2021;90:477–489.
3. Lu PJ, Barakovic M, Weigel M, Rahmanzadeh R, Galbusera R, Schiavi S, Daducci A, La Rosa F, Bach Cuadra M, Sandkühler R, Kuhle J. **GAMER-MRI in Multiple Sclerosis Identifies the Diffusion-Based Microstructural Measures That Are Most Sensitive to Focal Damage: A Deep-Learning-Based Analysis and Clinico-Biological Validation.** Frontiers in neuroscience. 2021 Apr 6;15:258.
4. Rahmanzadeh R, Lu PJ, Barakovic M, Weigel M, Nguyen TD, Spincemaille P, Schiavi S, Daducci A, La Rosa F, Reich DS, Sati P, et al. **Myelin and axon pathology in multiple sclerosis assessed by myelin water and multi-shell diffusion imaging.** Brain (2021).
5. Lu PJ, Yoo Y, Rahmanzadeh R, Galbusera R, Weigel M, Ceccaldi P, Nguyen TD, Spincemaille P, Wang Y, Daducci A, La Rosa F. **GAMER MRI: Gated-attention mechanism ranking of multi-contrast MRI in brain pathology.** NeuroImage: Clinical. 2021 Jan 1;29:102522.
6. Barquero G, La Rosa F, Kebiri H, Lu PJ, Rahmanzadeh R, Weigel M, Fartaria MJ, Kober T, Théaudin M, Du Pasquier R, Sati P. **RimNet: A deep 3D multimodal MRI architecture for paramagnetic rim lesion assessment in multiple sclerosis.** NeuroImage: Clinical. 2020 Jan 1;28:102412.
7. La Rosa F, Abdulkadir A, Fartaria MJ, Rahmanzadeh R, Lu PJ, Galbusera R, Barakovic M, Thiran JP, Granziera C, Cuadra MB. **Multiple sclerosis cortical and WM lesion segmentation at 3T MRI: a deep learning method based on FLAIR and MP2RAGE.** NeuroImage: Clinical. 2020 Jun 30:102335.
8. Rahmanzade R, Rahmanzadeh R, Tabarsi P, Hashemian SM**. Noninvasive Versus Invasive Ventilation in COVID-19 One Size Does Not Fit All!.** Anesthesia and Analgesia. 2020 May 12.
9. Rahmanzade R, Rahmanzadeh R, Hashemian SM. **Respiratory Distress in Postanesthesia Care Unit: First Presentation of Coronavirus Disease 2019 in a 17-Year-Old Girl: A Case Report.** A&a Practice. 2020 May;14(7):e01227.

10. Togha M, Martami F, Rahmanzadeh R, Ghorbani Z, Refaeian F, Behbahani S, Panahi P, Moghadam NB, Nafissi S, Shahbazi M. **The role of opening CSF pressure in response to treatment for idiopathic intracranial hypertension (IIH).** Journal of Clinical Neuroscience. 2020 Apr 21.
11. La Rosa F, Fartaria MJ, Abdulkadir A, Rahmanzadeh R, Lu PJ, Galbusera R, Granziera C, Thiran JP, Bach Cuadra M. **Deep learning-based detection of cortical lesions in multiple sclerosis patients with FLAIR, DIR, and MP2RAGE MRI sequences.** Multiple Sclerosis Journal. 2019 Sep 10;25(CONF):131-356.
12. Etesam Z, Nemati M, Ebrahimizadeh MA, Ebrahimi HA, Hajghani H, Khalili T, Jafarzadeh A. **Different expressions of specific transcription factors of Th1 (T-bet) and Th2 cells (GATA-3) by peripheral blood mononuclear cells from patients with multiple sclerosis.** Basic and clinical neuroscience. 2018 Nov;9(6):458.
13. Fartaria MJ, Sati P, Todea A, Radue EW, Rahmanzadeh R, O'Brien K, Reich DS, Cuadra MB, Kober T, Granziera C. **Automated detection and segmentation of multiple sclerosis lesions using ultra– high-field MP2RAGE.** Investigative radiology. 2019 Jun 1;54(6):356-64.
14. Rahmanzadeh R, Brück W, Minagar A, Sahraian MA. **Multiple sclerosis pathogenesis: missing pieces of an old puzzle. Reviews in the Neurosciences.** 2018 Dec 19;30(1):67-83.
15. Rahmanzadeh R, Mehrabi S, Barati M, Ahmadi M, Golab F, Kazmi S, Joghataei MT, Seifi M, Gholipourmalekabadi M. **Effect of co-administration of bumetanide and phenobarbital on seizure attacks in temporal lobe epilepsy.** Basic and clinical neuroscience. 2018 Nov;9(6):408.
16. Togha M, Shirbache K, Rahmanzadeh R, Ghorbani Z, Yari Z, Refaeian F, Behbahani S, Panahi P. **Prevalence of new-onset migraine in patients with idiopathic intracranial hypertension in comparison to the general population.** Iranian Journal of Neurology. 2018 Oct 7;17(4):161.
17. Rahmanzadeh R, Weber MS, Brück W, Navardi S, Sahraian MA. **B cells in multiple sclerosis therapy—A comprehensive review.** Acta Neurologica Scandinavica. 2018 Jun;137(6):544-56.
18. Sharifi G, Lotfinia M, Rahmanzade R, Lotfinia AA, Rahmanzadeh R, Omidbeigi M, Meybodi ET. **Congenital absence of the posterior element of C1, C2, and C3 along with bilateral absence of c4 pedicles: case report and review of the literature.** World Neurosurgery. 2018 Mar 1;111:395-401.
19. Rahmanzadeh R, Sahraian MA, Rahmanzade R, Rodriguez M. **Demyelination with preferential MAG loss: a complex message from MS paraffin blocks.** Journal of the Neurological Sciences. 2018 Feb 15;385:126-30.
20. Rahmanzadeh R, Moghadasi AN, Navardi S, Minagar A, Sahraian MA. **Multiple sclerosis: clinical features, pathophysiology, diagnosis, and management.** Neuroinflammation. 2018 Jan 1 (pp. 1-20).
21. Sharifi G, Rahmanzadeh R, Lotfinia M, Rahmanzade R. **Pilocytic astrocytoma of fornix mimicking a colloid cyst: report of 2 cases and review of the literature.** World Neurosurgery. 2018 Jan 1;109:31-5.

22. Togha M, Rahmanzadeh R, Nematgorgani S, Yari Z, Razeghi Jahromi S, Refaeian F. **Suppression of Menstrual-Related Migraine Attack Severity Using Pyridoxine, Thiamine, and Cyanocobalamin: A Quasi-Experimental Within-Subject Design.** Archives of Neuroscience. 2020 Jul 31;7(3).
23. Togha M, Yari Z, Rahmanzadeh R, Jahromi SR, Ghorbani Z. **Comorbidities in chronic and episodic migraine.** JOURNAL OF HEADACHE AND PAIN 2017
24. Rahmanzadeh R, Eftekhari S, Shahbazi A, Khodaei Ardakani MR, Rahmanzade R, Mehrabi S, Barati M, Joghataei MT. **Effect of bumetanide, a selective NKCC1 inhibitor, on hallucinations of schizophrenic patients; a double-blind randomized clinical trial.** Schizophr Res. 2017 Jun;184:145-146.
25. Rahmanzadeh R, Shahbazi A, Ardakani MR, Mehrabi S, Rahmanzade R, Joghataei MT. **Lack of the effect of bumetanide, a selective NKCC1 inhibitor, in patients with schizophrenia: A double-blind randomized trial.** Psychiatry and clinical neurosciences. 2017 Jan;71(1):72-3.
26. Rahmanzadeh R, Rahmanzade R, Zabihiyeganeh M. **Posterior reversible encephalopathy syndrome in a patient with mixed connective tissue disease: a case report.** Journal of medical case reports. 2016 Dec;10(1):1-4.
27. Eftekhari S, Mehrabi S, Soleimani M, Hassanzadeh G, Shahrokhi A, Mostafavi H, Hayat P, Barati M, Mehdizadeh H, Rahmanzadeh R, Hadjighassem MR. **BDNF modifies hippocampal KCC2 and NKCC1 expression in a temporal lobe epilepsy model.** Acta neurobiologiae experimentalis. 2014;74(3):276-87.

5.6. Patents

- **Patent Filing 9796-01-US:** "SYSTEM AND METHOD OF MAGNETIC RESONANCE IMAGING METHOD FOR MONITORING REMYELINATION"

5.7. Relevant technical skills

- **Programming languages:** Python, MATLAB & Bash
- **Statistical packages:** GraphPad Prism, SPSS & STATA
- **Neuroimaging tools:** Statistical Parametric Mapping (SPM), FMRIB Software Library (FSL) & FreeSurfer
- **Medical imaging segmentation software:** ITK-Snap, 3D Slicer

5.8. Books & Book chapters

- Book Title: **Neuroinflammation**, Second edition, Elsevier.
  Book Chapter: Reza Rahmanzadeh, Alireza Minagar, Mohammad Ali Sahraian. "Multiple
  sclerosis: Clinical features, Pathophysiology, Diagnosis, and Management."
- Book Title: **MRI Atlas of MS Lesions**, in press, Springer.
  Authors: Reza Rahmanzadeh, Ernst-Wilhelm Radue, Mohammad Ali Sahraian.
- Book Title: **Human anatomy (Muscluskeletal System, Head and Neck)**, 2011.
  Authors: Reza Rahmanzadeh, Homa Rasouli. In Persian.
- Book Title: **Gray's Anatomy for students**, translated, 2012.
  Authors: Reza Rahmanzadeh, Mehdi Mehdizadeh. In Persian.
- Book Title: **Systematic anatomy**, 2014.
  Authors: Reza Rahmanzadeh, Homa Rasouli. It is the current approaved textbook for anatomy in Iran University of Medical Sciences. In Persian.

6. PhD-related Publications

Original papers

1. Pietro Maggi, Jens Kuhle, Sabine Schaedelin, Franziska Van der Meer, Reza Rahmanzadeh, Pascal Benkert, Francesco La Rosa, Meritxell Bach cuadra, Pascal Sati, et al. **Chronic White Matter Inflammation and Serum Neurofilament Levels in Multiple Sclerosis.** Neurology.2021; 97 (6)
2. Oechtering J, Schaedelin S, Benkert P, Müller S, Achtnichts L, Vehoff J, Disanto G, Findling O, Fischer-Barnicol B, Orleth A, Chan A**. Intrathecal Immunoglobulin M synthesis is an independent biomarker for higher disease activity and severity in multiple sclerosis.** Annals of Neurology. ANN NEUROL 2021;90:477–489.
3. Lu PJ, Barakovic M, Weigel M, Rahmanzadeh R, Galbusera R, Schiavi S, Daducci A, La Rosa F, Bach Cuadra M, Sandkühler R, Kuhle J. **GAMER-MRI in Multiple Sclerosis Identifies the Diffusion-Based Microstructural Measures That Are Most Sensitive to Focal Damage: A Deep-Learning-Based Analysis and Clinico-Biological Validation.** Frontiers in neuroscience. 2021 Apr 6;15:258.
4. Rahmanzadeh R, Lu PJ, Barakovic M, Weigel M, Nguyen TD, Spincemaille P, Schiavi S, Daducci A, La Rosa F, Reich DS, Sati P, et al. **Myelin and axon pathology in multiple sclerosis assessed by myelin water and multi-shell diffusion imaging.** Brain (2021).
5. Lu PJ, Yoo Y, Rahmanzadeh R, Galbusera R, Weigel M, Ceccaldi P, Nguyen TD, Spincemaille P, Wang Y, Daducci A, La Rosa F. **GAMER MRI: Gated-attention mechanism ranking of multi-contrast MRI in brain pathology.** NeuroImage: Clinical. 2021 Jan 1;29:102522.
6. Barquero G, La Rosa F, Kebiri H, Lu PJ, Rahmanzadeh R, Weigel M, Fartaria MJ, Kober T, Théaudin M, Du Pasquier R, Sati P. **RimNet: A deep 3D multimodal MRI architecture for paramagnetic rim lesion assessment in multiple sclerosis.** NeuroImage: Clinical. 2020 Jan 1;28:102412.
7. La Rosa F, Abdulkadir A, Fartaria MJ, Rahmanzadeh R, Lu PJ, Galbusera R, Barakovic M, Thiran JP, Granziera C, Cuadra MB. **Multiple sclerosis cortical and WM lesion segmentation at 3T MRI: a deep learning method based on FLAIR and MP2RAGE.** NeuroImage: Clinical. 2020 Jun 30:102335.
8. La Rosa F, Fartaria MJ, Abdulkadir A, Rahmanzadeh R, Lu PJ, Galbusera R, Granziera C, Thiran JP, Bach Cuadra M. **Deep learning-based detection of cortical lesions in multiple sclerosis patients with FLAIR, DIR, and MP2RAGE MRI sequences.** Multiple Sclerosis Journal. 2019 Sep 10;25(CONF):131-356.
9. Rahmanzadeh R, Lu PJ, Weigel M, Nguyen TD, Schiavi S, Wang Y, Radue EW, Kuhle J, Kappos L, Granziera C. **An evaluation of axonal and myelin damage in multiple sclerosis lesions in living patients using myelin water and multi-shell diffusion MRI.** EUROPEAN JOURNAL OF NEUROLOGY 2019.
10. Fartaria MJ, Sati P, Todea A, Radue EW, Rahmanzadeh R, O'Brien K, Reich DS, Cuadra MB, Kober T, Granziera C. **Automated detection and**

segmentation of multiple sclerosis lesions using ultra– high-field MP2RAGE. Investigative radiology. 2019 Jun 1;54(6):356-64.

Congress Proceedings

11. Rahmanzadeh R, Lu PJ, Barakovic M, Weigel M, Schaedelin S, Nguyen TD, Schiavi S, Daducci A, La Rosa F, Wang Y, Cuadra MB. **Advanced magnetic resonance imaging for myelin and axonal density in ms: correlation with clinical disability and serum neurofilament levels.** MULTIPLE SCLEROSIS JOURNAL 2020.
12. Barakovic M, Melie-Garcia L, Weigel M, Rahmanzadeh R, Kuhle J, Kappos L, Granziera C. **Applying advanced diffusion MRI in MS: a comparison of 20 diffusion mri models to identify microstructural features of focal damage.** MULTIPLE SCLEROSIS JOURNAL 2020.
13. Rahmanzadeh R, Lu PJ, Barakovic M, Weigel M, Nguyen TD, Spincemaille P, Schiavi S, Daducci A, La Rosa F, Reich DS, Sati P. **Quantitative susceptibility mapping classifies white matter lesions with different myelin and axonal content and quantifies diffuse pathology in MS**. MULTIPLE SCLEROSIS JOURNAL 2020.
14. Sinnecker T, Ruberte E, Yaldizli O, Rahmanzadeh R, Galbusera R, Todea RA, Cagol A, Subramaniam S, Benkert P, Mueller S, Achtnichts L. **Role of gadolinium-based contrast agents to detect subclinical disease activity in clinically stable patients in the Swiss MS cohort study.** MULTIPLE SCLEROSIS JOURNAL 2020.
15. Todea R, Barquero G, Barakovic M, Kober T, Fartaria MJ, Cagol A, Rahmanzadeh R, Galbusera R, Psychogios M, Lieb J, Kappos L. **Automatic ms lesions segmentation using leman-pv as a clinical decision-support tool: a longitudinal analysis.** MULTIPLE SCLEROSIS JOURNAL 2020.
16. Barakovic M, Rahmanzadeh R, Lu PJ, Maggi P, Absinta M, La Rosa F, Bach-Cuadra M, Schiavi S, Daducci A, Sati P, Reich D. **Studying intralesional axonal damage in MS white matter lesions with diffusion MRI biophysical models.** MULTIPLE SCLEROSIS JOURNAL 2020.
17. Rahmanzadeh R, Lu PJ, Barakovic M, Weigel M, Schaedelin S, Nguyen TD, Schiavi S, Daducci A, La Rosa F, Wang Y, Cuadra MB. **Advanced magnetic resonance imaging for myelin and axonal density in ms: correlation with clinical disability and serum neurofilament levels.** MULTIPLE SCLEROSIS JOURNAL 2020.
18. Lu PJ, Barakovic M, Weigel M, Rahmanzadeh R, Galbusera R, Schiavi S, Daducci A, Kuhle J, Kappos L, Cattin P, Granziera C. **Attention-based deep learning identifies a new microstructural diffusion MRI contrast sensitive to focal pathology and related to patient disability.** MULTIPLE SCLEROSIS JOURNAL 2020.
19. Cagol A, Barakovic M, Benkert P, Todea RA, Rahmanzadeh R, Galbusera R, Schaedelin S, Lu PJ, Weigel M, Radue EW, Yaldizli O. **Focal inflammatory activity and lesion repair are associated with brain atrophy rates in MS patients.** MULTIPLE SCLEROSIS JOURNAL 2020.
20. Yaldizli Ö, Benkert P, Maceski A, Barakovic M, Todea RA, Cagol A, Schaedelin S, Disanto G, Oechtering J, Orleth A, Rey D. **Value of serum neurofilament light chain levels as a biomarker of suboptimal treatment**

response in MS clinical practice. MULTIPLE SCLEROSIS JOURNAL. 2020;26(3_SUPP):26-7.
21. Oechtering J, Schaedelin S, Benkert P, Barakovic M, Maceski A, Orleth A, Rey D, Sinnecker T, Rahmanzadeh R, Zadic S, Galbusera R. **Intrathecal immunoglobulin m synthesis is associated with higher serum neurofilament light chain levels and increased mri disease activity in MS.** MULTIPLE SCLEROSIS JOURNAL. 2020;26(3_SUPP):165.
22. Benkert P, Schaedelin S, Maceski A, Disanto G, Oechtering J, Barakovic M, Orleth A, Rey D, Sinnecker T, Yaldizli O, Rahmanzadeh R. **Serum nfl z-scores derived from a large healthy control group reflect different levels of treatment effect in a real-world setting.** MULTIPLE SCLEROSIS JOURNAL. 2020;26(3_SUPP):194-5.
23. Francesco La Rosa, Ahmed Abdulkadir, Mário João Fartaria, Reza Rahmanzadeh, Riccardo Galbusera, Jean-Philippe Thiran, Cristina Granziera, and Meritxell Bach Cuadra. **Automatic detection of Multiple Sclerosis cortical lesions based on 3D-FLAIR and MP2RAGE sequences**. ISMRM 2020.
24. Reza Rahmanzadeh, Po-Jui Lu, Muhamed Barakovic, Riccardo Galbusera, Matthias Weigel, Pietro Maggi, Thanh D. Nguyen, Simona Schiavi, Francesco La Rosa, Daniel S. Reich, Pascal Sati, Yi Wang, Meritxell Bach-Cuadra, Ernst-Wilhelm Radue, Jens Kuhle, Ludwig Kappos, and Cristina Granziera. **A quantification of myelin and axonal damage across multiple sclerosis lesions and clinical subtypes with myelin and diffusion MRI.** ISMRM 2020.
25. Po-Jui Lu, Reza Rahmanzadeh, Riccardo Galbusera, Matthias Weigel, Youngjin Yoo, Pascal Ceccaldi, Yi Wang, Jens Kuhle, Ludwig Kappos, Philippe Cattin, Benjamin Odry, Eli Gibson, and Cristina Granziera. **Attention-based convolutional network quantifying the importance of quantitative MR metrics in the multiple sclerosis lesion classification**. ISMRM 2020.
26. La Rosa F, Fartaria MJ, Abdulkadir A, Rahmanzadeh R, Lu PJ, Galbusera R, Granziera C, Thiran JP, Bach Cuadra M. **Deep learning-based detection of cortical lesions in multiple sclerosis patients with FLAIR, DIR, and MP2RAGE MRI sequences.** Multiple Sclerosis Journal. 2019 Sep 10;25(CONF):131-356.
27. Rahmanzadeh R, Lu PJ, Weigel M, Galbusera R, Nguyen TD, Schiavi S, Wang Y, La Rosa F, Cuadra MB, Radue EW, Kuhle J. **Axonal and myelin injury in white matter and cortex of relapsing-remitting and progressive multiple sclerosis patients: a combined myelin water and multi-shell diffusion MRI study.** MULTIPLE SCLEROSIS JOURNAL 2019.
28. Lu PJ, Rahmanzadeh R, Galbusera R, Odry B, Weigel M, La Rosa F, Cuadra MB, Nguyen T, Wang Y, Daducci A, Kuhle J. **Deep learning analysis applied to multi-parametric advanced MRI shows higher myelin content and neurite density in juxtacortical lesions compared to periventricular lesions.** MULTIPLE SCLEROSIS JOURNAL 2019.
29. Rahmanzadeh R, Lu PJ, Weigel M, Galbusera R, La Rosa F, Cuadra MB, Schiavi S, Radue EW, Kuhle J, Kappos L, Granziera C. **Axonal damage explains part of and extends beyond the diffuse pathology evidenced by T1 mapping in normal-appearing white matter of multiple sclerosis patients.** MULTIPLE SCLEROSIS JOURNAL 2019.

30. Rahmanzadeh R, Lu PJ, Weigel M, Nguyen TD, Schiavi S, Wang Y, Radue EW, Kuhle J, Kappos L, Granziera C. **An evaluation of axonal and myelin damage in multiple sclerosis lesions in living patients using myelin water and multi-shell diffusion MRI.** EUROPEAN JOURNAL OF NEUROLOGY 2019 (Vol. 26, pp. 245-246).

7. PhD Poster and presentations

7.1. Oral presentation

-11 Sep 2020 Joint American & European Committee for Treatment and Research in Multiple Sclerosis (ACTRIMS & ECTRIMS), Washington DC, USA.
Title: Quantitative susceptibility mapping classifies white matter lesions with different myelin content and axonal density and quantifies diffuse pathology in multiple sclerosis.
-10 Oct 2020 International Society for Magnetic Resonance in Medicine (ISMRM), Sydney, Australia.
Title: A quantification of microstructural damage across multiple sclerosis lesions and clinical subtypes with advanced quantitative MRI.
-11 Sep 2019 European Committee for Treatment and Research in Multiple Sclerosis (ECTRIMS), Stockholm, Sweden.
Title: Axonal damage explains part of and extends beyond the diffuse pathology evidenced by T1 mapping in normal-appearing white matter of multiple sclerosis patients.
-30 Jun 2019 European Congress of Neurology (EAN), Oslo, Norway.
Title: An Evaluation of Axonal and Myelin Damage in Multiple Sclerosis Lesions in Living Patients using Myelin Water and Multi-Shell Diffusion MRI.

7.2. Posters

- Axonal damage explains part of and extends beyond the diffuse pathology evidenced by T1 mapping in normal-appearing white matter of multiple sclerosis patients. ECTRIMS 2019.
- Advanced magnetic resonance imaging for myelin and axonal density in multiple sclerosis: correlation with clinical disability and serum neurofilament. ECTRIMS 2020.

-Axonal and myelin injury in white matter and cortex of relapsing-remitting and progressive multiple sclerosis patients: a combined myelin water and multi-shell diffusion MRI study. ECTRIMS 2020.

- A comparative assessment of sensitivity to myelin loss in multiple sclerosis and intra-scanner reproducibility for myelin-sensitive MRI measures. ECTRIMS 2021.

8. PhD courses (23 ETCS) *

8.1. Principles of Medical Imaging (3 ECTS)

8.2. Advanced Methods in Medical Image Analysis (6 ECTS)

8.3. Artificial Intelligence in Medical Imaging-2019 DBE Summer school (2 ECTS)

8.4. Biostatistics (2 ECTS)

8.5. Genetic Approaches in Biomedical Research (1 ECTS)

8.6. Chromatin and Epigenetics (2 ECTS)

8.7. Novel Approaches in Neurodegenerative Diseases- Seminar (2 ECTS)

8.8. Deutsch aktiv: Intensivkurs B1-Stufe- transferable skills (2 ECTS)

8.9. Out of the Box! Visualize Your Science- transferable skills (1 ECTS)

8.10. Presentation Training- transferable skills (1 ECTS)

8.11. Ethics in Science- transferable skills (1ECTS)

8.12. Visual communication of science- transferable skills workshop

***18 ETCS are required for PhD graduation.**

9. Bibliography

Aboul-Enein F, Rauschka H, Kornek B, Stadelmann C, Stefferl A, Bruck W, *et al.* Preferential loss of myelin-associated glycoprotein reflects hypoxia-like white matter damage in stroke and inflammatory brain diseases. J Neuropathol Exp Neurol 2003; 62(1): 25-33.

Absinta M, Nair G, Filippi M, Ray-Chaudhury A, Reyes-Mantilla MI, Pardo CA, *et al.* Postmortem magnetic resonance imaging to guide the pathologic cut: individualized, 3-dimensionally printed cutting boxes for fixed brains. J Neuropathol Exp Neurol 2014; 73(8): 780-8.

Absinta M, Sati P, Fechner A, Schindler MK, Nair G, Reich DS. Identification of Chronic Active Multiple Sclerosis Lesions on 3T MRI. AJNR Am J Neuroradiol 2018; 39(7): 1233-8.

Absinta M, Sati P, Masuzzo F, Nair G, Sethi V, Kolb H, *et al.* Association of Chronic Active Multiple Sclerosis Lesions With Disability In Vivo. JAMA Neurol 2019.

Absinta M, Sati P, Schindler M, Leibovitch EC, Ohayon J, Wu TX, *et al.* Persistent 7-tesla phase rim predicts poor outcome in new multiple sclerosis patient lesions. J Clin Invest 2016; 126(7): 2597-609.

Adamczyk B, Adamczyk-Sowa M. New Insights into the Role of Oxidative Stress Mechanisms in the Pathophysiology and Treatment of Multiple Sclerosis. Oxid Med Cell Longev 2016; 2016: 1973834.

Alcina A, Fedetz M, Ndagire D, Fernandez O, Leyva L, Guerrero M, *et al.* The T244I variant of the interleukin-7 receptor-alpha gene and multiple sclerosis. Tissue Antigens 2008; 72(2): 158-61.

Allan C, Burel JM, Moore J, Blackburn C, Linkert M, Loynton S, *et al.* OMERO: flexible, model-driven data management for experimental biology. Nat Methods 2012; 9(3): 245-53.

Amann M, Papadopoulou A, Andelova M, Magon S, Mueller-Lenke N, Naegelin Y, *et al.* Magnetization transfer ratio in lesions rather than normal-appearing brain relates to disability in patients with multiple sclerosis. J Neurol 2015; 262(8): 1909-17.

Andersson JLR, Sotiropoulos SN. An integrated approach to correction for off-resonance effects and subject movement in diffusion MR imaging. Neuroimage 2016; 125: 1063-78.

Androdias G, Reynolds R, Chanal M, Ritleng C, Confavreux C, Nataf S. Meningeal T cells associate with diffuse axonal loss in multiple sclerosis spinal cords. Ann Neurol 2010; 68(4): 465-76.

Antel J, Antel S, Caramanos Z, Arnold DL, Kuhlmann T. Primary progressive multiple sclerosis: part of the MS disease spectrum or separate disease entity? Acta Neuropathol 2012; 123(5): 627-38.

Bagnato F, Franco G, Thomas N, Smith S, Dortch R, Xu J. Multi-compartment Spherical Microscopic Diffusion Imaging Using Spherical Mean Techniques to Probe Axonal Injury in Multiple Sclerosis. Neurology 2018: P3. 383.

Bagnato F, Hametner S, Yao B, van Gelderen P, Merkle H, Cantor FK, *et al.* Tracking iron in multiple sclerosis: a combined imaging and histopathological study at 7 Tesla. Brain 2011; 134(Pt 12): 3602-15.

Bane O, Hectors SJ, Wagner M, Arlinghaus LL, Aryal MP, Cao Y, *et al.* Accuracy, repeatability, and interplatform reproducibility of T1 quantification methods used for DCE-MRI: Results from a multicenter phantom study. Magn Reson Med 2018; 79(5): 2564-75.

Baranzini SE, Srinivasan R, Khankhanian P, Okuda DT, Nelson SJ, Matthews PM, *et al.* Genetic variation influences glutamate concentrations in brains of patients with multiple sclerosis. Brain 2010; 133(9): 2603-11.

Baranzini SE, Wang J, Gibson RA, Galwey N, Naegelin Y, Barkhof F, *et al.* Genome-wide association analysis of susceptibility and clinical phenotype in multiple sclerosis. Hum Mol Genet 2009; 18(4): 767-78.
Barker GJ, Schreiber WG, Gass A, Ranjeva JP, Campi A, van Waesberghe JH, *et al.* A standardised method for measuring magnetisation transfer ratio on MR imagers from different manufacturers--the EuroMT sequence. MAGMA 2005; 18(2): 76-80.
Barnett MH, Prineas JW. Relapsing and remitting multiple sclerosis: pathology of the newly forming lesion. Ann Neurol 2004; 55(4): 458-68.
Bettencourt C, Santos C, Montiel R, Kay T, Vasconcelos J, Maciel P, *et al.* The (CAG)n tract of Machado-Joseph Disease gene (ATXN3): a comparison between DNA and mRNA in patients and controls. Eur J Hum Genet 2010; 18(5): 621-3.
Bian W, Tranvinh E, Tourdias T, Han M, Liu T, Wang Y, *et al.* In Vivo 7T MR Quantitative Susceptibility Mapping Reveals Opposite Susceptibility Contrast between Cortical and White Matter Lesions in Multiple Sclerosis. AJNR Am J Neuroradiol 2016; 37(10): 1808-15.
Bitsch A, Schuchardt J, Bunkowski S, Kuhlmann T, Bruck W. Acute axonal injury in multiple sclerosis. Correlation with demyelination and inflammation. Brain 2000; 123 (Pt 6): 1174-83.
Bjartmar C, Kinkel RP, Kidd G, Rudick RA, Trapp BD. Axonal loss in normal-appearing white matter in a patient with acute MS. Neurology 2001; 57(7): 1248-52.
Bodini B, Veronese M, Garcia-Lorenzo D, Battaglini M, Poirion E, Chardain A, *et al.* Dynamic Imaging of Individual Remyelination Profiles in Multiple Sclerosis. Ann Neurol 2016; 79(5): 726-38.
Bonnier G, Roche A, Romascano D, Simioni S, Meskaldji D, Rotzinger D, *et al.* Advanced MRI unravels the nature of tissue alterations in early multiple sclerosis. Ann Clin Transl Neurol 2014; 1(6): 423-32.
Boyd A, Zhang H, Williams A. Insufficient OPC migration into demyelinated lesions is a cause of poor remyelination in MS and mouse models. Acta Neuropathol 2013; 125(6): 841-59.
Bruck W. Inflammatory demyelination is not central to the pathogenesis of multiple sclerosis. J Neurol 2005; 252 Suppl 5: v10-5.
Cao G, Edden RAE, Gao F, Li H, Gong T, Chen W, *et al.* Reduced GABA levels correlate with cognitive impairment in patients with relapsing-remitting multiple sclerosis. Eur Radiol 2018; 28(3): 1140-8.
Caspers S, Rockner ME, Jockwitz C, Bittner N, Teumer A, Herms S, *et al.* Pathway-Specific Genetic Risk for Alzheimer's Disease Differentiates Regional Patterns of Cortical Atrophy in Older Adults. Cereb Cortex 2020; 30(2): 801-11.
Ceccarelli A, Rocca MA, Falini A, Tortorella P, Pagani E, Rodegher M, *et al.* Normal-appearing white and grey matter damage in MS. A volumetric and diffusion tensor MRI study at 3.0 Tesla. J Neurol 2007; 254(4): 513-8.
Cercignani M, Gandini Wheeler-Kingshott C. From micro- to macro-structures in multiple sclerosis: what is the added value of diffusion imaging. NMR Biomed 2019; 32(4): e3888.
Chen W, Gauthier SA, Gupta A, Comunale J, Liu T, Wang S, *et al.* Quantitative susceptibility mapping of multiple sclerosis lesions at various ages. Radiology 2014; 271(1): 183-92.
Choi JY, Lee J, Nam Y, Lee J, Oh SH. Improvement of reproducibility in quantitative susceptibility mapping (QSM) and transverse relaxation rates (R 2 *) after physiological noise correction. J Magn Reson Imaging 2019; 49(6): 1769-76.
Colgan N, Siow B, O'Callaghan JM, Harrison IF, Wells JA, Holmes HE, *et al.* Application of neurite orientation dispersion and density imaging (NODDI) to a tau pathology model of Alzheimer's disease. Neuroimage 2016; 125: 739-44.

Crow MK, Olferiev M, Kirou KA. Type I Interferons in Autoimmune Disease. Annu Rev Pathol 2019; 14: 369-93.
Cui QL, Khan D, Rone M, V TSR, Johnson RM, Lin YH, *et al.* Sublethal oligodendrocyte injury: A reversible condition in multiple sclerosis? Ann Neurol 2017; 81(6): 811-24.
Dal-Bianco A, Grabner G, Kronnerwetter C, Weber M, Hoftberger R, Berger T, *et al.* Slow expansion of multiple sclerosis iron rim lesions: pathology and 7 T magnetic resonance imaging. Acta Neuropathologica 2017a; 133(1): 25-42.
Dal-Bianco A, Grabner G, Kronnerwetter C, Weber M, Hoftberger R, Berger T, *et al.* Slow expansion of multiple sclerosis iron rim lesions: pathology and 7 T magnetic resonance imaging. Acta Neuropathol 2017b; 133(1): 25-42.
De Jager PL, Jia X, Wang J, de Bakker PI, Ottoboni L, Aggarwal NT, *et al.* Meta-analysis of genome scans and replication identify CD6, IRF8 and TNFRSF1A as new multiple sclerosis susceptibility loci. Nat Genet 2009; 41(7): 776-82.
De Stefano N, Giorgio A. GABA: a new imaging biomarker of neurodegeneration in multiple sclerosis? Brain 2015; 138(Pt 9): 2467-8.
Deh K, Kawaji K, Bulk M, Van Der Weerd L, Lind E, Spincemaille P, *et al.* Multicenter reproducibility of quantitative susceptibility mapping in a gadolinium phantom using MEDI+0 automatic zero referencing. Magn Reson Med 2019; 81(2): 1229-36.
Deh K, Nguyen TD, Eskreis-Winkler S, Prince MR, Spincemaille P, Gauthier S, *et al.* Reproducibility of quantitative susceptibility mapping in the brain at two field strengths from two vendors. J Magn Reson Imaging 2015; 42(6): 1592-600.
Deh K, Ponath GD, Molvi Z, Parel GT, Gillen KM, Zhang S, *et al.* Magnetic susceptibility increases as diamagnetic molecules breakdown: Myelin digestion during multiple sclerosis lesion formation contributes to increase on QSM. J Magn Reson Imaging 2018; 48(5): 1281-7.
Disanto G, Barro C, Benkert P, Naegelin Y, Schadelin S, Giardiello A, *et al.* Serum Neurofilament light: A biomarker of neuronal damage in multiple sclerosis. Ann Neurol 2017; 81(6): 857-70.
Enzinger C, Barkhof F, Ciccarelli O, Filippi M, Kappos L, Rocca MA, *et al.* Nonconventional MRI and microstructural cerebral changes in multiple sclerosis. Nat Rev Neurol 2015; 11(12): 676-86.
Euesden J, Lewis CM, O'Reilly PF. PRSice: Polygenic Risk Score software. Bioinformatics 2015; 31(9): 1466-8.
Farr CV, El-Kasaby A, Freissmuth M, Sucic S. The Creatine Transporter Unfolded: A Knotty Premise in the Cerebral Creatine Deficiency Syndrome. Front Synaptic Neurosci 2020; 12: 588954.
Filippi M. MRI measures of neurodegeneration in multiple sclerosis: implications for disability, disease monitoring, and treatment. J Neurol 2015; 262(1): 1-6.
Filippi M, Rocca MA, Martino G, Horsfield MA, Comi G. Magnetization transfer changes in the normal appearing white matter precede the appearance of enhancing lesions in patients with multiple sclerosis. Ann Neurol 1998; 43(6): 809-14.
Fischl B. FreeSurfer. Neuroimage 2012; 62(2): 774-81.
Friese MA, Schattling B, Fugger L. Mechanisms of neurodegeneration and axonal dysfunction in multiple sclerosis. Nat Rev Neurol 2014; 10(4): 225-38.
Frischer JM, Bramow S, Dal-Bianco A, Lucchinetti CF, Rauschka H, Schmidbauer M, *et al.* The relation between inflammation and neurodegeneration in multiple sclerosis brains. Brain 2009; 132(Pt 5): 1175-89.
Ganter C, Settles M, Dregely I, Santini F, Scheffler K, Bieri O. B1+-mapping with the transient phase of unbalanced steady-state free precession. Magn Reson Med 2013; 70(6): 1515-23.

Gao F, Yin X, Edden RAE, Evans AC, Xu J, Cao G, *et al.* Altered hippocampal GABA and glutamate levels and uncoupling from functional connectivity in multiple sclerosis. Hippocampus 2018; 28(11): 813-23.
Ge Y, Grossman RI, Udupa JK, Babb JS, Mannon LJ, McGowan JC. Magnetization transfer ratio histogram analysis of normal-appearing gray matter and normal-appearing white matter in multiple sclerosis. J Comput Assist Tomogr 2002; 26(1): 62-8.
Geurts JJ, Roosendaal SD, Calabrese M, Ciccarelli O, Agosta F, Chard DT, *et al.* Consensus recommendations for MS cortical lesion scoring using double inversion recovery MRI. Neurology 2011; 76(5): 418-24.
Goldschmidt T, Antel J, Konig FB, Bruck W, Kuhlmann T. Remyelination capacity of the MS brain decreases with disease chronicity. Neurology 2009; 72(22): 1914-21.
Goodin DS, Khankhanian P, Gourraud PA, Vince N. Genetic susceptibility to multiple sclerosis: interactions between conserved extended haplotypes of the MHC and other susceptibility regions. BMC Med Genomics 2021; 14(1): 183.
Goris A, Pauwels I, Gustavsen MW, van Son B, Hilven K, Bos SD, *et al.* Genetic variants are major determinants of CSF antibody levels in multiple sclerosis. Brain 2015; 138(Pt 3): 632-43.
Granberg T, Fan Q, Treaba CA, Ouellette R, Herranz E, Mangeat G, *et al.* In vivo characterization of cortical and white matter neuroaxonal pathology in early multiple sclerosis. Brain 2017; 140(11): 2912-26.
Granziera C, Wuerfel J, Barkhof F, Calabrese M, De Stefano N, Enzinger C, *et al.* Quantitative magnetic resonance imaging towards clinical application in multiple sclerosis. Brain 2021; 144(5): 1296-311.
Griswold MA, Jakob PM, Heidemann RM, Nittka M, Jellus V, Wang J, *et al.* Generalized autocalibrating partially parallel acquisitions (GRAPPA). Magn Reson Med 2002; 47(6): 1202-10.
Grussu F, Schneider T, Tur C, Yates RL, Tachrount M, Ianus A, *et al.* Neurite dispersion: a new marker of multiple sclerosis spinal cord pathology? Ann Clin Transl Neurol 2017; 4(9): 663-79.
Haider L. Inflammation, Iron, Energy Failure, and Oxidative Stress in the Pathogenesis of Multiple Sclerosis. Oxid Med Cell Longev 2015; 2015: 725370.
Hametner S, Endmayr V, Deistung A, Palmrich P, Prihoda M, Haimburger E, *et al.* The influence of brain iron and myelin on magnetic susceptibility and effective transverse relaxation - A biochemical and histological validation study. Neuroimage 2018; 179: 117-33.
Hametner S, Wimmer I, Haider L, Pfeifenbring S, Bruck W, Lassmann H. Iron and neurodegeneration in the multiple sclerosis brain. Ann Neurol 2013; 74(6): 848-61.
Harrison DM, Li X, Liu H, Jones CK, Caffo B, Calabresi PA, *et al.* Lesion Heterogeneity on High-Field Susceptibility MRI Is Associated with Multiple Sclerosis Severity. AJNR Am J Neuroradiol 2016; 37(8): 1447-53.
Helms G, Dathe H, Dechent P. Quantitative FLASH MRI at 3T using a rational approximation of the Ernst equation. Magn Reson Med 2008a; 59(3): 667-72.
Helms G, Dathe H, Kallenberg K, Dechent P. High-resolution maps of magnetization transfer with inherent correction for RF inhomogeneity and T1 relaxation obtained from 3D FLASH MRI. Magn Reson Med 2008b; 60(6): 1396-407.
Helms G, Dechent P. Increased SNR and reduced distortions by averaging multiple gradient echo signals in 3D FLASH imaging of the human brain at 3T. J Magn Reson Imaging 2009; 29(1): 198-204.
Helms G, Draganski B, Frackowiak R, Ashburner J, Weiskopf N. Improved segmentation of deep brain grey matter structures using magnetization transfer (MT) parameter maps. Neuroimage 2009; 47(1): 194-8.

Hoppenbrouwers IA, Aulchenko YS, Ebers GC, Ramagopalan SV, Oostra BA, van Duijn CM, *et al.* EVI5 is a risk gene for multiple sclerosis. Genes Immun 2008; 9(4): 334-7.
Howell OW, Rundle JL, Garg A, Komada M, Brophy PJ, Reynolds R. Activated microglia mediate axoglial disruption that contributes to axonal injury in multiple sclerosis. J Neuropathol Exp Neurol 2010; 69(10): 1017-33.
Inglese M, Bester M. Diffusion imaging in multiple sclerosis: research and clinical implications. NMR Biomed 2010; 23(7): 865-72.
Ingram G, Loveless S, Howell OW, Hakobyan S, Dancey B, Harris CL, *et al.* Complement activation in multiple sclerosis plaques: an immunohistochemical analysis. Acta Neuropathol Commun 2014; 2: 53.
International Multiple Sclerosis Genetics C. Multiple sclerosis genomic map implicates peripheral immune cells and microglia in susceptibility. Science 2019; 365(6460).
International Multiple Sclerosis Genetics C, Beecham AH, Patsopoulos NA, Xifara DK, Davis MF, Kemppinen A, *et al.* Analysis of immune-related loci identifies 48 new susceptibility variants for multiple sclerosis. Nat Genet 2013; 45(11): 1353-60.
International Multiple Sclerosis Genetics C, Bush WS, Sawcer SJ, de Jager PL, Oksenberg JR, McCauley JL, *et al.* Evidence for polygenic susceptibility to multiple sclerosis--the shape of things to come. Am J Hum Genet 2010; 86(4): 621-5.
International Multiple Sclerosis Genetics C, Hafler DA, Compston A, Sawcer S, Lander ES, Daly MJ, *et al.* Risk alleles for multiple sclerosis identified by a genomewide study. N Engl J Med 2007; 357(9): 851-62.
Isobe N, Keshavan A, Gourraud PA, Zhu AH, Datta E, Schlaeger R, *et al.* Association of HLA Genetic Risk Burden With Disease Phenotypes in Multiple Sclerosis. JAMA Neurol 2016; 73(7): 795-802.
Itoyama Y, Sternberger NH, Webster HD, Quarles RH, Cohen SR, Richardson EP, Jr. Immunocytochemical observations on the distribution of myelin-associated glycoprotein and myelin basic protein in multiple sclerosis lesions. Ann Neurol 1980; 7(2): 167-77.
Jenkinson M, Beckmann CF, Behrens TE, Woolrich MW, Smith SM. Fsl. Neuroimage 2012; 62(2): 782-90.
Jung S, Gamez-Diaz L, Proietti M, Grimbacher B. "Immune TOR-opathies," a Novel Disease Entity in Clinical Immunology. Front Immunol 2018; 9: 966.
Kaden E, Kelm ND, Carson RP, Does MD, Alexander DC. Multi-compartment microscopic diffusion imaging. Neuroimage 2016; 139: 346-59.
Kaunzner UW, Kang Y, Zhang S, Morris E, Yao Y, Pandya S, *et al.* Quantitative susceptibility mapping identifies inflammation in a subset of chronic multiple sclerosis lesions. Brain 2019; 142(1): 133-45.
Kirilina E, Helbling S, Morawski M, Pine K, Reimann K, Jankuhn S, *et al.* Superficial white matter imaging: Contrast mechanisms and whole-brain in vivo mapping. Sci Adv 2020; 6(41).
Kolb H, Absinta M, Beck ES, Ha SK, Song Y, Norato G, *et al.* 7T MRI Differentiates Remyelinated from Demyelinated Multiple Sclerosis Lesions. Ann Neurol 2021.
Kornek B, Storch MK, Weissert R, Wallstroem E, Stefferl A, Olsson T, *et al.* Multiple sclerosis and chronic autoimmune encephalomyelitis: a comparative quantitative study of axonal injury in active, inactive, and remyelinated lesions. Am J Pathol 2000; 157(1): 267-76.
Kozlowski P, Rosicka P, Liu J, Yung AC, Tetzlaff W. In vivo longitudinal Myelin Water Imaging in rat spinal cord following dorsal column transection injury. Magn Reson Imaging 2014; 32(3): 250-8.
Kuhlmann T, Lingfeld G, Bitsch A, Schuchardt J, Bruck W. Acute axonal damage in multiple sclerosis is most extensive in early disease stages and decreases over time. Brain 2002; 125(Pt 10): 2202-12.

Kuhlmann T, Ludwin S, Prat A, Antel J, Bruck W, Lassmann H. An updated histological classification system for multiple sclerosis lesions. Acta Neuropathol 2017; 133(1): 13-24.
Kuhlmann T, Miron V, Cui Q, Wegner C, Antel J, Bruck W. Differentiation block of oligodendroglial progenitor cells as a cause for remyelination failure in chronic multiple sclerosis. Brain 2008; 131(Pt 7): 1749-58.
Kumar D, Nguyen TD, Gauthier SA, Raj A. Bayesian algorithm using spatial priors for multiexponential T(2) relaxometry from multiecho spin echo MRI. Magn Reson Med 2012; 68(5): 1536-43.
Kurtzke JF. Rating neurologic impairment in multiple sclerosis: an expanded disability status scale (EDSS). Neurology 1983; 33(11): 1444-52.
Kutzelnigg A, Lucchinetti CF, Stadelmann C, Bruck W, Rauschka H, Bergmann M, *et al.* Cortical demyelination and diffuse white matter injury in multiple sclerosis. Brain 2005; 128(Pt 11): 2705-12.
La Rosa F, Abdulkadir A, Fartaria MJ, Rahmanzadeh R, Lu PJ, Galbusera R, *et al.* Multiple sclerosis cortical and WM lesion segmentation at 3T MRI: a deep learning method based on FLAIR and MP2RAGE. Neuroimage Clin 2020; 27: 102335.
Lassmann H. Multiple Sclerosis Pathology. Cold Spring Harb Perspect Med 2018a; 8(3).
Lassmann H. Pathogenic Mechanisms Associated With Different Clinical Courses of Multiple Sclerosis. Front Immunol 2018b; 9: 3116.
Lassmann H, van Horssen J, Mahad D. Progressive multiple sclerosis: pathology and pathogenesis. Nat Rev Neurol 2012; 8(11): 647-56.
Laule C, Leung E, Lis DK, Traboulsee AL, Paty DW, MacKay AL, *et al.* Myelin water imaging in multiple sclerosis: quantitative correlations with histopathology. Mult Scler 2006; 12(6): 747-53.
Laule C, Moore GRW. Myelin water imaging to detect demyelination and remyelination and its validation in pathology. Brain Pathol 2018; 28(5): 750-64.
Lee J, Nam Y, Choi JY, Kim EY, Oh SH, Kim DH. Mechanisms of T2 * anisotropy and gradient echo myelin water imaging. NMR Biomed 2017; 30(4).
Lee LE, Ljungberg E, Shin D, Figley CR, Vavasour IM, Rauscher A, *et al.* Inter-Vendor Reproducibility of Myelin Water Imaging Using a 3D Gradient and Spin Echo Sequence. Front Neurosci 2018; 12: 854.
Lee NJ, Ha SK, Sati P, Absinta M, Nair G, Luciano NJ, *et al.* Potential role of iron in repair of inflammatory demyelinating lesions. J Clin Invest 2019; 129(10): 4365-76.
Levy S, Guertin MC, Khatibi A, Mezer A, Martinu K, Chen JI, *et al.* Test-retest reliability of myelin imaging in the human spinal cord: Measurement errors versus region- and aging-induced variations. PLoS One 2018; 13(1): e0189944.
Li W, Wu B, Liu C. Quantitative susceptibility mapping of human brain reflects spatial variation in tissue composition. Neuroimage 2011; 55(4): 1645-56.
Li X, Harrison DM, Liu H, Jones CK, Oh J, Calabresi PA, *et al.* Magnetic susceptibility contrast variations in multiple sclerosis lesions. J Magn Reson Imaging 2016; 43(2): 463-73.
Lieury A, Chanal M, Androdias G, Reynolds R, Cavagna S, Giraudon P, *et al.* Tissue remodeling in periplaque regions of multiple sclerosis spinal cord lesions. Glia 2014; 62(10): 1645-58.
Liguori M, Healy BC, Glanz BI, Khoury SJ, Moscufo N, Weiner HL, *et al.* HLA (A-B-C and -DRB1) alleles and brain MRI changes in multiple sclerosis: a longitudinal study. Genes Immun 2011; 12(3): 183-90.
Lin PY, Chao TC, Wu ML. Quantitative susceptibility mapping of human brain at 3T: a multisite reproducibility study. AJNR Am J Neuroradiol 2015; 36(3): 467-74.

Liu T, Xu W, Spincemaille P, Avestimehr AS, Wang Y. Accuracy of the morphology enabled dipole inversion (MEDI) algorithm for quantitative susceptibility mapping in MRI. IEEE Trans Med Imaging 2012; 31(3): 816-24.
Lopez-Gongora M, Escartin A, Martinez-Horta S, Fernandez-Bobadilla R, Querol L, Romero S, *et al.* Neurophysiological Evidence of Compensatory Brain Mechanisms in Early-Stage Multiple Sclerosis. PLoS One 2015; 10(8): e0136786.
Lubetzki C, Zalc B, Williams A, Stadelmann C, Stankoff B. Remyelination in multiple sclerosis: from basic science to clinical translation. Lancet Neurol 2020; 19(8): 678-88.
Lublin FD, Reingold SC, Cohen JA, Cutter GR, Sorensen PS, Thompson AJ, *et al.* Defining the clinical course of multiple sclerosis: the 2013 revisions. Neurology 2014; 83(3): 278-86.
Lucchinetti C, Bruck W, Parisi J, Scheithauer B, Rodriguez M, Lassmann H. A quantitative analysis of oligodendrocytes in multiple sclerosis lesions. A study of 113 cases. Brain 1999; 122 (Pt 12): 2279-95.
Lucchinetti C, Bruck W, Parisi J, Scheithauer B, Rodriguez M, Lassmann H. Heterogeneity of multiple sclerosis lesions: implications for the pathogenesis of demyelination. Ann Neurol 2000; 47(6): 707-17.
Lurbke A, Hagemeier K, Cui QL, Metz I, Bruck W, Antel J, *et al.* Limited TCF7L2 expression in MS lesions. PLoS One 2013; 8(8): e72822.
Magliozzi R, Howell O, Vora A, Serafini B, Nicholas R, Puopolo M, *et al.* Meningeal B-cell follicles in secondary progressive multiple sclerosis associate with early onset of disease and severe cortical pathology. Brain 2007; 130(Pt 4): 1089-104.
Mahad D, Ziabreva I, Lassmann H, Turnbull D. Mitochondrial defects in acute multiple sclerosis lesions. Brain 2008; 131(Pt 7): 1722-35.
Mahad DH, Trapp BD, Lassmann H. Pathological mechanisms in progressive multiple sclerosis. Lancet Neurol 2015; 14(2): 183-93.
Mammana S, Bramanti P, Mazzon E, Cavalli E, Basile MS, Fagone P, *et al.* Preclinical evaluation of the PI3K/Akt/mTOR pathway in animal models of multiple sclerosis. Oncotarget 2018; 9(9): 8263-77.
Manfredonia F, Ciccarelli O, Khaleeli Z, Tozer DJ, Sastre-Garriga J, Miller DH, *et al.* Normal-appearing brain t1 relaxation time predicts disability in early primary progressive multiple sclerosis. Arch Neurol 2007; 64(3): 411-5.
Marees AT, de Kluiver H, Stringer S, Vorspan F, Curis E, Marie-Claire C, *et al.* A tutorial on conducting genome-wide association studies: Quality control and statistical analysis. Int J Methods Psychiatr Res 2018; 27(2): e1608.
Marik C, Felts PA, Bauer J, Lassmann H, Smith KJ. Lesion genesis in a subset of patients with multiple sclerosis: a role for innate immunity? Brain 2007; 130(Pt 11): 2800-15.
Marques JP, Kober T, Krueger G, van der Zwaag W, Van de Moortele PF, Gruetter R. MP2RAGE, a self bias-field corrected sequence for improved segmentation and T1-mapping at high field. Neuroimage 2010; 49(2): 1271-81.
Masterman T, Ligers A, Olsson T, Andersson M, Olerup O, Hillert J. HLA-DR15 is associated with lower age at onset in multiple sclerosis. Ann Neurol 2000; 48(2): 211-9.
Metz I, Weigand SD, Popescu BF, Frischer JM, Parisi JE, Guo Y, *et al.* Pathologic heterogeneity persists in early active multiple sclerosis lesions. Ann Neurol 2014; 75(5): 728-38.
Meyers SM, Laule C, Vavasour IM, Kolind SH, Madler B, Tam R, *et al.* Reproducibility of myelin water fraction analysis: a comparison of region of interest and voxel-based analysis methods. Magn Reson Imaging 2009; 27(8): 1096-103.
Moccia M, van de Pavert S, Eshaghi A, Haider L, Pichat J, Yiannakas M, *et al.* Pathologic correlates of the magnetization transfer ratio in multiple sclerosis. Neurology 2020; 95(22): e2965-e76.

Moore GR, Leung E, MacKay AL, Vavasour IM, Whittall KP, Cover KS, *et al.* A pathology-MRI study of the short-T2 component in formalin-fixed multiple sclerosis brain. Neurology 2000; 55(10): 1506-10.
Mottershead JP, Schmierer K, Clemence M, Thornton JS, Scaravilli F, Barker GJ, *et al.* High field MRI correlates of myelin content and axonal density in multiple sclerosis--a post-mortem study of the spinal cord. J Neurol 2003; 250(11): 1293-301.
Mustafi SM, Harezlak J, Kodiweera C, Randolph JS, Ford JC, Wishart HA, *et al.* Detecting white matter alterations in multiple sclerosis using advanced diffusion magnetic resonance imaging. Neural Regen Res 2019; 14(1): 114-23.
Narayana PA, Doyle TJ, Lai D, Wolinsky JS. Serial proton magnetic resonance spectroscopic imaging, contrast-enhanced magnetic resonance imaging, and quantitative lesion volumetry in multiple sclerosis. Ann Neurol 1998; 43(1): 56-71.
Nguyen TD, Deh K, Monohan E, Pandya S, Spincemaille P, Raj A, *et al.* Feasibility and reproducibility of whole brain myelin water mapping in 4 minutes using fast acquisition with spiral trajectory and adiabatic T2prep (FAST-T2) at 3T. Magn Reson Med 2016; 76(2): 456-65.
Okuda DT, Srinivasan R, Oksenberg JR, Goodin DS, Baranzini SE, Beheshtian A, *et al.* Genotype-Phenotype correlations in multiple sclerosis: HLA genes influence disease severity inferred by 1HMR spectroscopy and MRI measures. Brain 2009; 132(Pt 1): 250-9.
Ozawa K, Suchanek G, Breitschopf H, Bruck W, Budka H, Jellinger K, *et al.* Patterns of oligodendroglia pathology in multiple sclerosis. Brain 1994; 117 (Pt 6): 1311-22.
Parnell GP, Booth DR. The Multiple Sclerosis (MS) Genetic Risk Factors Indicate both Acquired and Innate Immune Cell Subsets Contribute to MS Pathogenesis and Identify Novel Therapeutic Opportunities. Front Immunol 2017; 8: 425.
Patani R, Balaratnam M, Vora A, Reynolds R. Remyelination can be extensive in multiple sclerosis despite a long disease course. Neuropathol Appl Neurobiol 2007; 33(3): 277-87.
Patrikios P, Stadelmann C, Kutzelnigg A, Rauschka H, Schmidbauer M, Laursen H, *et al.* Remyelination is extensive in a subset of multiple sclerosis patients. Brain 2006; 129(Pt 12): 3165-72.
Patsopoulos NA. Genetics of Multiple Sclerosis: An Overview and New Directions. Cold Spring Harb Perspect Med 2018; 8(7).
Paul AM, Branton WG, Walsh JG, Polyak MJ, Lu JQ, Baker GB, *et al.* GABA transport and neuroinflammation are coupled in multiple sclerosis: regulation of the GABA transporter-2 by ganaxolone. Neuroscience 2014; 273: 24-38.
Piredda GF, Hilbert T, Thiran JP, Kober T. Probing myelin content of the human brain with MRI: A review. Magn Reson Med 2021; 85(2): 627-52.
Popescu BF, Frischer JM, Webb SM, Tham M, Adiele RC, Robinson CA, *et al.* Pathogenic implications of distinct patterns of iron and zinc in chronic MS lesions. Acta Neuropathol 2017; 134(1): 45-64.
Purcell S, Neale B, Todd-Brown K, Thomas L, Ferreira MA, Bender D, *et al.* PLINK: a tool set for whole-genome association and population-based linkage analyses. Am J Hum Genet 2007; 81(3): 559-75.
Rahmanzadeh R, Bruck W, Minagar A, Sahraian MA. Multiple sclerosis pathogenesis: missing pieces of an old puzzle. Rev Neurosci 2018a.
Rahmanzadeh R, Lu PJ, Barakovic M, Weigel M, Maggi P, Nguyen TD, *et al.* Myelin and axon pathology in multiple sclerosis assessed by myelin water and multi-shell diffusion imaging. Brain 2021.
Rahmanzadeh R, Sahraian MA, Rahmanzade R, Rodriguez M. Demyelination with preferential MAG loss: A complex message from MS paraffin blocks. J Neurol Sci 2018b; 385: 126-30.

Rahmanzadeh R, Weber MS, Bruck W, Navardi S, Sahraian MA. B cells in multiple sclerosis therapy-A comprehensive review. Acta Neurol Scand 2018c; 137(6): 544-56.
Ramio-Torrenta L, Sastre-Garriga J, Ingle GT, Davies GR, Ameen V, Miller DH, *et al.* Abnormalities in normal appearing tissues in early primary progressive multiple sclerosis and their relation to disability: a tissue specific magnetisation transfer study. J Neurol Neurosurg Psychiatry 2006; 77(1): 40-5.
Reich DS, Lucchinetti CF, Calabresi PA. Multiple Sclerosis. N Engl J Med 2018; 378(2): 169-80.
Rodriguez M, Scheithauer B. Ultrastructure of multiple sclerosis. Ultrastruct Pathol 1994; 18(1-2): 3-13.
Rodriguez M, Scheithauer BW, Forbes G, Kelly PJ. Oligodendrocyte injury is an early event in lesions of multiple sclerosis. Mayo Clin Proc 1993; 68(7): 627-36.
Ropele S, Enzinger C, Fazekas F. Iron Mapping in Multiple Sclerosis. Neuroimaging Clin N Am 2017; 27(2): 335-42.
Ropele S, Filippi M, Valsasina P, Korteweg T, Barkhof F, Tofts PS, *et al.* Assessment and correction of B1-induced errors in magnetization transfer ratio measurements. Magn Reson Med 2005; 53(1): 134-40.
Rovaris M, Bozzali M, Iannucci G, Ghezzi A, Caputo D, Montanari E, *et al.* Assessment of normal-appearing white and gray matter in patients with primary progressive multiple sclerosis: a diffusion-tensor magnetic resonance imaging study. Arch Neurol 2002; 59(9): 1406-12.
Samson RS, Cardoso MJ, Muhlert N, Sethi V, Wheeler-Kingshott CA, Ron M, *et al.* Investigation of outer cortical magnetisation transfer ratio abnormalities in multiple sclerosis clinical subgroups. Mult Scler 2014; 20(10): 1322-30.
Santin MD, Didier M, Valabregue R, Yahia Cherif L, Garcia-Lorenzo D, Loureiro de Sousa P, *et al.* Reproducibility of R2 * and quantitative susceptibility mapping (QSM) reconstruction methods in the basal ganglia of healthy subjects. NMR Biomed 2017; 30(4).
Sati P, George IC, Shea CD, Gaitan MI, Reich DS. FLAIR*: a combined MR contrast technique for visualizing white matter lesions and parenchymal veins. Radiology 2012; 265(3): 926-32.
Schmierer K, Scaravilli F, Altmann DR, Barker GJ, Miller DH. Magnetization transfer ratio and myelin in postmortem multiple sclerosis brain. Ann Neurol 2004; 56(3): 407-15.
Schultz V, van der Meer F, Wrzos C, Scheidt U, Bahn E, Stadelmann C, *et al.* Acutely damaged axons are remyelinated in multiple sclerosis and experimental models of demyelination. Glia 2017; 65(8): 1350-60.
Seewann A, Kooi EJ, Roosendaal SD, Barkhof F, van der Valk P, Geurts JJ. Translating pathology in multiple sclerosis: the combination of postmortem imaging, histopathology and clinical findings. Acta Neurol Scand 2009; 119(6): 349-55.
Shin HG, Lee J, Yun YH, Yoo SH, Jang J, Oh SH, *et al.* chi-separation: Magnetic susceptibility source separation toward iron and myelin mapping in the brain. Neuroimage 2021; 240: 118371.
Smets I, Goris A, Vandebergh M, Demeestere J, Sunaert S, Dupont P, *et al.* Quantitative MRI phenotypes capture biological heterogeneity in multiple sclerosis patients. Sci Rep 2021; 11(1): 1573.
Solanky M, Maeda Y, Ming X, Husar W, Li W, Cook S, *et al.* Proliferating oligodendrocytes are present in both active and chronic inactive multiple sclerosis plaques. J Neurosci Res 2001; 65(4): 308-17.
Srivastava R, Aslam M, Kalluri SR, Schirmer L, Buck D, Tackenberg B, *et al.* Potassium channel KIR4.1 as an immune target in multiple sclerosis. N Engl J Med 2012; 367(2): 115-23.

Stadelmann C. Multiple sclerosis as a neurodegenerative disease: pathology, mechanisms and therapeutic implications. Curr Opin Neurol 2011; 24(3): 224-9.
Stephenson E, Nathoo N, Mahjoub Y, Dunn JF, Yong VW. Iron in multiple sclerosis: roles in neurodegeneration and repair. Nat Rev Neurol 2014; 10(8): 459-68.
Stys PK, Zamponi GW, van Minnen J, Geurts JJ. Will the real multiple sclerosis please stand up? Nat Rev Neurosci 2012; 13(7): 507-14.
Sun D, Yu Z, Fang X, Liu M, Pu Y, Shao Q, *et al.* LncRNA GAS5 inhibits microglial M2 polarization and exacerbates demyelination. EMBO Rep 2017; 18(10): 1801-16.
Tabelow K, Balteau E, Ashburner J, Callaghan MF, Draganski B, Helms G, *et al.* hMRI - A toolbox for quantitative MRI in neuroscience and clinical research. Neuroimage 2019; 194: 191-210.
Taylor AJ, Salerno M, Dharmakumar R, Jerosch-Herold M. T1 Mapping: Basic Techniques and Clinical Applications. JACC Cardiovasc Imaging 2016; 9(1): 67-81.
Tham M, Frischer JM, Weigand SD, Fitz-Gibbon PD, Webb SM, Guo Y, *et al.* Iron Heterogeneity in Early Active Multiple Sclerosis Lesions. Ann Neurol 2020.
Thompson AJ, Banwell BL, Barkhof F, Carroll WM, Coetzee T, Comi G, *et al.* Diagnosis of multiple sclerosis: 2017 revisions of the McDonald criteria. Lancet Neurol 2018; 17(2): 162-73.
Todorich B, Pasquini JM, Garcia CI, Paez PM, Connor JR. Oligodendrocytes and myelination: the role of iron. Glia 2009; 57(5): 467-78.
Trapp BD, Nave KA. Multiple sclerosis: an immune or neurodegenerative disorder? Annu Rev Neurosci 2008; 31: 247-69.
van Baarsen LG, van der Pouw Kraan TC, Kragt JJ, Baggen JM, Rustenburg F, Hooper T, *et al.* A subtype of multiple sclerosis defined by an activated immune defense program. Genes Immun 2006; 7(6): 522-31.
van der Weijden CWJ, Garcia DV, Borra RJH, Thurner P, Meilof JF, van Laar PJ, *et al.* Myelin quantification with MRI: A systematic review of accuracy and reproducibility. Neuroimage 2021; 226: 117561.
Vrenken H, Geurts JJ, Knol DL, Polman CH, Castelijns JA, Pouwels PJ, *et al.* Normal-appearing white matter changes vary with distance to lesions in multiple sclerosis. AJNR Am J Neuroradiol 2006a; 27(9): 2005-11.
Vrenken H, Geurts JJ, Knol DL, van Dijk LN, Dattola V, Jasperse B, *et al.* Whole-brain T1 mapping in multiple sclerosis: global changes of normal-appearing gray and white matter. Radiology 2006b; 240(3): 811-20.
Wang Y, Spincemaille P, Liu Z, Dimov A, Deh K, Li J, *et al.* Clinical quantitative susceptibility mapping (QSM): Biometal imaging and its emerging roles in patient care. J Magn Reson Imaging 2017; 46(4): 951-71.
Weber F, Fontaine B, Cournu-Rebeix I, Kroner A, Knop M, Lutz S, *et al.* IL2RA and IL7RA genes confer susceptibility for multiple sclerosis in two independent European populations. Genes Immun 2008; 9(3): 259-63.
Weiskopf N, Suckling J, Williams G, Correia MM, Inkster B, Tait R, *et al.* Quantitative multi-parameter mapping of R1, PD(*), MT, and R2(*) at 3T: a multi-center validation. Front Neurosci 2013; 7: 95.
Winges KM, Gilden DH, Bennett JL, Yu X, Ritchie AM, Owens GP. Analysis of multiple sclerosis cerebrospinal fluid reveals a continuum of clonally related antibody-secreting cells that are predominantly plasma blasts. J Neuroimmunol 2007; 192(1-2): 226-34.
Wisnieff C, Ramanan S, Olesik J, Gauthier S, Wang Y, Pitt D. Quantitative susceptibility mapping (QSM) of white matter multiple sclerosis lesions: Interpreting positive susceptibility and the presence of iron. Magn Reson Med 2015; 74(2): 564-70.

Yan W, Nguyen T, Yuki N, Ji Q, Yiannikas C, Pollard JD, *et al.* Antibodies to neurofascin exacerbate adoptive transfer experimental autoimmune neuritis. J Neuroimmunol 2014; 277(1-2): 13-7.
Yang X, Wu Y, Zhang B, Ni B. Noncoding RNAs in multiple sclerosis. Clin Epigenetics 2018; 10(1): 149.
Yao B, Bagnato F, Matsuura E, Merkle H, van Gelderen P, Cantor FK, *et al.* Chronic multiple sclerosis lesions: characterization with high-field-strength MR imaging. Radiology 2012; 262(1): 206-15.
Yushkevich PA, Piven J, Hazlett HC, Smith RG, Ho S, Gee JC, *et al.* User-guided 3D active contour segmentation of anatomical structures: significantly improved efficiency and reliability. Neuroimage 2006; 31(3): 1116-28.
Zhang F, Liu G, Wei C, Gao C, Hao J. Linc-MAF-4 regulates Th1/Th2 differentiation and is associated with the pathogenesis of multiple sclerosis by targeting MAF. FASEB J 2017; 31(2): 519-25.
Zhang H, Schneider T, Wheeler-Kingshott CA, Alexander DC. NODDI: practical in vivo neurite orientation dispersion and density imaging of the human brain. Neuroimage 2012; 61(4): 1000-16.

10. Acknowledgement

First of all, I would like to thank Prof. Dr. Granziera for her supervision over my PhD projects. She gave me the opportunity to pursue my life-long interest in genuine scientific research in her equipped laboratory of neuroimaging, where I gradually developed a deep interest in neuroradiology. In addition, I would highly thank Prof. Granziera for her availability for being of help for difficulties during my PhD study.

I would like also to thank Prof. Dr. Cichon my second supervisor for his remarks and supports for my PhD project. His high-level laboratory assisted me to perform advanced genetic analysis and to develop an insight into that. I would also highly thank Stefan Herms for supervising the genetic analyses.

I would highly like to thank Prof. Dr. Matilde Inglese for kindly accepting to be as the external reviewer of my PhD thesis.

My heartfelt special thanks go to Herr Prof. Dr. Ernst-Wilhelm Radü who supported me in all aspects of my life from beginning of my presence in Basel. Without his support, I could have faced with major difficulties. His deep scientific viewpoints to the neglected areas of science and his precious scientific advices coming from life-long experience in MS neuroradiology were very helpful during my PhD.

I would like to deeply thank my parents Mr Abbas Rahmanzadeh and Ms Fatemeh Hosseini for their life-long support and guidance throughout my life. Their warm words and wise remarks originating from hard life experiences backed me always in my way. And my treasury of words is not yet rich enough to express truly the contribution of my wife Dr. Sahar Taheri Otaghsara, then as always I benefit from Iranian Molana's poem:

"If there are numerous pitfalls on the way,
No Problem! When you're still with me,
I'll survive… There will not be any further pain…"